Experimental Investigation of the Effect of Composition on the Performance and Characteristics of PEM Fuel Cell Catalyst Layers

Jungshik Baik

Thesis Submitted to the Faculty of
Virginia Polytechnic Institute and State University
in partial fulfillment of the requirements for the degree of:

MASTER OF SCIENCE

in

Mechanical Engineering

Committee Members:

Dr. Michael W. Ellis, Chair
Dr. Douglas J. Nelson
Dr. Michael R. von Spakovsky

July 19, 2006
Blacksburg, Virginia

Keywords: PEM, GDL, Catalyst Layer

Experimental Investigation of the Effect of Composition on the Performance and Characteristics of PEM Fuel Cell Catalyst Layers

Jungshik Baik

Abstract

The catalyst layer of a proton exchange membrane (PEM) fuel cell is a mixture of polymer, carbon, and platinum. The characteristics of the catalyst layer play a critical role in determining the performance of the PEM fuel cell. This research investigates the role of catalyst layer composition using a Central Composite Design (CCD) experiment with two factors which are Nafion content and carbon loading while the platinum catalyst surface area is held constant. For each catalyst layer composition, polarization curves are measured to evaluate cell performance at common operating conditions, Electrochemical Impedance Spectroscopy (EIS), and Cyclic Voltammetry (CV) are then applied to investigate the cause of the observed variations in performance. The results show that both Nafion and carbon content significantly affect MEA performance. The ohmic resistance and active catalyst area of the cell do not correlate with catalyst layer composition, and observed variations in the cell resistance and active catalyst area produced changes in performance that were not significant relative to compositions of catalyst layers.

Dedication

Dedicate to Heyjin Kim, Seungdo Baik, and Jumoon Park for their continuous love and support.

Acknowledgements

I would like to thank everyone who contributed to this research and to my success. I am very thankful for the help of my committee members for their input throughout this process. I am especially thankful for the help of my committee chair, Dr. Mike Ellis, for all he made time for the past years. The help was absolutely critical to the completion of this research. Without his help, this research would not have been possible. He was always willing to help and was always accommodating.

I would also like to thank Josh Sole. He taught me how to fabricate the MEA samples and how to use fuel cell test stand. He was very giving in his knowledge and time, and was helpful in completing this research.

Finally, I would like to thank my parents to whom this work is dedicated, and my wife for always support.

Table of Contents

List of Figures

List of Tables

1. Introduction

A fuel cell converts reactants (hydrogen and oxygen) into water, and in the process produces electricity. Because reactants constantly flow into the cell, it is never exhausted like a battery. As long as reactants flow into the cell, electricity is produced. The Proton Exchange Membrane Fuel Cell (PEMFC) has received great attention because of its transportation applications and portable electronic power applications. PEMFCs are light, small, and exhibit good energy conversion efficiency and high power density at a relatively low operating temperature (about 80 ^{o}C).

1.1 PEM Fuel Cell Operation

The components of a PEM fuel cell are shown in Figure 1-1.

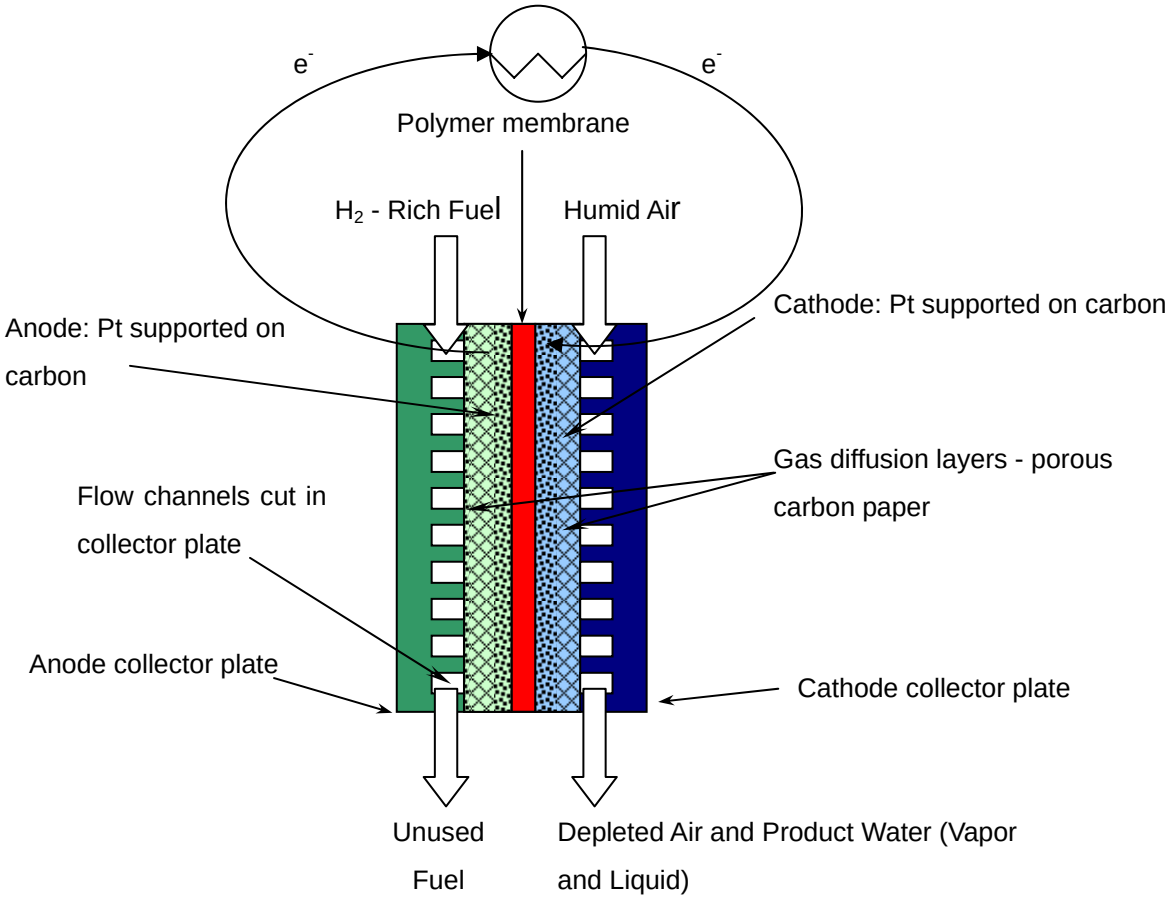

Figure 1-1. PEMFC structure.

The central element of a fuel cell is the membrane-electrode assembly (MEA) consisting of the electrodes (anode and cathode) and a polymer electrolyte membrane. Gas channels and diffusion layers adjacent to each electrode supply reactants and provide electrical continuity. Each component of the assembly is described in more detail in the following,

- **Anode** - the negative electrode of the fuel cell. At the anode, the hydrogen gas reacts as electrons are released, and hydrogen ions (protons) are created. This reaction supplies electrons through the external circuit and transfers ions to the electrolyte.

- **Cathode** - the positive electrode of the fuel cell. At the cathode, the oxygen reacts with electrons received from the anode through the external circuit, and hydrogen ions transferred through the electrolyte, to form water.
- **Electrolyte** - the proton exchange membrane. This ionic polymer conducts positively charged ions (H^+) and blocks the flow of electrons and reactant gas.
- **Gas Diffusion Layer (GDL)** – a porous carbon paper or carbon cloth treated with Polytetrafluoroethylene (PTFE), one located next to the anode and another next to the cathode. The porous nature of the GDL material ensures effective diffusion of each reactant gas to the electrode and allows the gas to disperse so that it contacts the entire surface area of the electrode. The GDL also allows transport of water in both liquid and vapor phases from the cathode into the flow channels.
- **Collector Plate** –an electrically conductive plate (usually graphite) with flow channels that supplies the reactant gases, removes the reaction products and unused reactant gases, and harvests the electrical current generated in the fuel cell. The channels in the flow field are usually a little less than 1 mm in width and height. The pressure drop along each channel should be greater than the surface tension that holds each water droplet in place so that water droplets do not stick in the channels (Larminie, [23]). The three most basic flow patterns are parallel, serpentine, and interdigitated.

The chemical half-reactions that govern the anode and cathode processes are shown in equations 1.1 and 1.2, respectively. The overall reaction is given in equation 1.3.

Anode side: $2H_2 \rightarrow 4H^+ + 4e^-$ (1.1)

Cathode side: $O_2 + 4H^+ + 4e^- \rightarrow 2H_2O$ (1.2)

Overall reaction: $2H_2 + O_2 \rightarrow 2H_2O$ (1.3)

In a fuel cell the electrodes are porous regions referred to as catalyst layers in which the electrochemical reactions occur. The catalyst layers must allow transport of reactants, ions, electrons, and other products to support electrochemical reactions and must provide a large catalyst surface area to promote these reactions.

The catalyst itself is a chemical substance that increases the rate of a reaction without being consumed in the process. The catalyst lessens the activation energy, allowing the reaction to proceed more quickly or at a lower temperature. In a fuel cell, the catalyst facilitates each half reaction. Platinum has proven to be the standard catalyst for many oxidation and reduction reactions in PEM fuel cells. To increase the platinum surface area, the catalyst is usually made of very small (~ 0.2 nm) platinum particles supported on larger (~ 30 nm) carbon particles. The catalyst layer is porous so that the maximum surface area of the platinum can be exposed to the hydrogen or oxygen. The catalyst layer structure is shown in a simplified form in Figure 1-2.

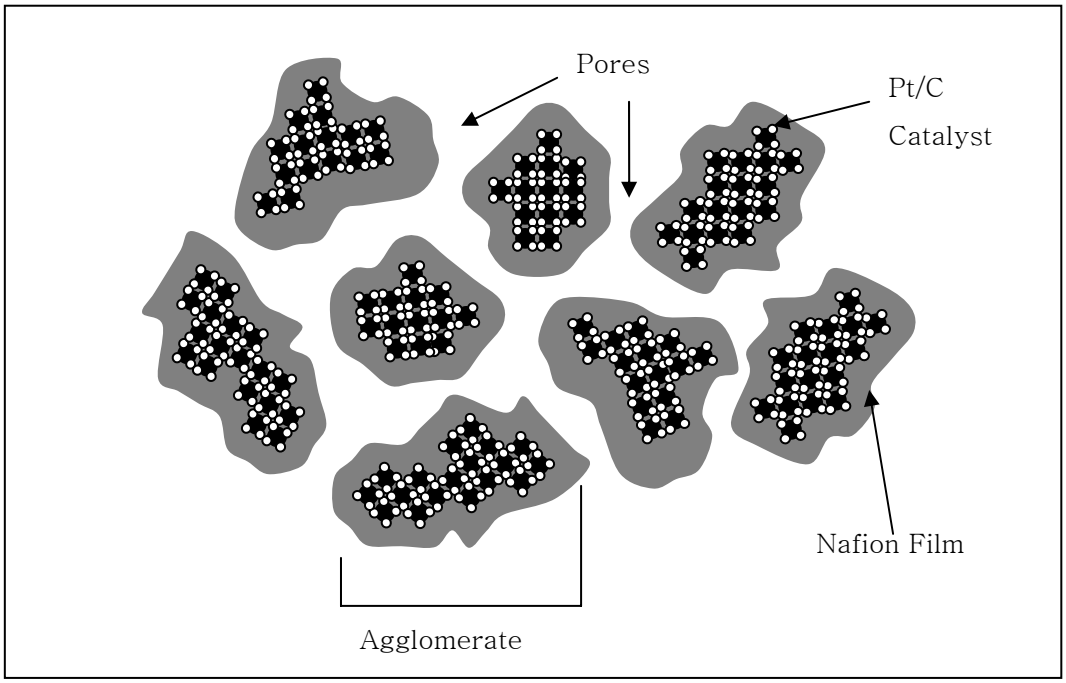

Figure 1-2. Simplified structure of the fuel cell catalyst layer.

1.2 Characteristics of the Catalyst Layer

PEM fuel cells require platinum or platinum-rich alloy catalysts to provide sufficient catalytic activity because in such cells the oxygen reduction reaction takes place in an acidic electrolyte at a relatively low temperature and has very slow kinetics in the absence of a catalyst. The use of low temperature is very important because the fuel cell is used with transportation and portable devices. At the same time, a rapid reaction rate is needed to achieve high current density. Thus a catalyst is regarded to achieve both low temperature and high reaction kinetics.

Early PEM fuel cells did not provide good contact between the electrolyte and the catalyst. For this reason, electrodes with very high platinum loading (about 4 mg-Pt /cm^2) were previously used to achieve high power density. A major breakthrough on electrode development, accomplished by Srinivasan and coworkers in 1988 [1], was

the reduction of catalyst loading from 4 to 0.4 mg-Pt /cm^2 by using carbon supported catalysts and by introducing polymer electrolyte into the gas diffusion electrodes and then hot-pressing the electrodes to the polymer membrane. In the following years many improvements were made in the design and fabrication processes for the catalyst layer. Currently, electrodes can run satisfactorily with loading as low as 0.20 mg-Pt /cm^2 for the oxygen electrode and 0.05 mg-Pt/cm^2 for the hydrogen (Gasteiger, et al. [7]).

The characteristics that are needed for a high performance catalyst layer include

1. Large platinum surface area
2. High electrical and ionic conductivities
3. Low mass transport resistance

A large platinum surface area enhances the reaction rate. This is not the same as simply having more platinum in the catalyst layer – the only portion of the platinum used is that which is on the surface of the platinum particle and connected ionically to the electrolyte and electrically to the diffusion layer. Surface area is maximized by using platinum particles with smaller radii thus yielding greater surface area for a given amount of platinum. Proper dispersion of the platinum is also essential because if two platinum particles touch within the catalyst layer, some of the surface area of each is lost. Thus, platinum particles with a very small radius are typically supported on carbon particles and then mixed with Nafion to form the catalyst layer.

Electrical conductivity and ionic conductivity affect the transport of electrons

and ions from the reaction sites to the other fuel cell components. Electrons must travel from the reaction sites through the electrical circuit. Ions must travel from the reaction sites through the electrolyte. The catalyst layer must have sufficient carbon to provide an electrical path and sufficient Nafion to provide an ion transport path. On the other hand, too much carbon or Nafion can constrict the pores and increase the thickness of the catalyst layer. This means that an optimum content of Nafion and carbon must exists for optimum performance within the catalyst layer.

Mass transport resistance controls the rate of flow of reactants and products. Reactants (hydrogen and oxygen) must flow to the reactant sites at a rate sufficient to sustain the reaction. Likewise products must be able to flow from the reaction sites. Reactants and products must travel through the pores of the catalyst layer and through the layer of electrolyte (i.e. Nafion) that blankets the catalyst surface. Achieving low mass transport resistance requires a thin porous catalyst layer and a thin film of electrolyte covering the catalyst surface. High porosity helps the product water flow out of the catalyst layer and the reactant gas flow to the reaction sites. Too much porosity increases the electrical and ionic resistances of the layer by restricting the paths for electron and ion flow. An electrolyte film on the catalyst surface is essential for transporting ions to and from the reaction site. Making the film thin reduces the resistance to the transport of reactants through the electrolyte film to the platinum catalyst sites.

The key characteristics of the catalyst layer, platinum surface area, electrical and ionic conductivities, and mass transport resistance are affected by its composition.

The composition of the catalyst layer is specified by;

1. *Platinum loading* (L_{Pt} in mg/cm^2): As platinum loading is increased, the active surface area is increased as well, but the cost of the catalyst layer becomes much higher.
2. *Carbon loading* (L_C in mg/cm^2): The carbon provides electrical conductivity and enhances the active surface area in the catalyst layer, but little research has been done to explore these effects.

3. *Nafion loading* (L_{Naf} in mg/cm^2): At the optimal Nafion content, all the catalyst particles are connected for optimum ionic conduction with no excess Nafion blocking the pores. The literature commonly defines a parameter called *NFP*, which is the weight percentage of Nafion in the catalyst layer, and calculated by equation 1.4,

$$NFP = \frac{L_{Naf}}{L_{Naf} + L_{Pt} + L_C} \tag{1.4}$$

1.3 Purpose of Research

The main goal of this research is to explore the effect of carbon and Nafion content on the performance and characteristics of the catalyst layer. To isolate the effects of these components, the platinum loading expressed as gross catalyst surface area is held constant. Combinations of carbon and Nafion are explored in a two-factor, five-level experiment in which nine possible combinations are created. All other

factors that affect the fuel cell performance remain constant for all nine combinations.

The state-of -the-art platinum loading reported in the literature ranges from 0.1 to 0.5 mg/cm^2. In this research, 0.3 mg/cm^2 was chosen as representative platinum loading. A commonly used catalyst is 20 % platinum on carbon with a specific surface area, α_{Pt}, value of 128 m^2/g (E-TEK). The loading and catalyst specific surface area can be used to determine a representative catalyst area using equation 1.5,

$$A_{Pt} = \frac{L_{Pt} \times \alpha_{Pt}}{1000} = \frac{0.3mg/cm^2 \times 128m^2/g}{1000mg/g} = 0.0384m^2/cm^2 \qquad (1.5)$$

This catalyst area is held constant for all experiments in this research. Thus, one goal of this work is to determine the Nafion and carbon loadings that lead to optimal performance for this given catalyst surface area. In addition, having determined a relationship between catalyst layer composition and performance, a second goal of the research is to examine how catalyst layer characteristics such as physical characteristics, activation losses, ohmic losses, and mass transfer resistance are affected by composition.

2. Literature Review

2.1 Overview

The economic future of PEM fuel cells depends on lowering the costs of the ionomeric membranes, the catalysts, and the bipolar plates. Cost savings can be approached in several ways, such as reducing electrocatalyst loadings, increasing current density, or simplifying the cell design and manufacturing process. Achieving high performance catalyst layers is one of the important goals that must be achieved to improve cell performance and to lower the platinum loading in the electrodes. To make PEM fuel cells a commercial reality, much developmental work in the past 10-15 years has focused on improving the performance of polymer electrolytes, electrocatalysts, and electrode materials.

Since the first description of low catalyst-loading, carbon-supported, gas-diffusion electrodes for polymer electrolyte fuel cells (PEMFC), several improvements have been made in the design, composition, and loading of platinum in such systems. A major breakthrough in electrode development was accomplished by Srinivasan, et al [1] and involved a ten fold reduction of the catalyst loading, from 4 to 0.35 mg-Pt/cm^2, by impregnating gas diffusion electrodes with Nafion and hot pressing the electrodes to the membrane.

The catalyst fabrication process presented by Wilson and Gottesfeld [3] improved upon the previous techniques by significantly increasing the contact area between the polymer electrolyte and the platinum clusters by mixing solubilized Nafion

ionomer with a carbon supported platinum catalyst (Pt/C). The catalyst layers are cast from solution as thin films that utilize the ionomer itself as a binder. The thin films are then hot pressed directly onto the ionomer membranes, and the hydrophobic gas diffusion backings are inserted when the cells are assembled. This technique increases performance in several ways. First, the supported catalyst increases the gross platinum surface area. Second, the contact area between the ionomeric additive and catalyst is increased by completely eliminating the Teflon component (formerly used as a binder) from the catalyst layer and by improving the dispersion of the ionomer throughout the catalyst layer to increase the ionic conductivity.

A variety of research efforts refined these new approaches to PEM fuel cell catalyst layers. For example, Ticianelli et al. [4] examined the effect of Nafion loading for various ranges of current density. In the low current density region (0-300 mA/cm^2), an increase in Nafion loading increases the cell performance. This can be explained by an increased active area in the electrodes. For the high current density region (300-600 mA/cm^2), the increase of Nafion content has positive effects only up to 33 % of Nafion, after which the performance starts to decrease rapidly. In the high current density region, low Nafion loading leads to poor internal electrolytic conductivity that accounts for the poor cell performance. With increased Nafion loading, the conductivity increases, but a thicker layer of polymer inside the pores of the electrode introduces mass transport problems either by retarding the access of gases to the active sites or by encouraging flooding. Thus, for the high current density region, Ticianelli found that a Nafion content of about 33 % appears to be optimum for minimizing both ohmic and mass transport limitations.

Wantanbe et al. [5] investigated the influence of Nafion thickness on electrocatalytic properties using Nafion coated platinum electrodes. Platinum electrodes with a thin Nafion film show catalytic activities that are the same as those of a bare platinum electrode, i.e. kinetically controlled. The critical thickness of Nafion film on the catalyst surface is 0.2 μm, when the diffusion rate of reactant gases to catalyst sites becomes a rate determining step for H_2 oxidization. With thickness more than 0.2 μm, the diffusion of reactant gases in the film is the rate determining step. These results indicated the possibility that high performance catalysts embedded in very thin Nafion films can be designed for PEMFC.

Modern catalyst layers fabricated by processes similar to those described in these early works ([1], [3], [4]) can yield dramatic reductions in platinum loading. According to Gasteiger et al. [7], the effect of platinum loading reductions in both anode and cathode can be accomplished without significant voltage losses. In their work, the anode platinum loading is reduced from 0.4 to 0.05 mgPt/cm^2 at 80 ^{o}C, fully humidified condition, and 150 kPa with 50 cm^2 single-cell. The differences in cell voltage are only of the order of 10 mV and do not reflect their predicted differences of 30 mV. The cell voltage losses at the cathode are only 20 mV with reduction of platinum loading from 0.40 to 0.20 mg-Pt/cm^2 in state-of-the-art MEAs operated with H_2/air. Further improvements in the Pt-specific power density are possible with thinner membranes, allowing the same cell voltage at even higher current densities.

2.2 Construction Methods

Catalyst layers can be fabricated by application to the gas diffusion layer (GDL) or by application to the membrane.

2.2.1 Gas Diffusion Layer Application

Spraying: In the spraying method described by Srinivasan [11], the electrolyte is suspended in a mixture of water, alcohol, and colloidal polytetrafluoroethylene (PTFE, DuPont's Teflon). This mixture is then repeatedly sprayed onto wet-proofed carbon cloth. Between each spraying, the electrode is sintered in order to prevent the components from re-dissolving in the next layer. The last step is rolling of the electrode. This operation has been found to produce a thin catalyst layer of uniform thickness and of low porosity on the GDL surface.

Spreading: The spreading method described by Mehta et al. [12], consists of preparing a catalyzed carbon and PTFE dough by mechanical mixing and spreading it on a wet-proofed carbon cloth using a heavy stainless steel cylinder on a flat surface. This operation leads to a thin and uniform active catalyst layer on the surface of GDL for which the Pt loading is directly related to the thickness.

Sputtering: O'Hayre et al. [13] describe a method in which a 5 nm layer is sputter deposited on a wet-proofed GDL. Platinum was sputtered through shadow masks to define 5 cm^2 active regions on both sides of each membrane. The samples

were taken out of the vacuum chamber, exposed to ambient atmosphere, flipped, and then returned to vacuum to sputter the second side. The deposited platinum thickness was controlled by the sputtering time. Sputter conditions were 100 W and 30 SCCM Argon at 0.67 Pa, resulting in a sputter deposition rate of approximately 1 nm/s. Also, a remarkable improvement in performance was achieved when the catalyzed GDL was over-coated with a very thin layer of sputter deposited Nafion at the anode.

Dry spraying: According to Schulze, et al [6], reaction materials (Pt/C, PTFE) are mixed in a knife mill. The mixture is then atomized and sprayed in a nitrogen stream through a slit nozzle directly onto the membrane. Although adhesion of the catalytic material on the surface is strong, in order to improve the electric and ionic contact, the layer is fixed by hot pressing (Schulze, et al. [6]).

2.2.2 Membrane Application

Catalyst decaling and hot pressing: In the catalyst decaling method described by Wilson and Gottesfeld [3], platinum ink is prepared by thoroughly mixing the catalyst and solubilized perfluorosulfonic acid (PFSA). The paintability of the ink and stability of the suspension can be improved by the addition of glycerol. Membranes are catalyzed using a decal process in which the ink is cast onto PTFE blanks for transfer to the membrane by hot pressing. In the hot pressing, the coated blank, a polymer electrolyte membrane, and a second coated blank are sandwiched together. The assembly is inserted into a hot press at 100 ^{o}C and a light load is applied as the press is heated to 125 ^{o}C at which point the assembly is pressed at 70-90 atm for 90

seconds. The membrane/catalyst assembly is removed from the press and allowed to cool, and then the Teflon blanks are peeled away from the membrane, leaving the thin catalyst layers adhering to each side of the membrane. In the last step, the catalyzed membranes are rehydrated and ion-exchanged to the H^+ form by immersing them in light boiling sulfuric acid followed by rinsing in deionized water. The following table compares hot pressing conditions reported in the recent literature.

Table 2-1. Summary of previous decal brushing and hot pressing conditions.

Reference	Temperature	Pressure	Time
Henderson [23], 2005	200 ^oC	97 atm	5 min-rotate 90^o-2 min
Sole [24], 2006	210 ^oC	70 atm	4 min
Russell [25], 2003	210 ^oC	9-44 atm	1-5 min
Srinivasan et al.[1], 1988	120 ^oC	50-60 atm	30-40 sec
Xie et al. [9], 2004	205 ^oC	440 atm	5 min
Chun et al. [22], 1998	145 ^oC	193 atm	3 min
Wilson et al. [3], 1992	125 ^oC	70-90 atm	90 sec

Painting: In the painting method described by Wilson and Gottesfeld [15], Pt ink is prepared in a method similar to that used for the decaling method. A layer of ink is painted directly onto a dry membrane in the Na^+ form and baked at 160 to 190 ^oC to dry the ink. The reverse side is then prepared in a similar way. When using thinner membranes or heavy ink applications, there is considerable distortion of the painted area. The distortion is managed through drying on a specially heated and fixtured vacuum table. Also, the bulk of the solvent is removed at a lower temperature to alleviate cracking, and the final traces of solvent are rapidly removed at higher temperatures. In the last step, the catalyzed membranes are rehydrated and ion-exchanged to the H^+ form by immersing them in lightly boiling sulfuric acid followed by rinsing in deionized

water.

Refinements to the membrane application method: The most common method of preparing catalyst layers (described above) involves painstaking application by hand of thin coats of the liquid catalyst suspension to a hot press transfer decal, with drying and careful weighing of the decal between coats to determine when the appropriate platinum loading has been reached. This process can take from six hours to several days, depending on the degree of precision required. Bender and coworkers [8] have demonstrated that by use of a water-based catalyst ink along with Kapton film as a hot press transfer material, high precision fuel cell MEAs for research can be rapidly fabricated using a simple machine-driven coater. The Kapton film was chosen since it is more hydrophilic than Teflon. They also show that careful calibration of the ink/substrate combination can allow a predictable catalyst loading, with precision nearly three times better than that achievable under the best circumstances with the conventional ink formulation transferred from a Teflon decal. This is attributable to the superior release characteristics of the water ink/Kapton system.

Xie and coworkers [9] discovered that a perfluorosulfonated ionomer-rich film exists on the surface of the catalyst layer prepared by the traditional method of decal preparation. Under certain fabrication conditions, a dense skin consisting of recast Nafion formed on the outer surface of the catalyst layer of the completed MEA (surface adjacent to the decal). This skin was found to form during decal preparation and was attributed to the strong interaction between the dissolved Nafion ionomer in the catalyst ink solution and the hydrophobic Teflon decal surface. MEA evaluation indicated a

strong correlation between the presence of the catalyst layer skin with a significant decrease in performance in the mass-transport region of the polarization curve. This performance loss was attributed to an increased resistance to the transport of oxygen through the skin to the catalytic sites. Equally likely was the slow removal of water formed in the cathode reaction, leading to flooding at higher current density. Methods of preventing the catalyst layer skin formation include use of a less hydrophobic decal substrate, such as replacing Teflon-coated fiberglass with Kapton, use of a single ink application, for example, with blade-coating instead of multiple hand paintings, and elimination of the use of Crown dry film lubricant or other hydrophobic surface wetting agents.

2.3 Catalyst Layer Composition

Electrocatalysts for PEM fuel cells have been platinum or platinum based alloys with relatively high activities for H_2 oxidation and O_2 reduction at a low temperature. Due to the high cost of platinum, many researchers have been studying the catalyst layer composition as a way to reduce the content of platinum in the electrocatalyst layer while maintaining the performance.

One approach for reducing is to identify an optimal platinum reduction could be made by controlling Nafion content in the catalyst layer. Impedance spectroscopic measurements of electrodes with different Nafion loadings provide evidence for a variation of ionic resistance with the amount of polymer. The ionic resistance is the main factor which controls the electrochemical performance. According to

Poltarzewski and coworkers [10], at low Nafion loadings, the polymeric electrolyte uniformly fills the micro and macro pores of the electrode structure and increases its ionic conductivity. The pores are completely filled in the range from 0.8 to 1.0 mg of Nafion/cm^2 of electrode, and further addition of polymer results in the formation of a film on the external surface of the electrode. At 0.8 to 1.0 mg of polymer/cm^2 of electrode, a maximum in electrochemical activity was found for both anode and cathode respectively. In this range, the ionic conductivity of the electrodes reaches its highest value. This phenomenon has been explained with reference to a physical model that indicates that the electrolyte is located within the pores of the electrodes and resistance decreases when the pores fill with Nafion. Above 0.9 mg/cm^2, due to the hydrophobic-hydrophilic properties of the Nafion structure, a further supply of electrolyte does not fill the pores but forms films on the external surface of the electrodes. This film causes additional electrical and diffusive resistances in series with the ionic resistance in the active layer.

A similar explanation is offered by Passalacqua et al. [16] who assert that at low Nafion content, some catalyst particles are not connected to the membrane by a Nafion bridge. However, too much Nafion in the catalyst layer creating complex path way for electron transport and increases the electronic resistance. At the optimal Nafion content in the catalyst layer, all the catalyst particles are properly connected for both ionic and electronic conduction. In Figure 2-1, a schematic of the internal structure of the catalyst layer is shown.

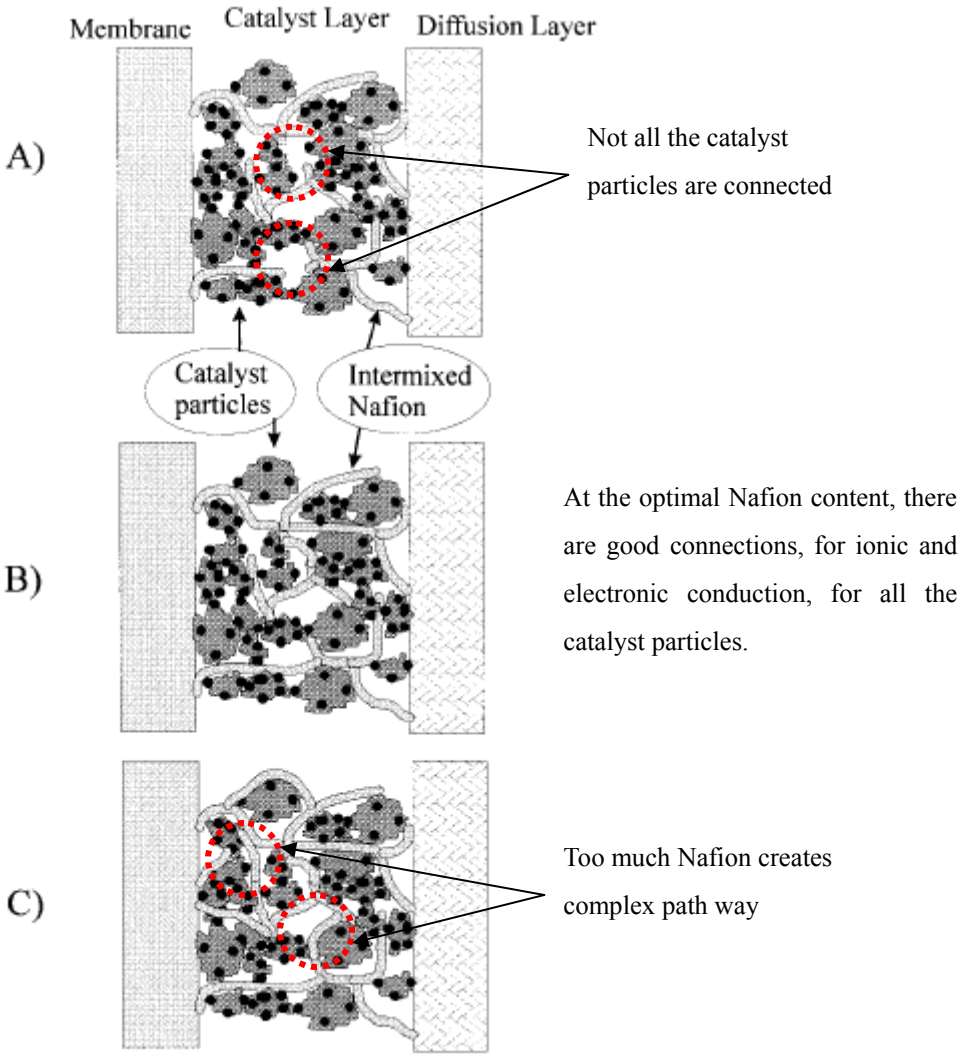

Figure 2-1. **Effect of Nafion content of the catalyst layer (Passalacqua et al. [16]).**

Based on the descriptions suggested by Poltarzewski or Passalacqua, many researchers have investigated the optimal Nafion content of catalyst layer for reducing the electronic and ionic resistances. Wilson and Gottesfeld [3] used a weight ratio of Nafion to carbon of 1 to 3 and they suggest that the optimal catalyst layer is very dense and very thin. Also, Uchida and coworkers [21] used ionomer loadings from 0.1 to 1.4 mg/cm^2 and 0.5 mg/cm^2 of platinum using 25 % weight platinum on carbon. They defined the best ionomer loading is 1.0 mg/cm^2 and the cell performance increased over

the entire operating range. Other works have reported similar results. For example, Paganin and coworkers [2] defined the best ionomer loading is 1.0 mg/cm^2 and they used Nafion loadings from 0.87 to 2.6 mg/cm^2 and a platinum loading of 0.4 mg/cm^2 using 10 % platinum on carbon.

Antolini and coworkers [17] investigated the effect of Nafion loading on gas diffusion electrode performance. They used 20 % platinum on carbon catalyst and Nafion by brushing the mixture onto a GDL, and Nafion loadings from 0 to 1.46 mg/cm^2. They found that the best Nafion loading is 0.67 mg/cm^2. They defined this loading minimized the activation overpotential and polarization resistance and maximized the electrochemical active area.

Passalacqua and coworkers [16] defined a parameter called NFP, which is the weight percentage of Nafion in the catalyst layer and found that the optimal NFP is 33 %. They used 20 % platinum on Vulcan XC-72 carbon at a platinum loading of 0.1 mg/cm^2. Also, Ticianelli and coworkers [4] found their best NFP is 33 %. They used 20 % platinum on carbon catalyst with a platinum loading of 0.35 mg/cm^2. Another researcher agreed with NFP of 33 %. Russell [25] investigated the effect of catalyst layer composition. He used 20 % platinum on carbon catalyst with a platinum loading of 0.322 mg/cm^2 and found the best NFP is 33 %

2.4 Summary of Current Catalyst Layer Literature and Relation to Current Work

A summary of platinum loading, Nafion content, construction method, and

operating conditions in recent literature is given in Table 2-2.

Table 2-2. Summary of previous findings on optimal conditions.

Authors	Platinum Type & Loading (mg/cm^2)	Carbon Loading (mg/cm^2)	Ionomer Content of Best MEA Loading (mg/cm^2) & NFP	Operating Pressure (atm)	Operating Temperature (^oC)	Fabrication Technique
Russell [25], 2003	20% Pt /C 0.322	1.30	0.792 33 %	2	80	Decal brushing and Hot press
Wilson and Gottesfeld [3], 1992	20% Pt/C 0.17	0.68	N/A 25-28 %	Anode: 3 Cathode: 5	N/A	Decal brushing and Hot press
Uchida et al. [21], 1995	25% Pt/C 0.5	1.5	1.0 33 %	N/A	N/A	Spreading on GDL and Hot press
Paganin et al. [2], 1996	20% Pt/C 0.4	1.6	1.1 33 %	N/A	80	Brushing on GDL and Hot press
Antolini et al. [17], 1999	20% Pt/C 0.2	0.8	0.67 40 %	N/A	N/A	Brushing on GDL and Hot press
Passalacqua et al. [16], 2001	20% Pt/C 0.1	0.4	0.24 33 %	N/A	70	Spraying on GDL and Hot press
Ticianelli et al. [4], 1988	20% Pt/C 0.35	1.4	N/A 33 %	Anode: 3 Cathode: 5	80	Brushing on GDL and Hot press

The current work investigates the effect of catalyst layer composition on the performance of a PEM fuel cell, and then explores the performance variation in terms of catalyst layer characteristics. Different compositions of catalyst layers are constructed, the performance of each MEA is evaluated, and the characteristics of each MEA including physical characteristics, activation losses, ohmic losses, and mass transport

losses are analyzed. The analysis identifies the characteristics of the catalyst layer and how they relate to the performance. The results of this work will improve the understanding of the characteristics of the catalyst layer and help to identify the best composition of catalyst layers for PEM fuel cells.

3. Experimental Procedures

This section explains the experimental procedures used for the investigation of the catalyst layer. Procedures and equipment used to conduct performance tests, impedance tests, and cyclic voltammetry tests are described. Performance tests describe the variation of cell voltage with current density and allow comparison of the current density of different membrane-electrode assembles at a common cell voltage. Impedance tests and cyclic voltammetry were used to measure ohmic losses, activation losses, and the active catalyst area of the catalyst layer.

3.1 Design of Experiment

The goal of this investigation is to determine the effect of Nafion and carbon loadings on catalyst layer performance for a given gross catalyst surface area. A Central Composite Design (CCD) was chosen for the investigation of the carbon and Nafion contents. The CCD is one of the most common design tools for Response Surface Methodology (RSM) designs in statistical studies. Good RSM designs allow finding a suitable approximating function for the purpose of predicting response and determining what values of the independent variables are optimums as far as the response is concerned. Good RSM designs should also give rise to a model with a small prediction error and permit a judgment of the adequacy of the model. This latter aspect means that the design must contain replicated experiments enabling the performance of a lack of fit test (Eriksson et al. [14]). Figure 3-1 shows the Central Composite Design model.

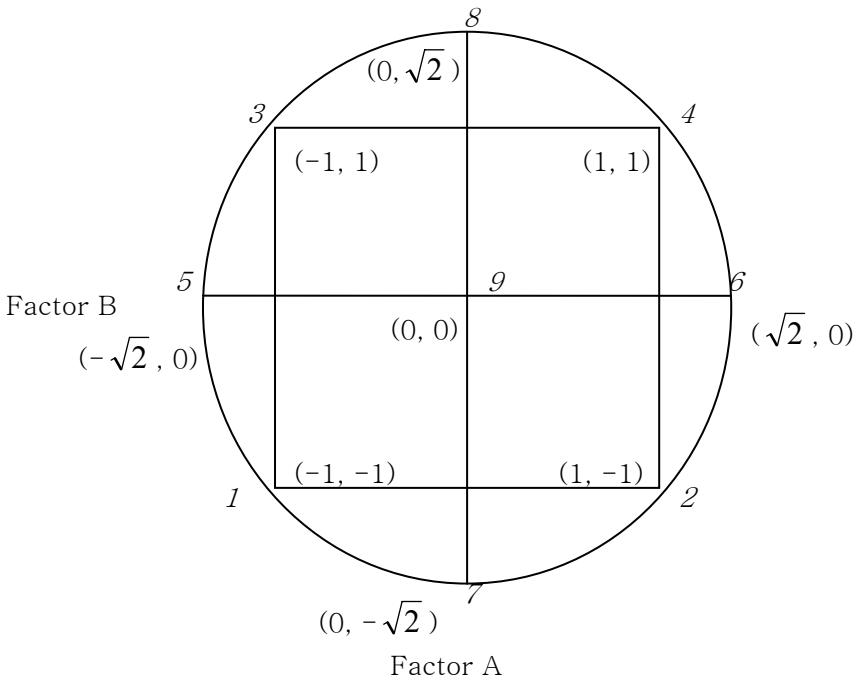

Figure 3-1. Central composite design.

A Central Composite Design contains an imbedded factorial or fractional factorial design with center points that is increased with a group of star points which are 5, 6, 7, and 8 in Figure 3-1 that allow estimation of curvature. If the distance from the center of the design space to a factorial point is ±1 unit for each factor, the distance from the center of the design space to a star point is ±α with $|\alpha| > 1$. The precise value of α depends on certain properties desired for the design and on the number of factors involved. For this research, $\sqrt{2}$ was chosen for α value.

Based on the literature review, the carbon range was chosen to be 0.57 to 2.42 mg/cm^2 with a center point of 1.5 mg/cm^2. The Nafion content was originally centered at 33 % but preliminary testing suggested that the performance was very poor at loadings exceeding 33 %. Therefore, the NFP range was established as 17 to 33 %

Nafion with a central point of 25 %.

The state-of -the-art platinum loading reported in the literature ranges from 0.1 to 0.5 mg/cm^2. As discussed in Chapter 1, 0.3 mg/cm^2 was chosen as a representative platinum loading while a specific surface area of 128 m^2/g yields a gross platinum surface area of 0.0384 m^2/cm^2. To achieve a range of carbon loadings which maintaining a constant gross platinum surface area, two different catalysts were mixed. Catalyst 1 has 10 % by weight platinum supported on XC-72 carbon particles. Catalyst 2 has 40 % by weight platinum on the same carbon support.

With the following two equations, 3.1 and 3.2, catalysts can be mixed to meet the desired carbon loading, L_c, and the common platinum area A_{pt}.

$$L_{cp}X_1(1-Y_1)+L_{cp}(1-X_1)(1-Y_2)=L_c \tag{3.1}$$

$$L_{cp}X_1Y_1\alpha_1+L_{cp}(1-X_1)Y_2\alpha_2=A_{pt} \tag{3.2}$$

where, L_{cp} is the carbon loading plus platinum loading,

X_1 is the mass fraction of catalyst 1

Y_1 is the platinum percent (mass basis) of catalyst 1

Y_2 is the platinum percent (mass basis) of catalyst 2

L_c is the desired carbon loading

α_1 is the surface area per gram of platinum for catalyst 1 (m^2/g-Pt)

α_2 is the surface area per gram of platinum for catalyst 2 (m^2/g-Pt)

A_{pt} is the desired platinum surface area (0.0384 m^2/cm^2)

The following Table 3-1 shows the carbon loadings and the Nafion weight percent for fit into the CCD model. Table 3-2 shows the characteristics of each catalyst used in the catalyst mixtures.

Table 3-1. The Central Composite Design for the Carbon and Nafion contents.

		Carbon Loadings L_c (mg/cm^2)				
		0.56885	0.8406	1.4965	2.1524	2.4241
		Platinum Loadings L_{Pt} (mg/cm^2)				
		0.384	0.3676	0.3282	0.2887	0.2723
Nafion %	33			**MEA 8**		
	30.7		**MEA 3**		**MEA 4**	
	25	**MEA 5**		**MEA 9**		**MEA 6**
	19.3		**MEA 1**		**MEA 2**	
	17			**MEA 7**		
Catalyst Mixture	Catalyst 1 (%)	100	67.3	26.1	5.7	0
	Catalyst 2 (%)	0	32.7	73.9	94.3	100

Table 3-2. The catalyst specification.

Designation	% Pt	α_{Pt} (m^2/g-Pt)
Catalyst 1	40.3% Pt	100
Catalyst 2	10.1% Pt	141

3.2 Preparation of MEA Samples

The MEAs used in this experiment were constructed by means of the Wilson and Gottesfeld [3] techniques. Following Wilson and Gottesfeld, the catalyst inks were mixed; the ink was painted onto Teflon coated decals and baked in an oven; the decals were weighed and the process repeated to achieve the desired loading. Finally, decals were hot-pressed onto a pre-treated Nafion membrane. The process is described in more detail in the following.

Catalyst inks were prepared using platinum-on-carbon catalysts from E-Tek

(see Table 3-2), a 5 % by weight Nafion solution, and glycerol. The carbon supported catalysts which were mixed in accordance with equations (3.1) and (3.2) were weighed and stored in a vial. The 5 % Nafion solution (Ion Power, Inc., DuPont DE 521) was then added to the vial to achieve the desired composition as specified in Table 3-1. Glycerol (ACROS, 41098-5000) was then added to the mixture in a ratio of one part glycerol to one part Nafion solution. The mixture was stirred for 30 minutes at room temperature using a magnetic stirrer and a hot plate. The ink was further mixed using an ultrasonic homogenizer (Biologics, Inc., 300 V/T) using a setting of 50 % pulse for one minute.

The Teflon blank was sprayed with PTFE release agent (SAINT-GOBAIN, Fluoroglide) and weighed to determine its mass. The prepared ink was brushed from left to right onto the Teflon blanks to form the catalyst layer. After coating, the blank was dried in an oven at 140 ^{o}C for 15-20 minutes to remove solvents from the ink. The painted blank was weighed and the mass of just the sprayed blank subtracted to determine the mass of the catalyst layer. The process was repeated until the desired catalyst layer mass was achieved. Each painting yielded an incremental loading of 1.8 to 2.3 mg of total catalyst layer. Between the brushing processes, 90 degree rotation prevented uneven thickness of brushing. The blank was then baked for 20 minutes to remove solvents possibly still left on the catalyst layer. The sample was weighed again to determine the final catalyst layer mass.

The Nafion membrane (Ion Power, Inc., Nafion 112) was boiled in deionized water for one hour and boiled again in 1 % NaOH by weight for one hour. These preparations were to convert the Nafion membrane to the sodium (Na^{+}) form from the standard proton (H^{+}) form. This process gives a higher glass transition temperature,

which improves the Nafion melting characteristics during catalyst layer hot-pressing. Catalyst coated blanks were then placed on both sides of the pretreated Nafion membrane, to form a sandwich. The sandwich was placed between two aluminum plates and placed in a hot press. The conditions for hot pressing described in Table 2-2 were reviewed and a procedure was chosen that consisted of preheating the hot press and the pressing the membrane-decal assembly at 70 atm for four minutes. The assembly was then removed and cooled under light pressure for at least 30 minutes. The Teflon blanks were removed leaving the catalyst layer adhered to the Nafion membrane to form an MEA. The remaining Teflon blanks were weighed to calculate the deposited mass of the catalyst layers. The MEA was boiled in solution of 20 ml of 18 M sulfuric acid (H_2SO_4) and 700 ml of deionized water for 90 minutes to return the membrane to the original H^+ form. The MEA was then boiled in deionized water for one hour to remove the acid.

The GDL was prepared from woven PAN carbon fiber cloth (E-Tek, B-1/A). The carbon cloth was immersed in a solution of 93% deionized water and 7% Teflon solution (ElectroChem, Inc. TFE 30) for 40 seconds and baked in an oven 20 minutes. The GDL treatment produced a hydrophobic content of 20% Teflon by weight on the carbon cloth. The Teflon treatment of the GDL helps to prevent flooding of the catalyst layer due to water production at the cathode.

3.3 Construction and Assembly of the Fuel Cell

The fuel cell test fixture (Fuel Cell Technologies, Inc.) used in this experiment

has a 5 cm^2 active area. The fuel cell is composed of eleven pieces: two end plates, two current collectors, two graphite plates, two Teflon gaskets, two gas diffusion layers, and the MEA. The assembly is illustrated in Figure 3-2.

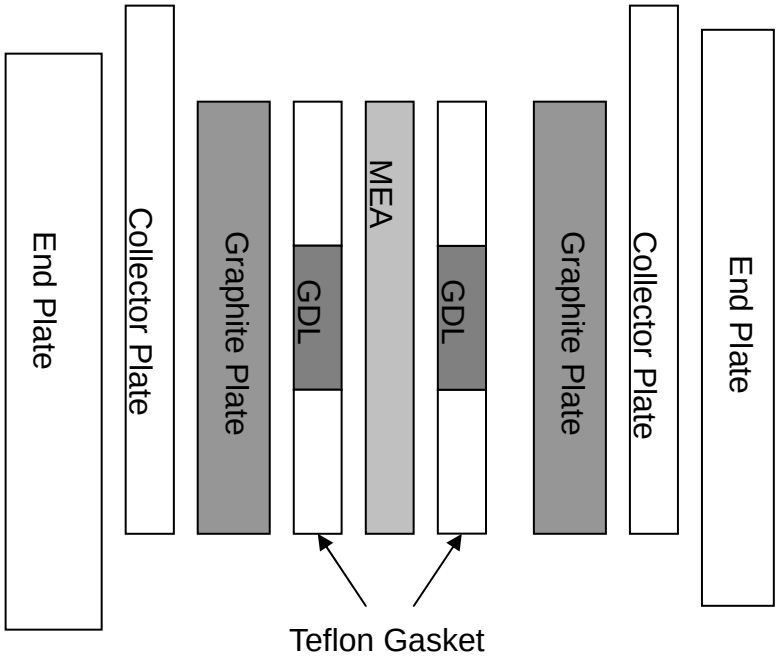

Figure 3-2. Schematic of the fuel cell assembly.

The end plates serve as a clamp that holds all of the parts together and connects the gas supply lines for the reactants. Eight quarter-inch bolt holes are located around the edge of the end plates. The end plates also contain cartridge heaters that maintain a constant temperature during cell operation. Gold-plated copper collector plates collect the current produced by the cell. The current produced by the cell is transmitted to the collector plates from the graphite plates. The graphite plates contain the gas flow channels that bring gases the MEA and conveys unused gases and product water to the cell outlet. The gas channels are serpentine in shape, winding back and forth across the active area of the MEA. The GDL is placed over the gas channels to evenly

distribute the gas over the MEA and to transfer current. The next component of the cell fixture is the fiberglass-reinforced Teflon gaskets which serve as both spacer and seal. Combinations of gaskets were used to achieve a total gasket thickness of 0.35 mm. The gaskets surround the GDL to prevent it from being crushed when the cell is compressed together with the end plates. The gaskets also prevent gas from exiting through the side of the cell rather than flowing through the gas channels in the graphite plates. Controlling the gasket thickness effectively controls the GDL compression.

Before the fuel cell was assembled, the parts were cleaned using alcohol to ensure minimal contact resistance within the hardware and to achieve the best cell performance. Teflon gaskets were cut with a razor blade using a plastic template that reflects the dimensions of the MEA and were then rinsed in alcohol. The GDL was then cut to fit inside of the gaskets. After the gaskets and GDLs were cut, a gasket was placed on one half of the assembled cell and a GDL carefully placed inside the gasket. The assembly was checked to ensure that the GDL and the gasket did not overlap, which could cause uneven pressure on the MEA. The MEA was then placed over the gasket and GDL and covered by the other gasket and GDL. The other half of the fuel cell fixture was then placed over the assembly, and the bolts were tightened in a cross pattern by hand. The bolts were tightened incrementally in a cross pattern at 10 inch pounds per increment and were tightened to a final torque of 50 inch pounds each. The cross pattern gives a uniform pressure distribution across the MEA. A picture of the two halves of the fuel cell fixture and MEA is shown in Figure 3-3.

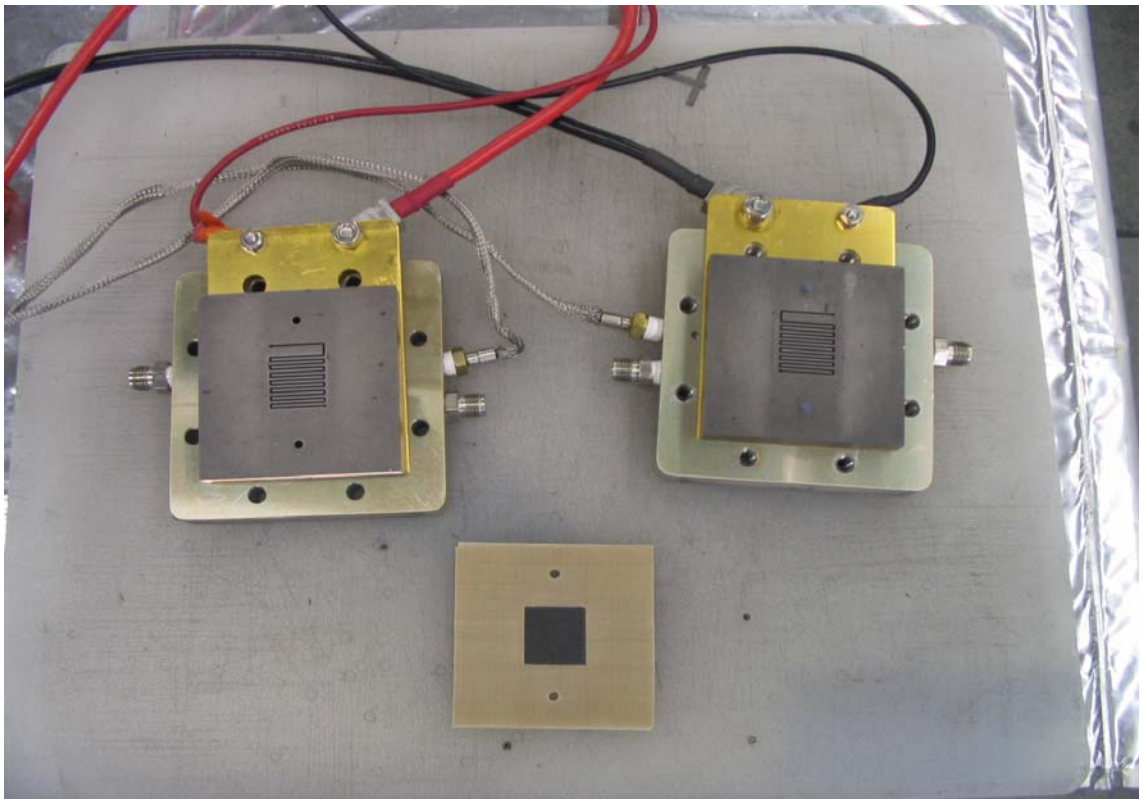

Figure 3-3. Fuel cell fixture with end plates, current collectors, graphite plates, and MEA.

3.4 Test Apparatus

The test stand in this experiment is from Fuel Cell Technologies, Inc. The test stand can control cell temperature, cell voltage, cell current as well as, dew point temperature, inlet temperature, pressure, and flow rate for both anode and cathode gas streams. These controls are operated with LABView software. A schematic diagram of the test stand is shown in Figure 3-4 and a picture is shown in Figure 3-5.

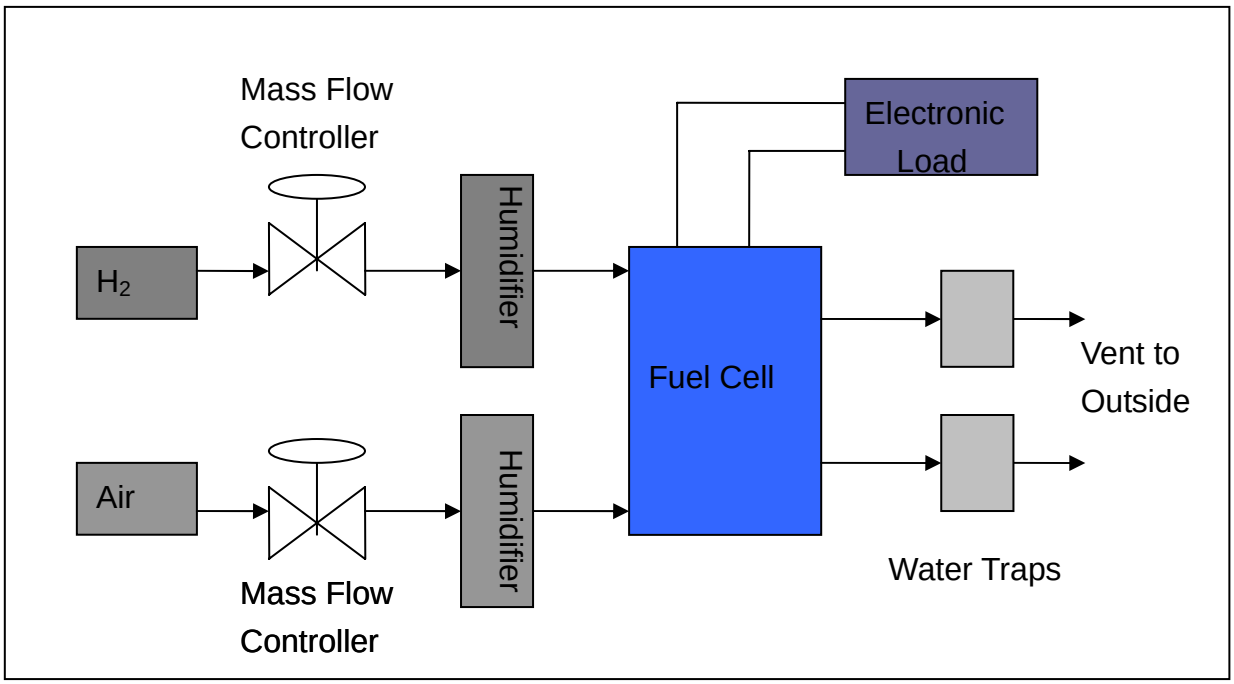

Figure 3-4. Schematic diagram of fuel cell test stand.

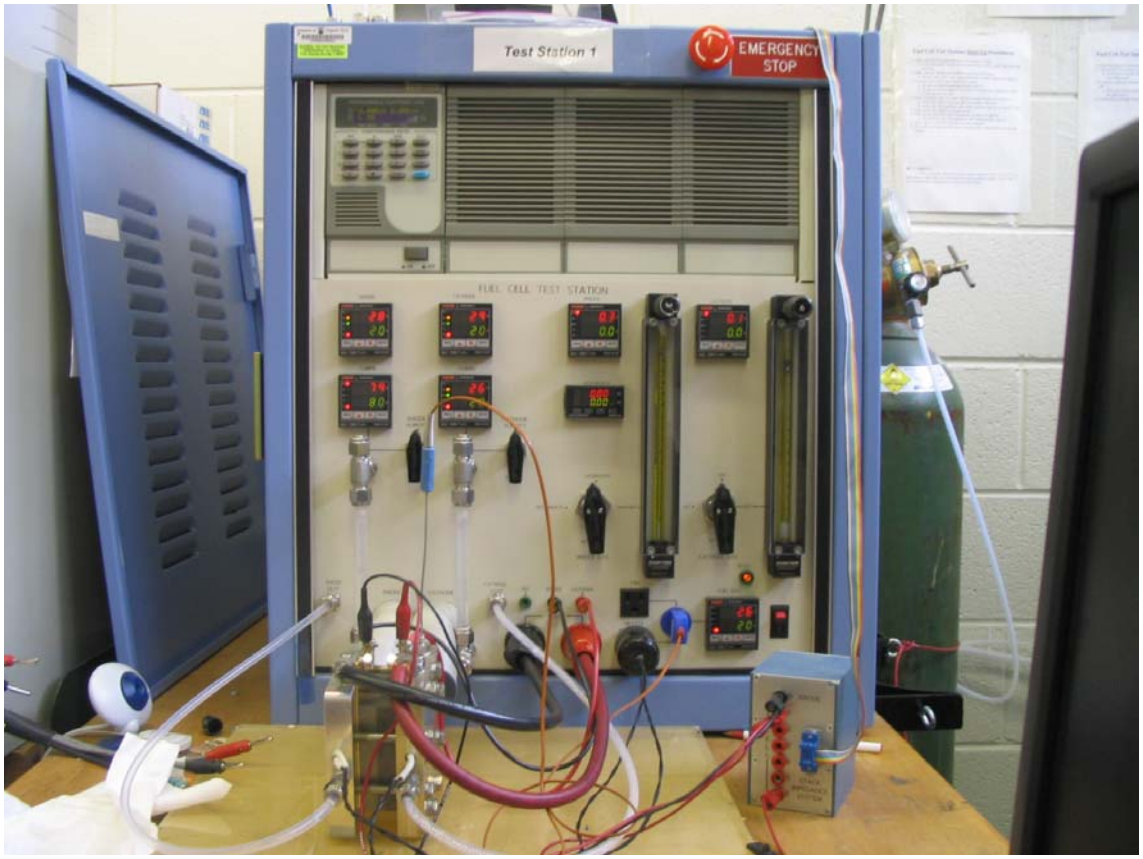

Figure 3-5. Picture of fuel cell test stand.

3.5 Performance Tests

The catalyst layer experiments were conducted in accordance with a consistent procedure. The MEAs were first conditioned, and polarization curves were obtained. The MEAs must be conditioned before they are used for the first time to achieve maximum performance. The MEAs were conditioned by operating the cell at 0.5 Volts for at least 24 hours or until stable performance was achieved. After the MEAs were fully conditioned, polarization curves were measured. The polarization curves were obtained potentiostatically both from high to low voltage and from low to high voltage. All tests were conducted with a cell temperature of 80 ºC using 60 % relative humidity air as the cathode gas and 100 % relative humidity hydrogen as the anode gas. The anode and cathode gases were supplied to the cell at a flow rate six times that required for stoichiometric operation at a current of 5 Amps (1 A/cm^2) equivalent to 225 SCCM for hydrogen and 550 SCCM for air. Following the performance test, diagnostic tests including electrochemical impedance spectroscopy tests, cyclic voltammetry tests, and microscopy were conducted to understand performance characteristics.

3.6 Diagnostic Tests

3.6.1 Electrochemical Impedance Spectroscopy Test

Electrochemical Impedance Spectroscopy (EIS) tests were conducted to distinguish between components of the overpotential. At low current densities, activation losses are most important. Activation losses are associated with the potential difference required to drive the electrochemical reaction at a finite rate. At

the middle current densities, ohmic losses tend to be most significant. Ohmic losses are caused by resistance to the flow of electrons through the electrodes and the flow of ions through the electrolyte. At high current densities, mass transport losses dominate the cell performance behavior. Mass transport losses result from restrictions along the reactant flow path. Figure 3-6 shows a typical polarization curve and identifies the region in which each of the three losses is most important.

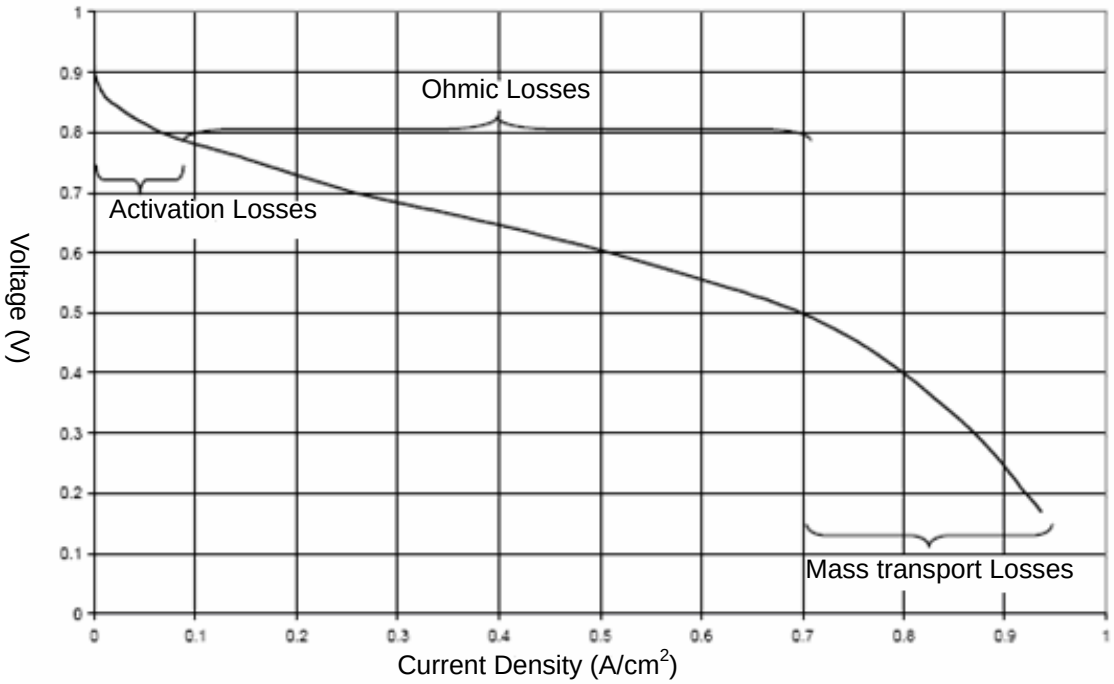

Figure 3-6. Polarization curve identifying major losses.

The processes that occur inside the fuel cell can be modeled using circuit elements. The losses associated with ion and electron transport can be modeled as a simple resister. At the electrodes the behavior is more complex. During an electrochemical reaction, a significant separation of charge occurs across the reaction interface, with electron accumulation in the electrode matched by ion accumulation in the electrolyte. The separation between the negative charge in the electrode and the

positive charge in the electrolyte causes the interface to behave like a capacitor. The overall impedance behavior of the reaction interface can be modeled as parallel combination of a resistor and a capacitor. This circuit element occurs at both the anode and cathode. However in hydrogen-air fuel cells, the anode kinetic is assumed to have fast reaction kinetics compared to the cathode and thus the anode can generally be neglected. The cathode mass transfer process can be modeled as an infinite Warburg impedance element. The physical picture as a equivalent simple circuit model and corresponding Nyquist plot are shown in Figure 3-7.

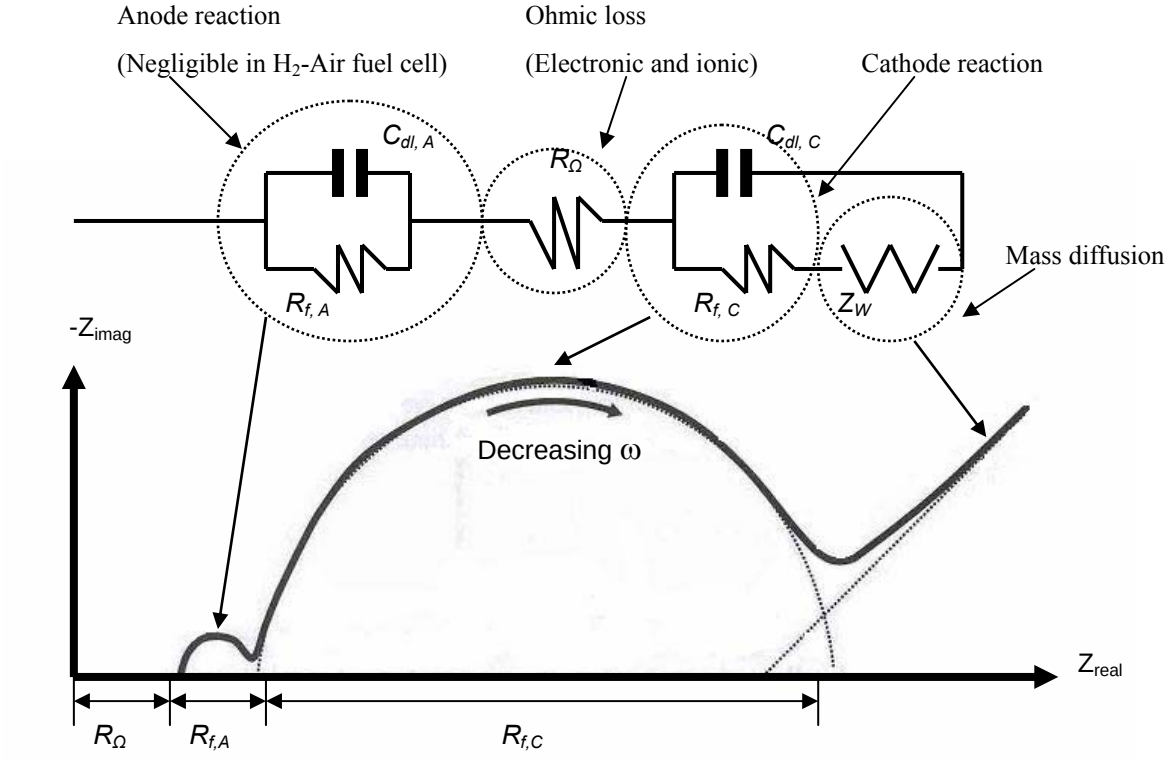

Figure 3-7. Physical picture of circuit diagram and Nyquist plot.

The Nyquist plot shows two semicircles and the real component of impedance always increases as frequency decreases. The first loop corresponds to the RC model of the anode activation kinetics ($R_{f,A}$) and the second loop corresponds to the RC model

of the cathode activation kinetics ($R_{f,C}$). The cathode loop is significantly larger than the anode loop because the cathode activation losses are significantly greater than the anode activation losses. The high-frequency, real axis intercept is indicative of to the ohmic resistance of fuel cell model. The diagonal line at low frequency is due to mass transport as modeled by the infinite Warburg impedance (Z_W). In many real fuel cells, the RC loop of the cathode dominates the RC loop of the anode. The high frequency resistance (R_Ω) was measured to determine the ohmic losses. At low current densities, the mass transfer losses are negligible. Thus, by subtracting ohmic losses from the total overpotential at low current density, it is possible to isolate the activation overpotential. The results can then be fit to the Tafel equation to describe the activation losses.

3.6.2 Cyclic Voltammetry

Cyclic voltammetry tests were conducted to determine the actual active electrochemical surface area of each MEA. The electrochemical surface area is a very important factor in an MEA's performance. All MEAs in this study had the same gross catalyst surface area, which is 0.0384 m^2/cm^2. However, the *active* area can be affected by differences in catalyst layer structure and composition of the MEAs. Cyclic voltammetry provides a method for quantifying the catalyst area that is active. Humidified hydrogen at 80 ^oC and 100 % RH was supplied to the anode (the counter electrode), while humidified nitrogen at 80 ^oC and 60 % RH was supplied to the cathode (the working electrode). The counter electrode also served as the reference electrode due to its negligible overpotential. In this experiment, the voltage was linearly cycled

from -0.1 V to 1 V and back to -0.1 V using a potentiostat (Solartron 1480 MultiStat). The current between the counter and working electrodes was recorded by the potentiostat. Three cycles of this voltage sweep were conducted, and the last cycle was recorded. Figure 3-8 shows the response current density as a function of the applied voltage.

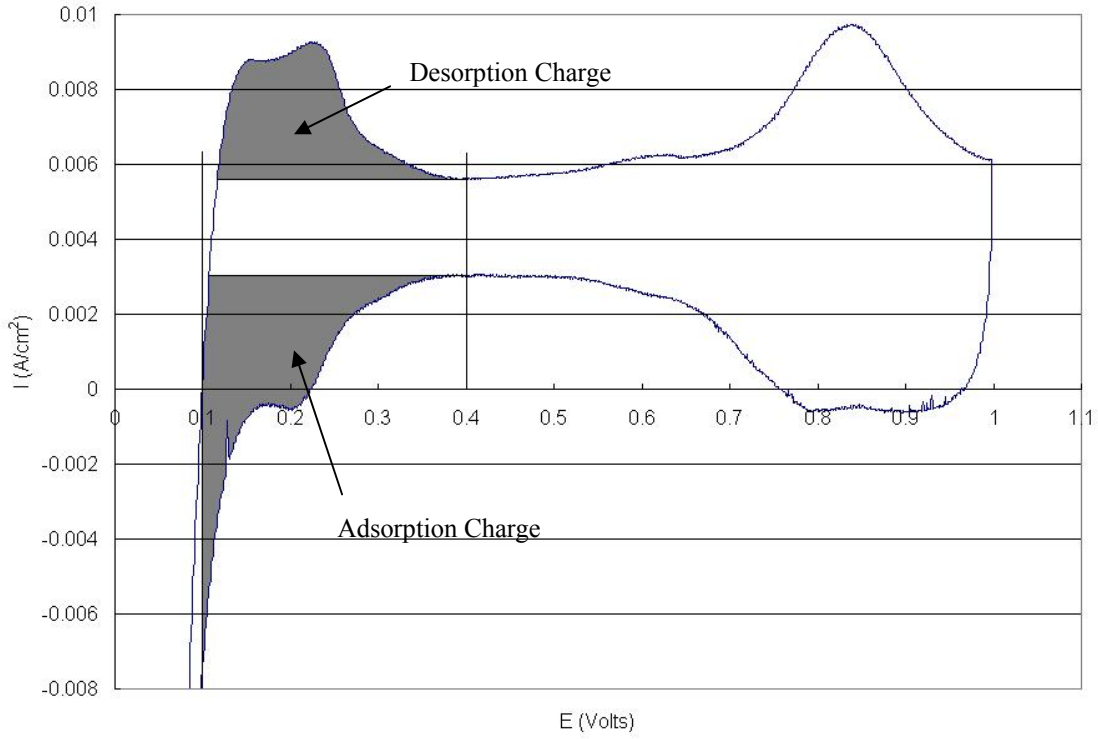

Figure 3-8. Cyclic voltammetry waveform.

The charge transferred to or from the electrode corresponds to the charge transfer associated with adsorption and desorption of a hydrogen monolayer on the active platinum surface. The charge transfer is obtained by integrating the current between 0.1 and 0.4 volt after subtracting the baseline current reading at 0.4 volt, as indicated by the shaded area in Figure 3-8. The average of the adsorption and desorption charges, $Q_{a/d}$, is taken as the charge transferred during the

adsorption/desorption of a hydrogen monolayer. Previous work has determined that the charge of an adsorbed monolayer of hydrogen on atomically smooth platinum, Q_m, is 210 μC/cm^2. Thus, the active surface area, A_{act}, can be calculated by

$$A_{act} = \frac{Q_{a/d}}{Q_m} \tag{3.3}$$

where $Q_{a/d}$ is the average of the adsorption/desorption charges (Russell [20]).

3.6.3 Scanning Electron Microscopy (SEM)

Scanning electron microscopy was used to obtain a cross-sectional view of the MEA. This technique provided information about the catalyst layer thickness.

The catalyst layer thickness was obtained by measuring at three randomly selected points along the catalyst layer cross-section. These measurements were averaged to obtain the thickness value used for calculations.

The porosity of the layer can be determined using the measured catalyst layer thickness with the area of the catalyst layer and the known values for density of platinum, Nafion and carbon.

The porosity as a percentage of the total volume is calculated by

$$Porosity = V_{actual} - \frac{\left(L_{Pt}/\rho_{Pt} + L_{Naf}/\rho_{Naf} + L_C/\rho_C\right)/1000 \times 5}{V_{actual}} \tag{3.4}$$
$$V_{actual} = Thickness \times 5cm^2$$

where variables are as previously defined and density values for the catalyst layer

materials are as specified in Table 3-3.

Table 3-3. Densities of catalyst layer components [26].

Material	Density (g/cm^3)
Platinum	$\rho_{Pt} = 21.45$
Nafion	$\rho_{Naf} = 1.97$
Carbon	$\rho_{C} = 1.8$

Samples were prepared for SEM examination using a freeze-cutting technique. With this technique, the sample and a razor blade were held in liquid nitrogen for 1 minute. The razor blade was then pushed vertically through the sample until the sample fractured. This fractured edge was used for investigation

3.7 Summary of Experimental Methods

The compositions of the MEAs in this research were designed on the basis of equal gross active platinum surface area. These MEAs were fabricated using the decal technique from Wilson and Gottesfeld [3]. A total of 11 MEAs were prepared at five different carbon loadings and five different Nafion percentages. Performance tests, electrochemical impedance spectroscopy tests, cyclic voltammetry, and microscopy were used to determine the performance, to characterize the effects of composition, and to relate the performance variation to physical characteristics, activation losses, ohmic losses, and mass transfer losses. Specifically, performance was evaluated from polarization curves for each MEA. Impedance tests were used to determine the ohmic losses. Cyclic voltammetry indicated the active catalyst area of each MEA.

Scanning electron microscopy was used to obtain a thickness and cross-sectional view of each MEAs. Results from these tests establish the effects of composition of the catalyst layer and lead to an improved understanding of catalyst layer characteristics.

4. Experimental Results

4.1 Overview

This chapter describes the results of tests to evaluate the effect of catalyst layer composition on fuel cell performance and to investigate the catalyst layer characteristics that have the most significant impact on performance. The effect of composition on performance was quantified in the form of polarization curves and a response surface with carbon loading and Nafion content as factors. To understand how composition affects performance, the effects of composition on the catalyst layer physical characteristics (thickness, porosity, and apparent film thickness), area specific resistance, activation losses, and mass transport losses were investigated. The effect of each of these characteristics on performance was then evaluated. The results help to demonstrate that carbon and Nafion loading have a significant effect on MEA performance and to suggest an improved catalyst layer composition.

4.2 Gasket Thickness Optimization

The compression of the gas diffusion layer can have a significant effect on cell performance. Insufficient compression leads to high contact resistance and excessive ohmic losses. Excessive compression can diminish the porosity of the diffusion media and lead to high diffusive losses. To properly evaluate MEA performance, the appropriate GDL compression that leads to best performance must first be determined. The gas diffusion layer compression is determined by the difference between the

uncompressed thickness and the compressed thickness. The gasket surrounding the GDL is assumed to be incompressible so that the uncompressed thickness is equal to the gasket thickness. Thus for a given GDL thickness, the gasket thickness determines the compression.

The fuel cell gaskets are made out of the fiberglass-reinforced Teflon. In addition to controlling the compressed GDL thickness, gaskets also prevent gas from leaking from the edges of the GDL rather than flowing through the gas channels in the graphite plates. According to previous work from Henderson [23] conducted using the same cell fixture and GDL, the optimum gasket choice was 0.21 mm for both sides. In this research, another investigation was done with available gasket sizes as 0.21, 0.14, 0.13, and 0.07 mm. Five major thickness combinations were tested while the cell operating conditions were maintained the same. The thickness combinations are shown in Table 4-1 and the performance test results are shown in Figure 4-1.

Table 4-1. **Gasket thickness combinations.**

Designation	Thickness combination	Total Thickness (mm)
1	0.21 (mm) + 0.21 (mm)	0.42
2	0.21 (mm) + 0.14 (mm)	0.35
3	0.21 (mm) + 0.13 (mm)	0.34
4	0.14 (mm) + 0.14 (mm)	0.28
5	0.14 (mm) + 0.07 (mm)	0.21

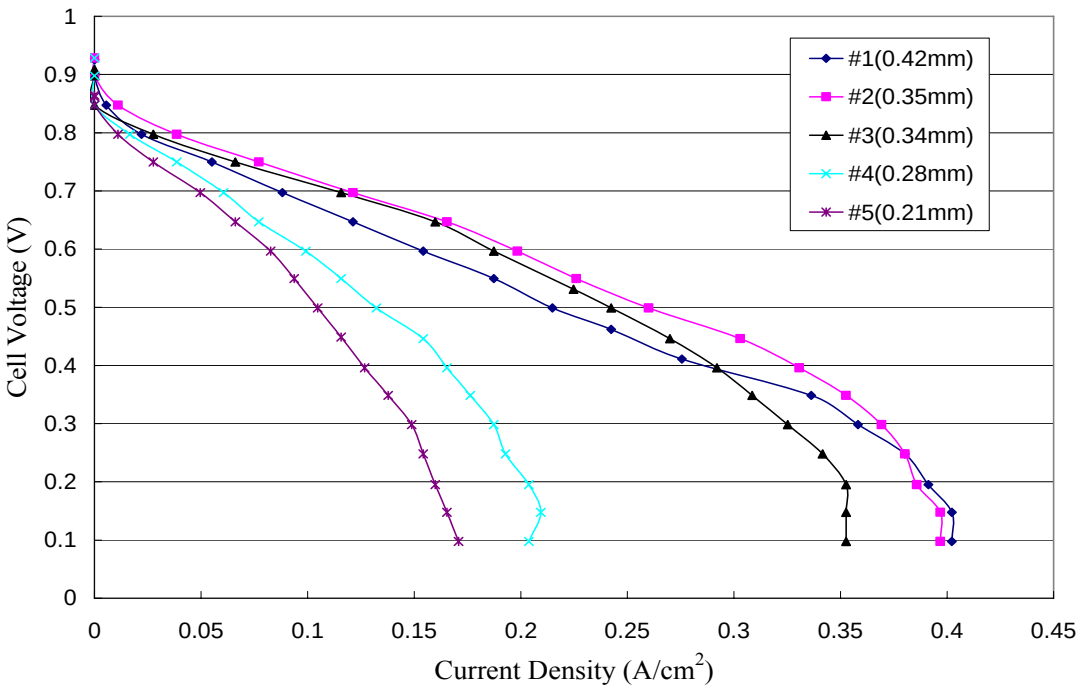

Figure 4-1. Effect of gasket size on cell performance.

After the polarization curves were investigated, the gasket thickness of 0.42 mm (two 0.21 mm) and 0.35 mm (0.21 mm + 0.14 mm) had very similar performance at low voltage. However, the gasket thickness of 0.35 mm performed better at middle voltage range which is the normal operating voltage range in a fuel cell. Thus, the gasket thickness used in this research was 0.35 mm. This gasket thickness was used all nine MEA samples.

4.3 Effect of Catalyst Layer Composition on Fuel Cell Performance

4.3.1 Basis for Evaluation

To insure a fair comparison, all catalyst layers were subjected to the same

conditions prior to testing and were tested at common conditions. After the MEAs were constructed, all of them were conditioned at least 24 hours or until a steady current density of 0.5 V was achieved. During the conditioning process, the cell conditions were maintained at the values presented in Table 4-2. These same conditions were maintained during the test procedure.

Table 4-2. Fuel cell operating conditions for MEA evaluation.

Cell temperature	80 ºC	
Reactant gas conditions	Anode	Cathode
Composition	Humidified hydrogen	Humidified air
Temperature	80 ºC	80 ºC
Pressure	200 kPa	200 kPa
Relative humidity	100 % RH	60 % RH
Mass flow rate	225 SCCM	550 SCCM
Stoichiometric ratio	6 at 1 A/cm^2	6 at 1 A/cm^2

4.3.2 Evaluation of Polarization Curves

Polarization curves for all MEA samples are shown in Figure 4-2. Complete polarization data for all samples are provided in Appendix A. For convenience, the composition of each catalyst layer is repeated in Table 4-3. As discussed in chapter 3, all catalyst layers have the same gross platinum surface area (~ 0.0384 m^2/cm^2).

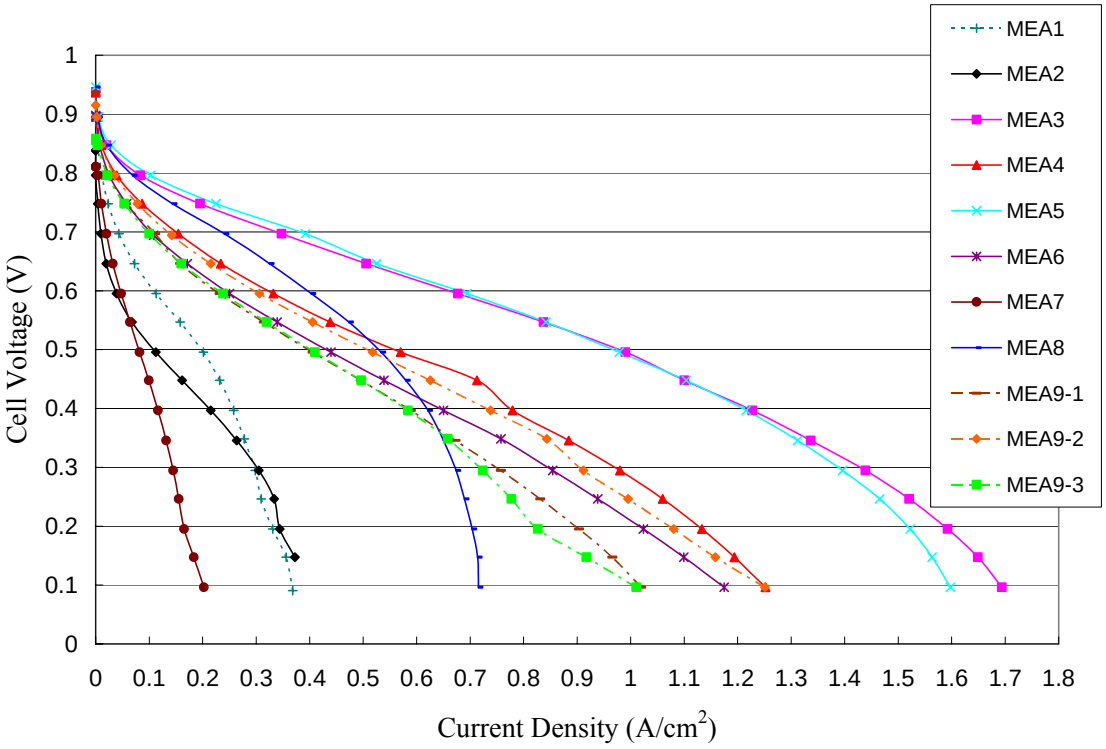

Figure 4-2. Effect of composition on cell performance.

Table 4-3. Summary of MEA composition.

		Carbon Loadings L_c (mg/cm^2)				
		0.56885	0.8406	1.4965	2.1524	2.4241
NFP (%)	33			**MEA 8**		
	30.7		**MEA 3**		**MEA 4**	
	25	**MEA 5**		**MEA 9***		**MEA 6**
	19.3		**MEA 1**		**MEA 2**	
	17			**MEA 7**		

*Replicated three times as MEA 9-1, 9-2, and 9-3.

The best performing MEAs were MEA 3 and MEA 5. These MEAs exhibited low activation losses as demonstrated by the low slopes of polarization curves at low current density. These MEAs also had very little mass transport resistance, since the curve slowly and linearly declines as current density increases. For these MEAs, limiting current density values exceeded 1.5 A/cm^2. The worst performing MEAs

were MEA 1 and MEA 2. These MEAs showed very poor performance with steep slope, in the activation region and limiting values for current density as low as 0.4 A/cm^2. The MEAs with low Nafion loadings (1, 2, and 7) were found to have the highest activation losses.

Overall, MEA 3 was the best MEA and contained 30.7 % Nafion and a carbon loading of 0.8406 mg/cm^2 with a catalyst mixture consisting of 40 % catalyst 1 and 10 % catalyst 2. This construction generated a maximum power density of 0.493 W/cm^2 and had a maximum current density of 1.59 A/cm^2 at 0.2V.

For this research, the repeatability of construction of the MEAs is very important factor because without repeatability, it is not possible to make a meaningful comparison of MEA performance. The repeatability reflects human error and test measurement error. In this research, three MEA samples were constructed with the same catalyst composition at the center point of the CCD model designated 9-1, 9-2, and 9-3. Comparison of the current density values at 0.5 V for these three MEA's indicates a repeatability of ± 8 %. This level of repeatability is sufficient for comparing MEA composition.

4.3.3 Effect of Carbon Loading and Nafion Content

Figures 4-3 shows the effect of composition on the performance of MEAs in this research. In this analysis performance is defined as current density at 0.5 V. MEAs constructed with medium-low carbon loadings performed best with 30.7 % Nafion in the catalyst layer. Performance for medium-low, medium, and medium-high

carbon loadings all increased with Nafion content, although at the higher Nafion loadings (33 %) the rate of increase diminished. This is consistent with the work of other researchers who found that medium carbon loading and 33 % Nafion loading were the best combinations in the catalyst layer.

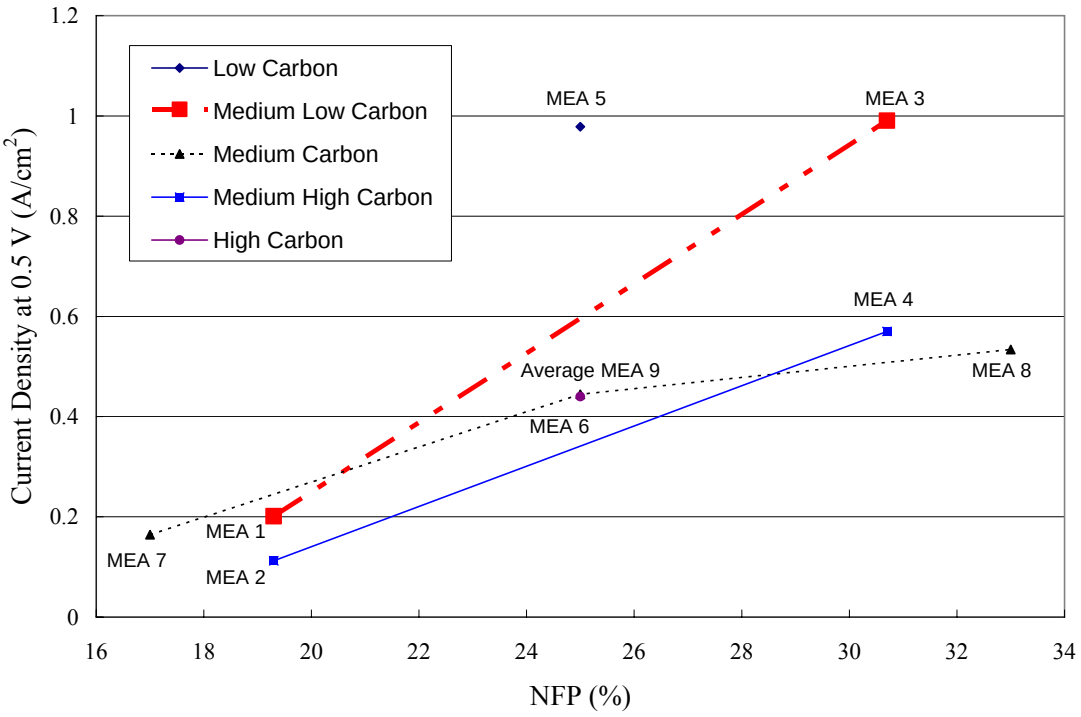

Figure 4-3. Effect of NFP on performance.

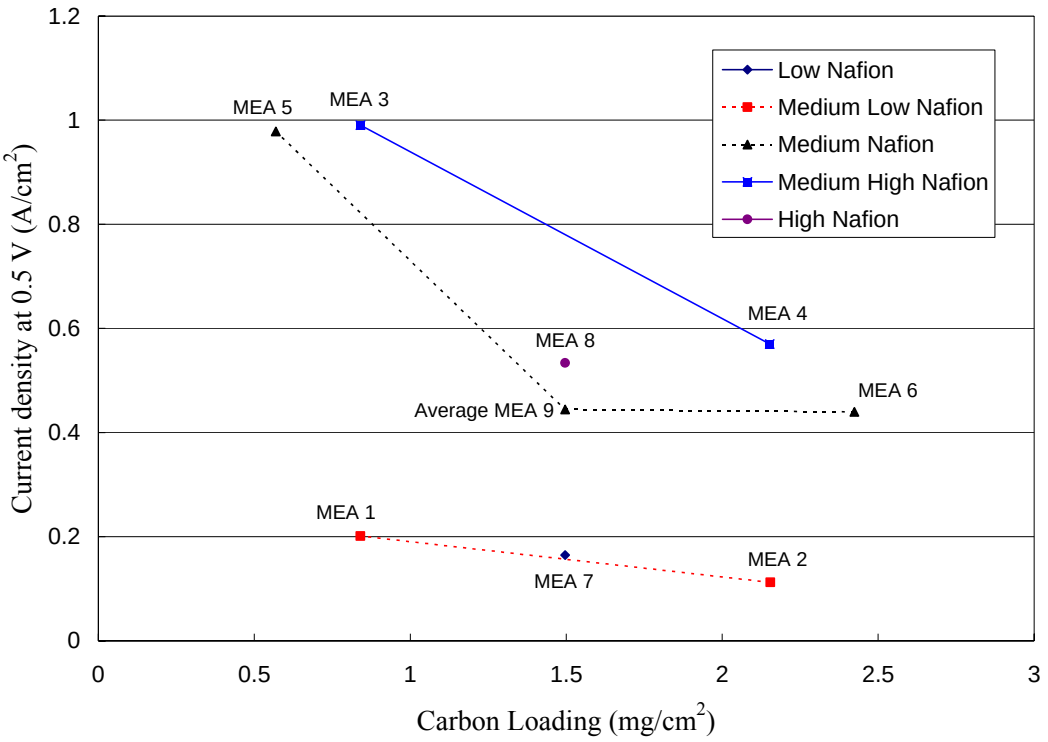

Figure 4-4. Effect of carbon loadings on performance.

The results from Figures 4-4 show the effect of carbon loading in the catalyst layer. Carbon provides support for the platinum particles and provides electrical conductivity. On the other hand, too much carbon can reduce the catalyst layer porosity and inhibit reactant transport. For all Nafion loadings considered here, performance decreases with increasing carbon. A maximum in performance is shown at the lowest tested carbon loading, containing about 0.57 mg/cm^2.

4.3.4 Response Surface with ANOVA

After completion of all performance tests, performance depended on two

factors: carbon and Nafion loading. The MINITAB* software was used to resolve the full fitted model equation. Equation 4.1 shows the fitted model from the analysis:

$$j = -1.6217 + 0.1706 \times N - 0.4997 \times C - 0.00196 \times N^2 + 0.2725 \times C^2 - 0.0223 \times N \times C \quad (4.1)$$

where j is the current density at 0.5 V, N is the Nafion content, and C is carbon loading.

The plot for this equation is shown in Figure 4-5. Complete analysis of variance and an ANOVA table for the results are provided in Table 4-4. Figure 4-5 shows that the current density is increased as the carbon loading is decreased.

Table 4-4. Analysis of variance for current density.

Source	Degree of freedom	Sum of square	Adjust sum of square	Adjust mean square	F	P
Regression	5	0.756652	0.756652	0.151330	8.51	0.017
Linear	2	0.593111	0.593111	0.296556	16.67	0.006
Square	2	0.136101	0.136101	0.068050	3.82	0.098
Interaction	1	0.027440	0.027440	0.027440	1.54	0.269
Residual Error	5	0.088959	0.088959	0.017792		
Lack-of-Fit	3	0.080926	0.080926	0.026975	6.72	0.132
Pure Error	2	0.008033	0.008033	0.004017		
Total	10	0.845611				
R^2 = 89.5 % R^2(adj) = 79.0 %						

* MINITAB version of 14 from Minitab Inc.

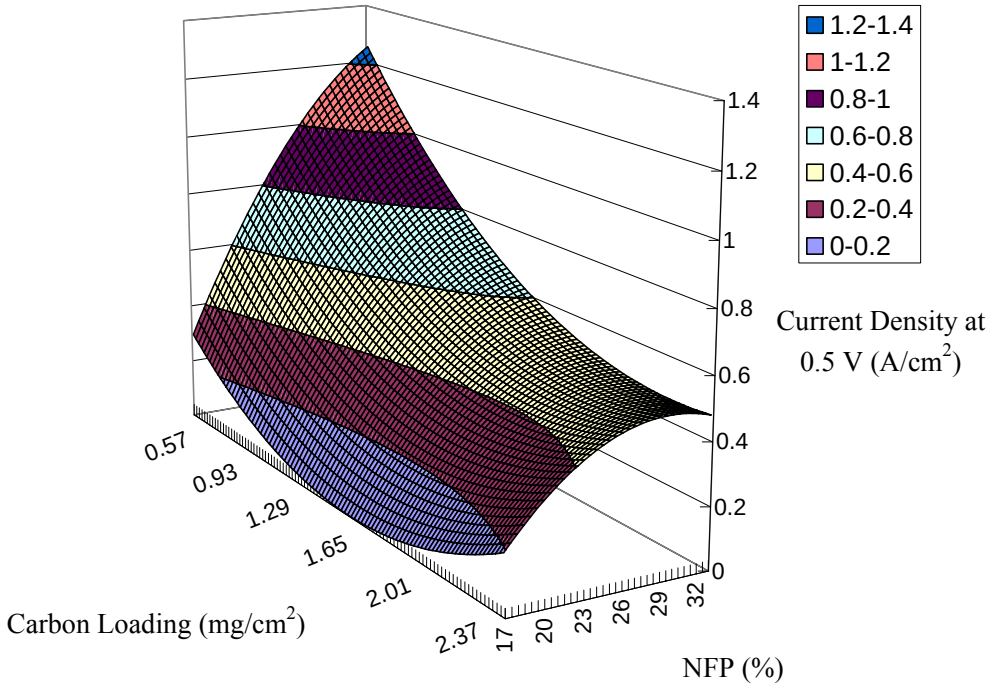

Figure 4-5. The performance plot for carbon and Nafion loading.

4.4 Effect of Composition on Catalyst Layer Characteristics

Based on the results of the previous section, it is clear that fuel cell performance is affected by catalyst layer composition. However, the mechanism by which composition affects performance is not clear. For example, changes in physical structure or conductivity could in turn cause the observed variations in performance. To explore these mechanisms, the effect of composition on physical characteristics, activation losses, area specific resistance, and mass transport losses was evaluated. Then, the effect of each of these factors on cell performance was assessed.

4.4.1 Physical Characteristics of Catalyst Layer

The carbon in the catalyst layer creates the porous structure, and Nafion fills in some of these pores. Thus, more carbon creates a larger-volume structure, leading to a thicker catalyst layer. Greater catalyst layer thickness is expected to reduce performance because of thicker catalyst layer creates longer pathways for mass transport and electronic and ionic conduction. In addition, gas must flow through the pores of the catalyst layer to the reaction sites, suggesting that porosity also affects fuel cell performance. At the micro-scale, increased agglomerate size creates longer paths for electron and proton conduction and species diffusion to and from the reaction sites. Larger agglomerates also reduce the active platinum area by concealing platinum surface area deep within the agglomerate. The various physical characteristics of the catalyst layer that affect these phenomena include thickness, porosity, and Nafion film thickness. Each of these characteristics is investigated in the following sections.

4.4.1.1 Thickness

Scanning electron microscopy was used to obtain a cross-sectional view of the MEA samples. Each cross section provided a view of two identically prepared catalyst layers. Thickness measurements were taken at three randomly selected points along the catalyst layer cross-section and averaged to determine the catalyst layer thickness. Figure 4-6 shows an SEM picture of MEA 2 at 3,000 times magnification and the location of the thickness measurements. A complete set of SEM pictures at different magnifications for each MEA is provided in Appendix B.

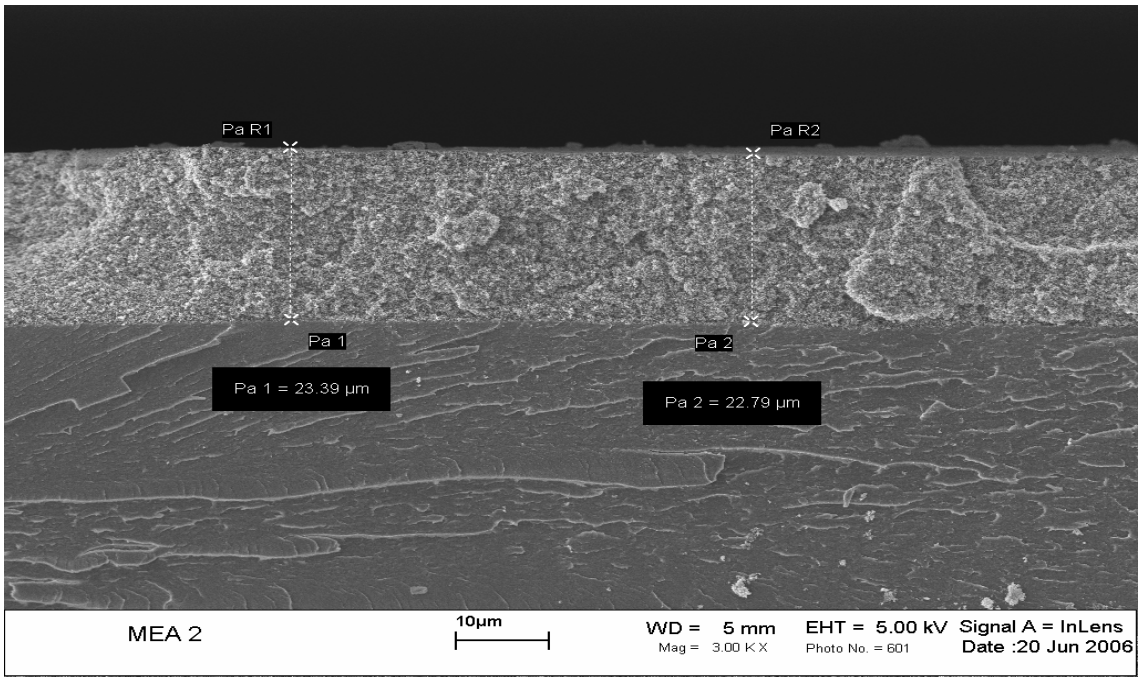

Figure 4-6. MEA 2 at 3,000x magnification.

The thicknesses of all three points were consistent for each MEA and the maximum variation in thickness for a particular catalyst layer was 20 percent. The cause of this relatively large variation is that all MEAs were compressed and operated in the cell fixture before the SEM pictures were taken. Table 4-5 shows the average thickness for the catalyst layers of each MEA. Table 4-5 also shows results for porosity which are discussed further in the following section. Figure 4-7 shows the effects of carbon loading on catalyst layer thickness.

Table 4-5. Thickness, pore volume and porosity of MEAs.

	Thickness (μm)	Actual Volume (cm^3)	Solid Volume (cm^3)	Pore Volume (cm^3)	Porosity (% Volume)
MEA1	8.026	0.004013	0.003154	0.000859	21.4
MEA 2	23.09	0.011545	0.007528	0.004017	34.8
MEA 3*	9.26	0.00463	0.003779	0.000851	18.4
MEA 4	18.35	0.009175	0.008791	0.000384	4.2
MEA 5	8.73	0.004365	0.002476	0.001889	43.3
MEA 6	20.32	0.01016	0.009078	0.001082	10.6
MEA 7	21.8	0.0109	0.005182	0.005718	52.5
MEA 8	16.98	0.00849	0.006514	0.001976	23.3
MEA 9-1	17.3	0.00865	0.005777	0.002873	33.2
MEA 9-2	12.35	0.006175	0.005777	0.000398	6.4
MEA 9-3	18.46	0.00923	0.005777	0.003453	37.4

* Catalyst layer thickness measured before installation in cell fixture.

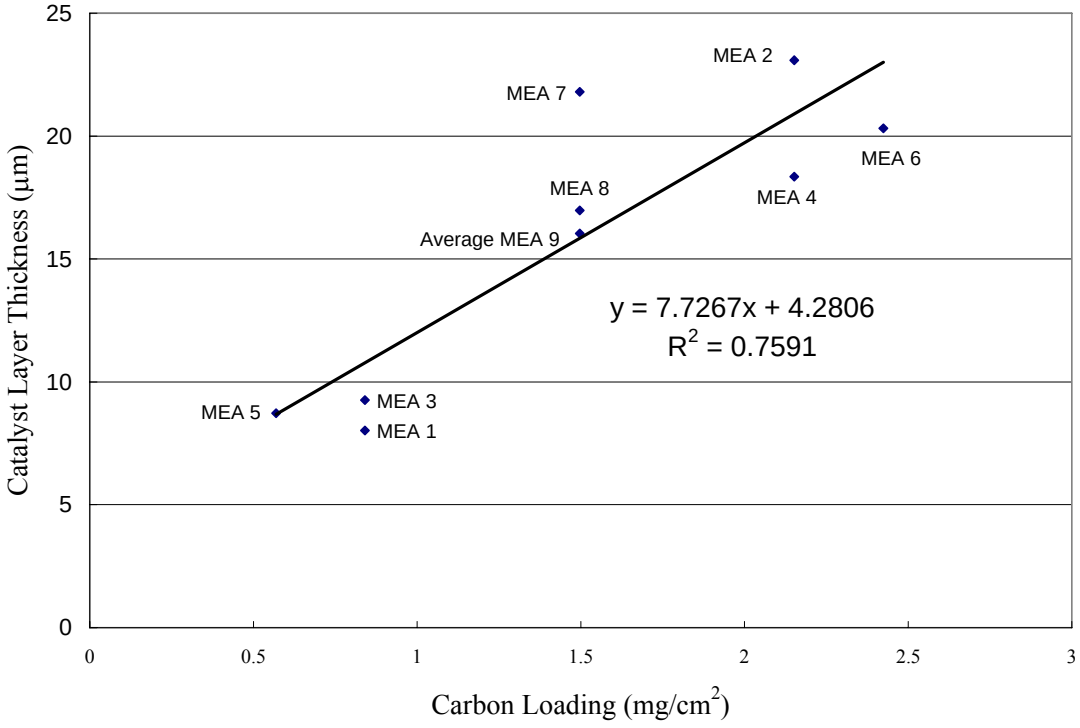

Figure 4-7. Effect of Carbon loading on catalyst layer thickness.

The catalyst layer thickness increased as the carbon loading increased and ranged from approximately 6 to 23 μm. Since the carbon creates the porous structure in the catalyst layer, more carbon creates a larger volume structure, leading to a thicker catalyst layer. In general, the catalyst layer thickness decreased as the Nafion loading increased. However, no strong relationship exists between the Nafion weight percentage and catalyst layer thickness in the range of NFP considered in this study.

The significance of the catalyst layer thickness was evaluated by plotting performance (expressed as current density at 0.5 V) against thickness. The results are shown in Figure 4-8. The results show that performance generally decreases with increasing catalyst layer thickness. However the correlation is relatively poor (R^2 = 0.35 for a linear fit).

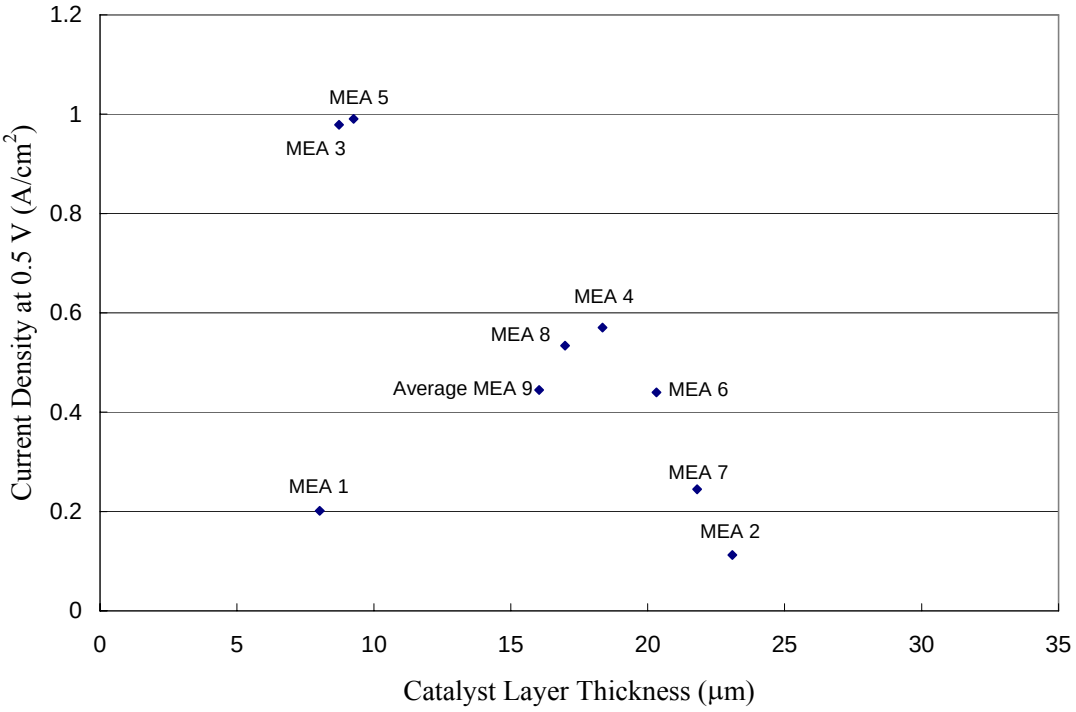

Figure 4-8. Effect of thickness on performance.

4.4.1.2 Porosity

Reactant must flow through the pores of the catalyst layer to the reaction sites, suggesting that porosity is an important factor affecting performance. The average thickness measurement values were used to calculate the porosity of each catalyst layer according to equation (3.4). Figure 4-9 shows the effect of composition on porosity.

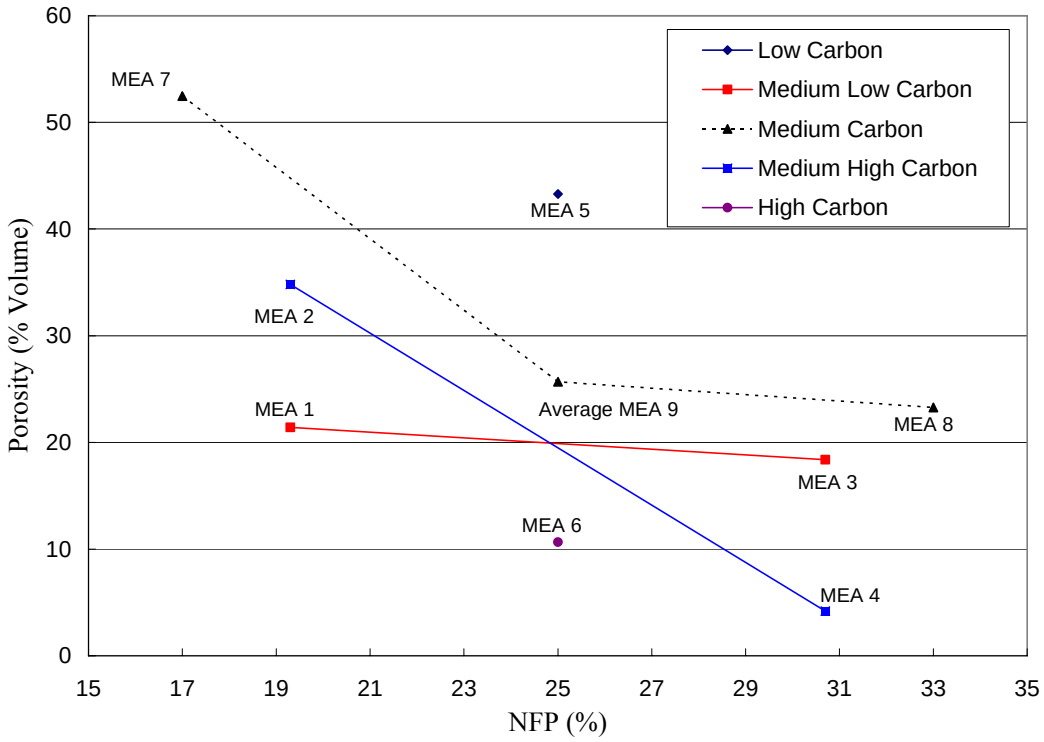

Figure 4-9. Effect of Nafion loading on porosity.

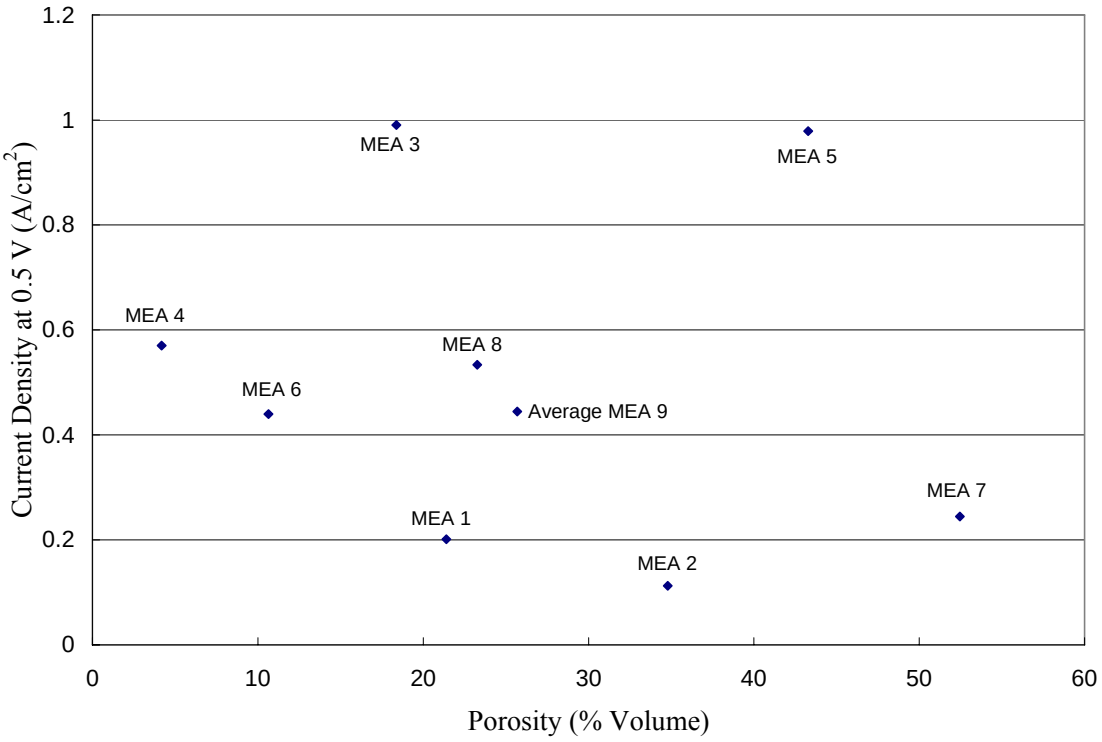

Figure 4-10. Effect of porosity on performance.

For the range of composition considered here, there was no clear relationship between carbon loading and porosity. For a given carbon loading, increased NFP led to decreased porosity suggesting that pores are being filled by Nafion. Figure 4-10 shows performance as function of porosity and shows that for the range of porosity considered here, there was no significant relationship between porosity and performance.

4.4.1.3 Apparent Film Thickness (Volume Ratio)

The catalyst layer can be modeled as a group of carbon particles with platinum catalyst deposited on the carbon particle surface and a film of Nafion surrounding the carbon particle. Figure 4-11 shows a diagram of this geometry. The Nafion film

must be thick enough to provide continuity of ion transport to adjacent particles and/or the membrane. On the other hand, reactants and products must diffuse through the Nafion film to the platinum reaction sites, so the film represents a diffusive resistance. Thus, the thickness of the film surrounding the catalyst particles could be expected to influence performance and to exhibit an optimum value.

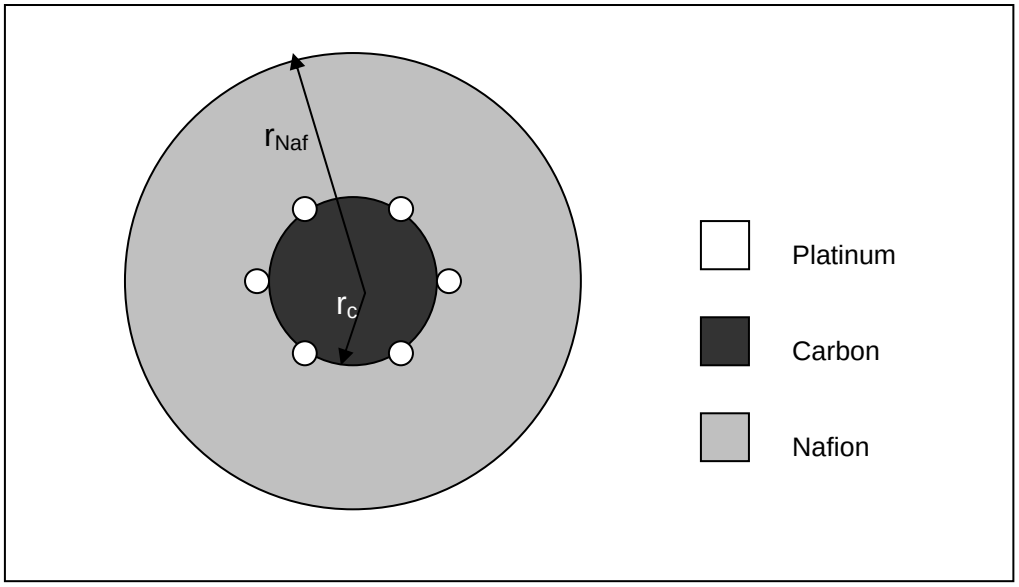

Figure 4-11. Assumed geometry for apparent Nafion film thickness.

If the catalyst particle is assumed to be a sphere and Nafion is assumed to cover the particle in a film of uniform thickness, then the volume of Nafion, V_{Naf}, is determined by equation (4.2),

$$V_{Naf} = \frac{4}{3}\pi\left(r_{Naf}^3 - r_{Car}^3\right) \tag{4.2}$$

where r_{Naf} and r_{Car} are the radius of Nafion and carbon. As suggested by Wilson and Gottesfeld [3], the volume ratio, R_V, of Nafion and carbon, is calculated by equation (4.3),

$$R_V = \frac{V_{Naf}}{V_C} = \frac{L_{Naf} \times \rho_C}{L_C \times \rho_{Naf}} \tag{4.3}$$

where L_{Naf} and L_C are loadings of Nafion and carbon, and ρ_C and ρ_{Naf} are the density of carbon and Nafion respectively. Assuming that all of the Nafion in the catalyst layer exists only as a film surrounding carbon particles, a dimensionless apparent film thickness, $t_{Naf,}$ can be determined by combining equations (4.2) and (4.3),

$$t_{Naf} = \frac{r_{Naf} - r_c}{r_c} = (R_V + 1)^{\frac{1}{3}} - 1 \tag{4.4}$$

Figure 4-12 shows the effect of the apparent Nafion film thickness on the performance (expressed as current density at 0.5 V). For the range of thickness considered in this work, the current density increases as the apparent Nafion film thickness increases. The second line in Figure 4-12 reflects the results from Russell [25]. In this previous work, the current density is decreased as the apparent Nafion film thickness decreases. In this work, the range of Nafion content relatively lower than previous and in the previous work, the range of Nafion content relatively higher than this work. Combining these works suggest that there is a optimum apparent Nafion film thickness exist within both works range.

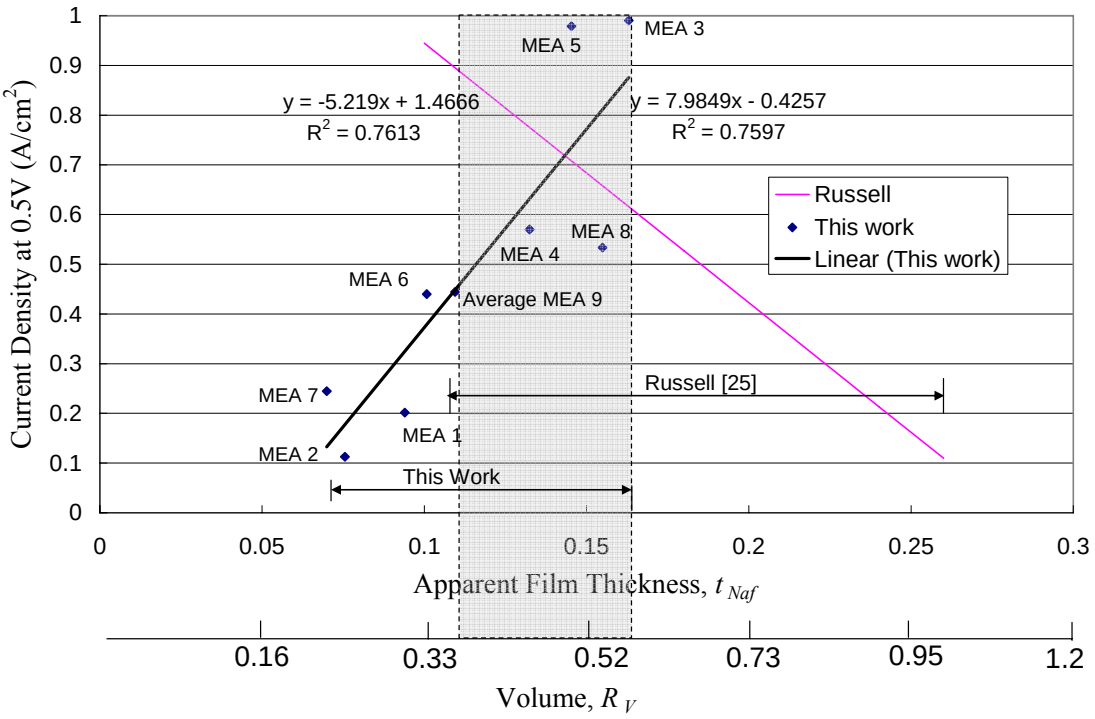

Figure 4-12. Effect of apparent film thickness on cell performance.

Figure 4-12 is also presented in terms of the volume ratio. Wilson and Gottesfeld [3] concluded that increasing the volume ratio of the electrode is beneficial up to a critical volume ratio. However, their work does not report a particular value for this ratio. For this research, volume ratios ranged from 0.2 to 0.6, and from Russell [25] work, volume ratios ranged from 0.35 to 1.05. Combining these works suggest that the optimal volume ratio range is between 0.38 and 0.57 corresponding to an apparent film thickness of 0.113 and 0.163. With a carbon particle size of 30 nm this implies a film thickness of 4.5 nm.

4.4.2 Area Specific Resistance of Catalyst Layer

After completion of the performance tests, the MEAs were subjected to electrochemical impedance spectroscopy tests to determine their ohmic resistance. The current density of the cell was maintained at 0.1 A/cm^2 at which mass transport limitations were not significant. As described in chapter 3, the high frequency resistance corresponds to the purely ohmic component of the cell resistance. The area specific resistance, *ASR*, in Ω·cm^2 was then determined from

$$ASR = R_{ohm} \times area \tag{4.5}$$

The *ASR* for each MEA is presented in Table 4-6 and ranges from 0.39 to 0.625 Ω cm^2

Table 4-6. Calculated resistances and ASR for each MEAs.

Samples	Membrane Electrode Assembly										
	1	2	3	4	5	6	7	8	9-1	9-2	9-3
Ohmic Resistance, R_{ohm} (Ω)	0.125	0.098	0.096	0.099	0.117	0.098	0.101	0.1	0.08	0.078	0.097
ASR (Ω·cm^2)	0.625	0.490	0.479	0.495	0.585	0.49	0.505	0.5	0.4	0.39	0.485

The results for ASR are presented in Figures 4-13 and 4-14 as functions of NFP and carbon loading, respectively. The results show that there is no significant correlation between ASR and either NFP or carbon loading for the ranges considered here. This result suggests that the minimum values of NFP and carbon considered here are sufficient to insure that the ionic and electrical losses in the catalyst layer are small

compared to losses in other cell components.

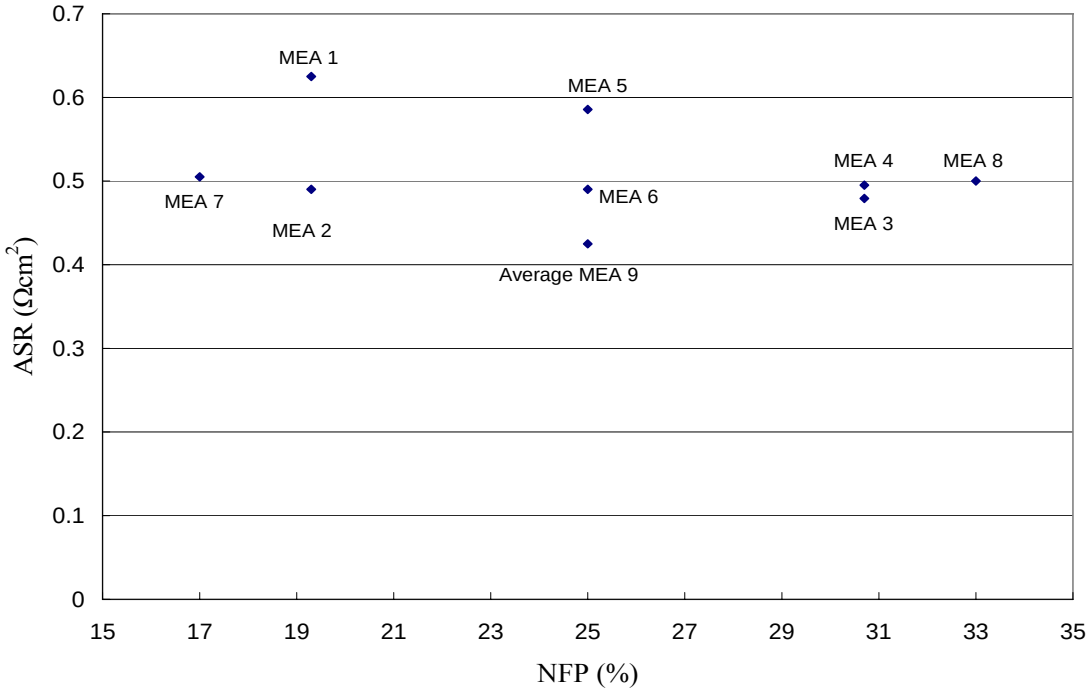

Figure 4-13. Effect of Nafion loadings on ASR at 0.1 A/cm^2.

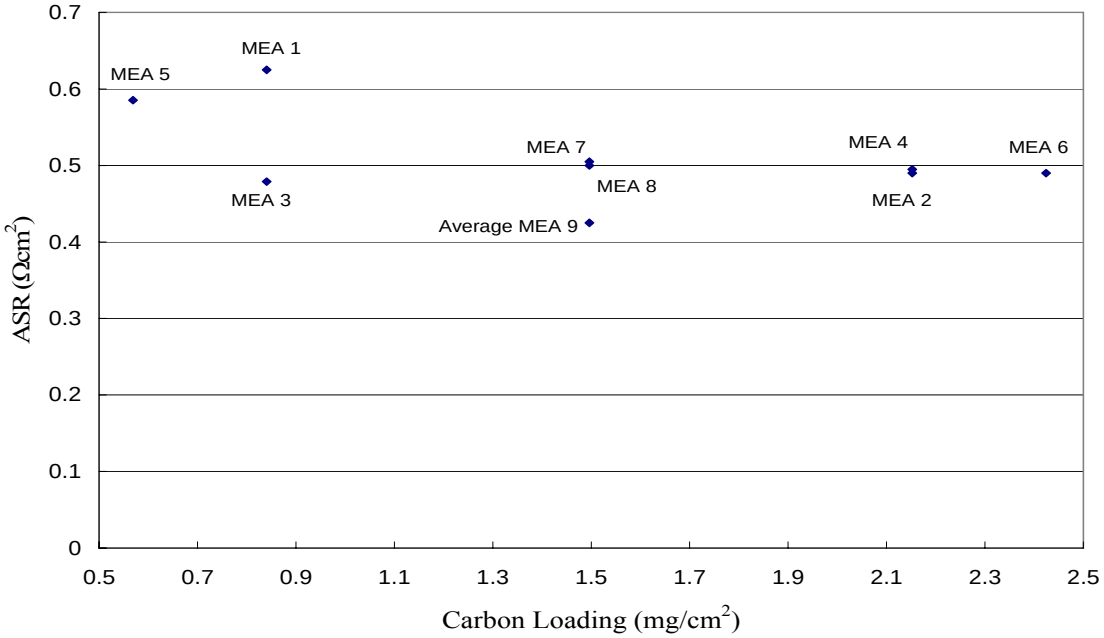

Figure 4-14. Effect of carbon loading on ASR at 0.1 A/cm^2.

4.4.3 Activation Losses Associated with Catalyst Layer

Activation losses were explored in two ways. First activation losses were fit to the Tafel equation to determine values for the Tafel slope and exchange current density for each MEA. In addition, cyclic voltammetry was used to determine the electrochemically active surface area for each MEA. Results were compared to NFP and carbon loading to determine whether there was a relationship.

The Tafel slope and exchange current density were determined at very low current densities where mass transport losses could be neglected. With mass transport neglected, the activation overpotential is given by

$$\eta_{act} = V_{OC} - V_{cell} - j \times ASR \tag{4.6}$$

The activation overpotential was then fit to the equation,

$$\eta_{act} = A \times \ln\left(\frac{j}{j_o}\right) \tag{4.7}$$

using liner regression to determine values for A and j_o. The analysis was conducted for a range of current density from 0.0022 to 0.1740 A/cm^2 and the results were generally very good with values for R^2 ranging from 0.93 to 0.99. The results for each MEA along with the R^2 for the fit are presented in Table 4-7.

Table 4-7. Calculated Tafel parameters each MEAs.

Samples	MEA 1	MEA 2	MEA 3	MEA 4	MEA 5	MEA 6	MEA 7	MEA 8	Average MEA 9
Tafel Slope, *A*	0.058	0.063	0.018	0.030	0.016	0.040	0.055	0.017	0.039
Exchange Current Density, j_0 (mA/cm^2)	1.18	0.825	0.283	0.759	0.197	1.98	2.01	0.196	2.15
Coefficient of Determination, R^2	0.97	0.99	0.96	0.99	0.93	0.97	0.98	0.97	0.96

The results for Tafel slope and exchange current density are presented in Figures 4-15 and 4-16 as functions of composition. The results show that there is significant correlation between the NFP and Tafel slope for the ranges considered here. The Tafel slope decreases as the NFP increases. However, no such relationship existed between the carbon loading and the Tafel slope. Also, the results show that there is no significant correlation between the exchange current density and either the NFP or carbon loading for the ranges considered here.

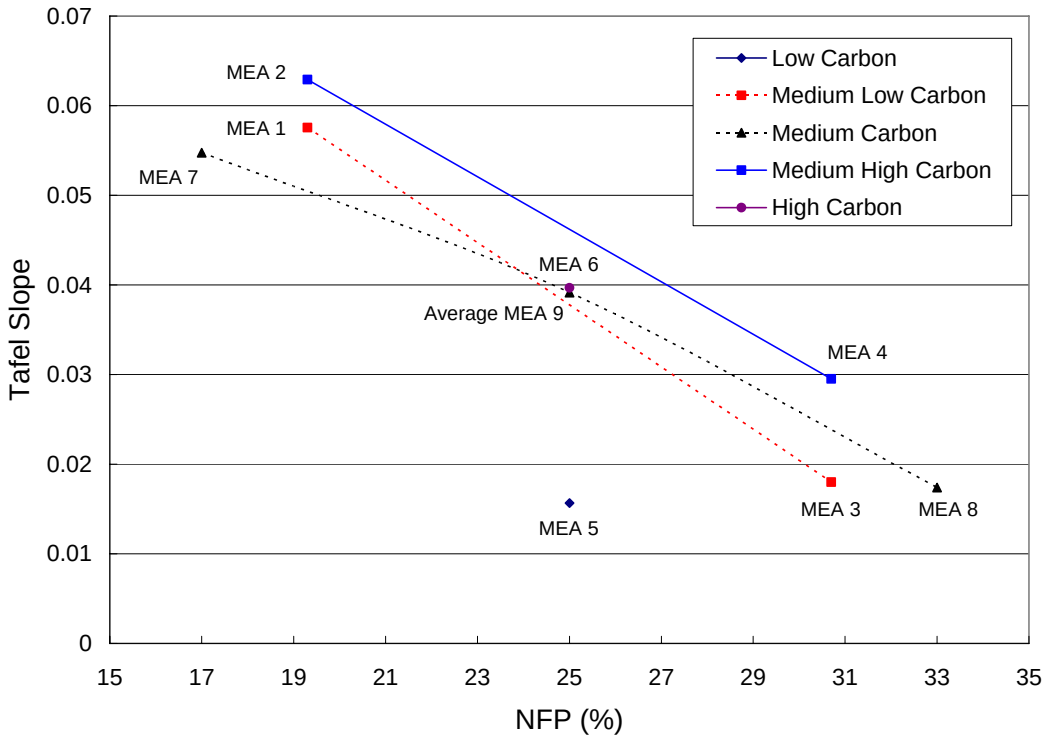

Figure 4-15. Effect of composition on the Tafel slope.

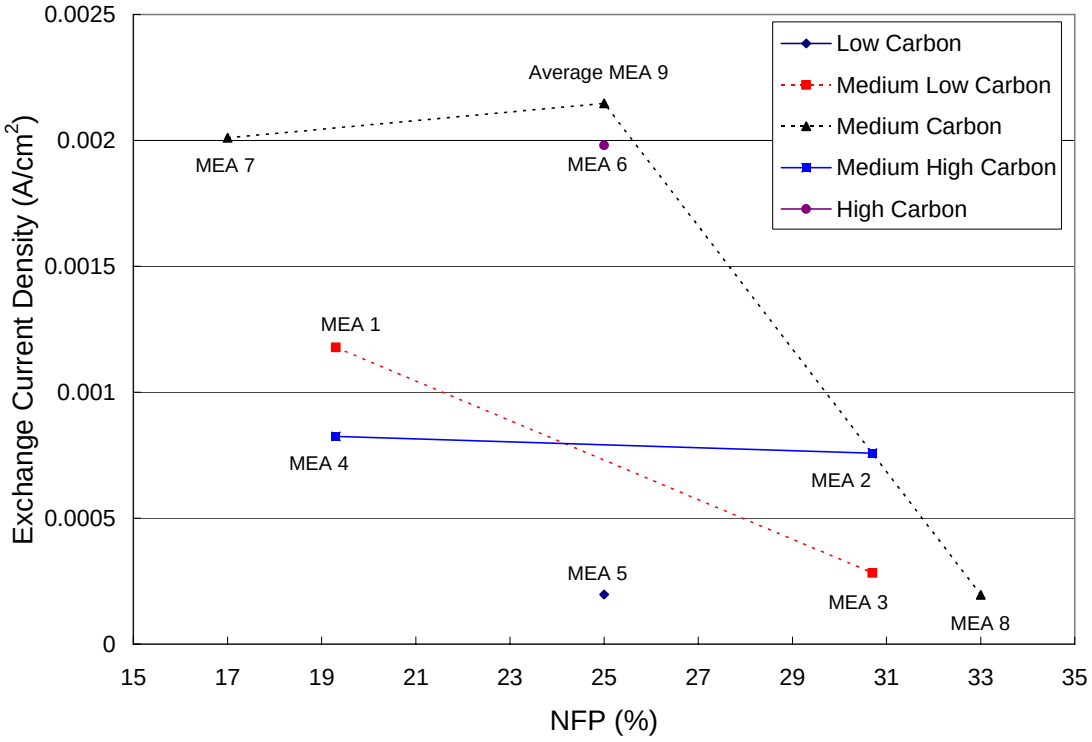

Figure 4-16. Effect of composition on the exchange current density.

In addition to Tafel plots, cyclic voltammetry tests were conducted for each MEA. The areas under the adsorption and desorption peaks of each waveform were calculated to determine the active platinum area of each MEA using Equation (3.3). Table 4-8 shows the adsorption and desorption charges of each MEA and the active platinum area. In most cases, the difference between the adsorption and desorption charges was significant suggesting a relatively large uncertainty in the charge measurement. The average of the adsorption and desorption charges was used for the active area calculations.

Table 4-8. Calculated platinum areas based on hydrogen adsorption and desorption charges.

Sample	Adsorption Charge (Coul/cm^2)	Desorption Charge (Coul/cm^2)	Average Charge (Coul/cm^2)	Active Platinum Area (m^{2}Pt/cm^2)	Active Percentage of Gross Platinum Area
MEA 1	0.008437	0.004016	0.006227	0.002965	7.72
MEA 2	0.001812	0.000169	0.00099	0.000472	1.23
MEA 3	0.01044	0.004774	0.007607	0.003622	9.43
MEA 4	0.007973	0.006375	0.007174	0.003416	8.90
MEA 5	0.013445	0.009461	0.011453	0.005454	14.20
MEA 6	0.009471	0.005143	0.007307	0.003479	9.06
MEA 7	0.01200	0.004429	0.008214	0.003912	10.19
MEA 8	0.008211	0.004757	0.006484	0.003088	8.04
MEA 9-1	0.00525	0.004641	0.004946	0.002355	6.13
MEA 9-2	0.00888	0.005246	0.007067	0.003365	8.76
MEA 9-3	0.013585	0.001843	0.007714	0.003673	9.57

Overall, the results from this section show that the most direct effect of composition on performance is through the Tafel slope. The Tafel slope reflects the innate reaction kinetics and the work required to get species from the vicinity of the reaction site to and from the reaction site. Increasing Nafion appears to provide a

better path for ion transport to the reaction site.

Figure 4-17 shows the effect of carbon and Nafion loading on active platinum surface area. The results from Figure 4-17 shows that there is no relationship between the active platinum surface area and the Nafion or carbon loadings for the ranges considered here. Figure 4-18 shows that performance generally increases with increasing active platinum surface area. However the correlation is relatively poor (R^2 = 0.47 for a liner fit). Since the exchange current density is directly related to the active surface area, this result is consisted with the prior result indicating no correlation of composition with exchange current density. This result suggests that even at the minimum values of NFP and carbon loading, there is sufficient Nafion and carbon to provide the minimal connectivity required to activate accessible platinum surface area for the cyclic voltammetry test. The reason for the generally low values of active surface area relative to the gross area is likely due to obstruction of platinum surface by the carbon support or by adjacent platinum particles.

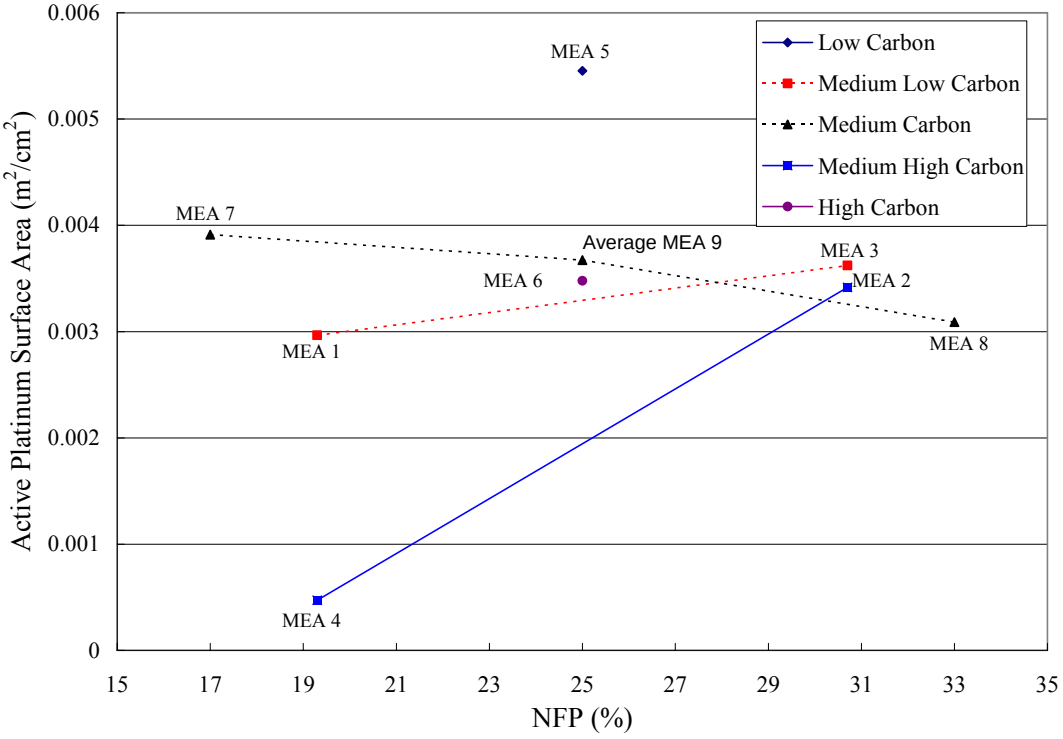

Figure 4-17. Effect of composition on active platinum surface area.

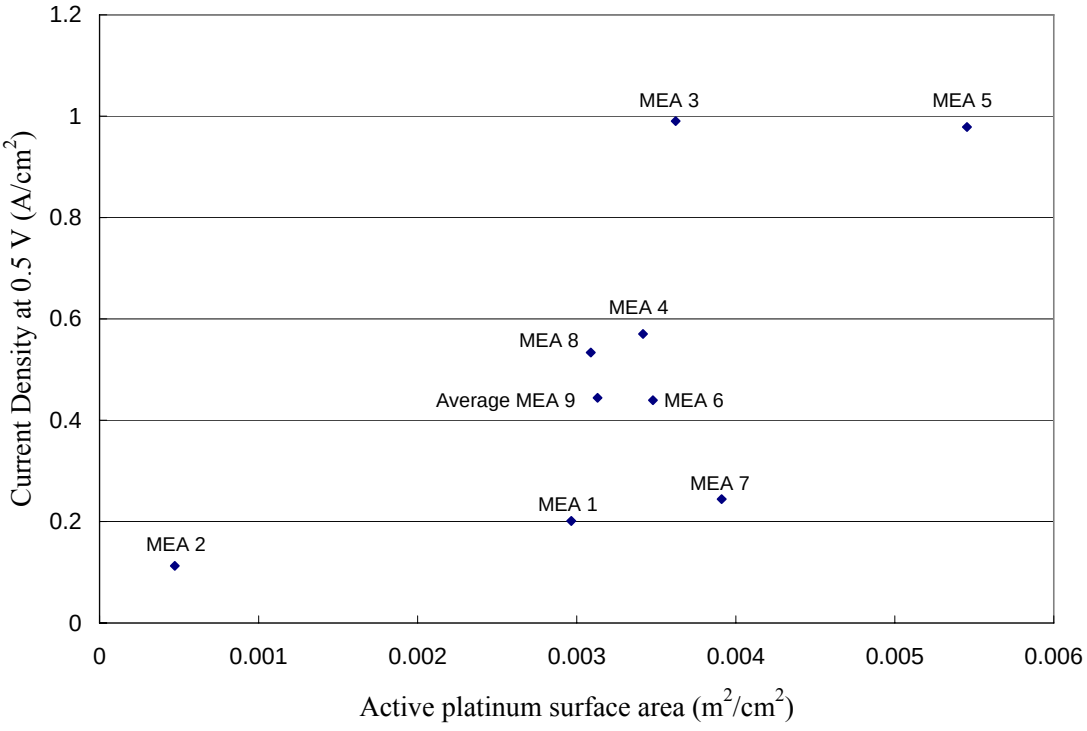

Figure 4-18. Effect of active platinum surface area on performance.

4.4.4 Mass Transport Losses Associated with Catalyst Layer

Mass transport losses were explored by comparing theoretical values with experimental values. First voltage was calculated with the Tafel slope, A, and the exchange current density, j_0, from Section 4.4.3 using the following equation,

$$V = V_{OC} - A \times \ln\left(\frac{j}{j_0}\right) - j \times ASR \tag{4.8}$$

Then, the voltage were plotted with the corresponding current density and compared with the experimental plot.

The results show that there is a significant correlation between the NFP and mass transport losses for the ranges considered here. MEA 8 with the highest NFP shows mass transfer losses at a relatively low current density of 0.7 A/cm^2. For MEAs with medium to medium-high NFP, most showed no evidence of mass transfer limitations (MEA 4, 6, 9-1, 9-2, and 9-3). Those with NFP that did exhibit mass transfer limitation (MEA 3, 5) did so only at very high current density. The performance of MEA 1, 2, and 7 with low NFP is dominated by high Tafel slopes. These Tafel slopes reflect the difficulty in ionic transfer at the microscopic scale. The results show that adding Nafion is beneficial in reducing the Tafel slope, but the benefits of more Nafion in reducing the Tafel slope are outweighed by mass transfer losses at higher Nafion content (greater than ~33%)..

4.5 Summary of Effects of Catalyst Layer Characteristics

Both the percentage of Nafion and the carbon loading in the catalyst layer were shown to be important parameters. The carbon loading was shown to be significant even when the gross platinum surface area was held constant. MEA 3 constructed with a medium high Nafion percentage of 30.7 % and a low carbon loading of 0.569 mg/cm^2 showed the best performance.

The catalyst layer thickness increased as the carbon loading increased and ranged from approximately 6 to 23 μm. In general, the catalyst layer thickness decreased as the Nafion loading increased. However, no strong relationship exists between the Nafion weight percentage and catalyst layer thickness in the range of NFP considered in this study.

For the range of composition considered here, there was no clear relationship between carbon loading and porosity. For a given carbon loading, porosity decreased as NFP increased. However, there was no relationship between porosity and performance. In this work, the current density increased as the apparent Nafion film thickness increased. Combining this work and the work of Russell [25] suggests that the best performance occurs when the Nafion to carbon volume ratio is between 0.38 and 0.57 corresponding to an apparent film thickness of 0.113 to 0.163.

Other characteristics of the catalyst layer including area specific resistance and active catalyst area had no effect on performance for the range tested here.

Furthermore, the area specific resistance and active catalyst area of the cell did not correlate with catalyst layer composition for the range tested here. This result suggests that the minimum values of NFP and carbon considered here are sufficient to insure that the ionic and electrical losses in the catalyst layer are small compared to losses in other cell components.

The results for the Tafel slope, exchange current density, and limiting current density show that there is significant correlation between the NFP and activation losses and mass transport losses for the ranges considered in this research. At a low NFP, high Tafel slopes are dominant; at a medium range of NFP, Tafel slopes and there is evidence of mass transport limitations only at very high current density. At high NFP, mass transport losses are apparent. However no relationship exists between the carbon loading and activation or mass transport losses. A summary of the characteristics of the catalyst layer and how these relate to composition and cell performance in this work is given in Table 4-9.

Table 4-9. Summary of the findings for this work.

Characteristic	Measurement technique	Relation to composition	Relation to cell performance
Catalyst layer thickness	SEM	Linear increase with increasing carbon loading; ref. Fig. 4-8. NC with Nafion.	NC; ref. Fig. 4-9
Catalyst layer porosity	Analysis based on layer thickness and calculated solid volume	Decreases with increasing Nafion; ref. Fig. 4-10. NC for carbon loading.	NC; ref. Fig. 4-11
Apparent film thickness (t_{Naf})	Analysis based on composition	Direct; ref. Eq. 4.3 and Eq. 4.4	Increases linearly with film thickness for tested range; ref. Fig. 4-14.
Volume ratio (R_v)	Analysis based on composition	Direct; ref. Eq. 4.3	Increases linearly with $R_v^{1/3}$; ref. Fig. 4-14.
Area specific resistance	EIS	NC; Ref. Fig. 4-15 and Fig. 4-16	$\eta_{ohm} = j \times ASR$
Tafel slope	Tafel curve fit to IR-corrected low current density results	Tafel slope decreases linearly with Nafion loading; ref. Fig. 4-17.	$\eta_{act} = A \ln\left(\frac{j}{j_0}\right)$
Exchange current density	Tafel curve fit to IR-corrected low current density results	NC for exchange current density.	$\eta_{act} = A \ln\left(\frac{j}{j_0}\right)$
Electrochemically active surface area	Cyclic voltammetry	NC; ref Fig. 4-17	NC ref Fig. 4-18
Mass transfer losses	Analysis based on comparison of polarization curves and Eq. 4.8.	Increases with increasing Nafion. NC for carbon loading.	No effect at low current density, significant effect at higher current density,

Notes:

1. Shaded rows indicated a characteristic that is affected by composition and that also affects performance.
2. NC = no correlation within the tested range.

5 Conclusions

This research investigated the effect of catalyst layer composition on the performance and characteristics of a PEM fuel cell. In this experiment, the gross catalyst surface area, 0.0384 m^2/cm^2, was held constant while the carbon and Nafion content of the catalyst layer were varied using a central composite design. The purpose of this experiment was to determine the optimum composition of catalyst layer and set up a full model equation. In addition to diagnostics, experiments were undertaken to determine the catalyst characteristics that had the most significant effect on performance.

5.1 Conclusions Regarding the Effect of Composition on Catalyst Layer Characteristics and Performance

The optimum composition of catalyst layer was 0.841 mg/cm^2 of carbon and 30.7 % of Nafion. The full model equation is as follows:

$$j = -1.6217 + 0.1706 \times N - 0.4997 \times C - 0.00196 \times N^2 + 0.2725 \times C^2 - 0.0223 \times N \times C \quad (5.1)$$

where j is the current density at 0.5 V, N is the Nafion content, and C is carbon loading.

In this equation, the square and interaction terms are not significant since the P values are greater than 0.05 however including these terms lead to higher adjust R2 value. Therefore, the square and interaction terms were incleased in order to explane whole respons.

The performance of a PEMFC catalyst layer was shown to be affected by both the carbon loading and the percentage of Nafion in the catalyst layer. The carbon loading was significant even when the gross platinum surface area was held constant. Lower carbon loadings with around 30 % of Nafion enhanced performance. Table 5-1 compares the results of this work to that of previous studies of catalyst layer composition.

Table 5-1. Comparison of the results of this work to that of previous work.

Authors	Platinum Type & Loading	Carbon Loading	NFP	Operating Pressure anode/cathode (atm)	Operating Temperature (^{o}C)
This Research	10 & 40% Pt/C 0.3676 mg/cm^2	0.8406 mg/cm^2	30.7 %	2	80
Russell [25], 2003	20% Pt /C, 0.322 mg/cm^2	1.30 mg/cm^2	33 %	2	80
Wilson and Gottesfeld [15], 1992	20% Pt/C 0.17 mg/cm^2	0.68 mg/cm^2	25-28 %	3/5	N/A
Uchida et al. [21], 1995	25% Pt/C 0.5 mg/cm^2	1.5 mg/cm^2	33 %	N/A	N/A
Paganin et al. [2], 1996	20% Pt/C 0.4 mg/cm^2	1.6 mg/cm^2	33 %	N/A	80
Antolini et al. [17], 1999	20% Pt/C 0.2 mg/cm^2	0.8 mg/cm^2	40 %	N/A	N/A
Passalacqua et al. [16], 2001	20% Pt/C 0.1 mg/cm^2	0.4 mg/cm^2	33 %	N/A	70
Ticianelli et al. [4], 1988	20% Pt/C 0.35 mg/cm^2	1.4 mg/cm^2	33 %	3/5	80

In addition to identifying catalyst layer compositions that achieved the highest performance, this work demonstrated that the most significant catalyst layer property is the apparent film thickness or the related property of Nafion to carbon volume ratio. Combining the work of Russell [25] and the current work suggests that the optimal range of apparent Nafion film thickness is 0.113 to 0.163 corresponding to a Nafion to carbon volume ratio range of 0.38 to 0.57.

Characteristics of the catalyst layer including activation losses and mass transport losses were significantly affected by Nafion content. The activation losses decreased as the NFP increased. However mass transfer losses increased as the NFP increased

Catalyst layer thickness was shown to increase with increasing carbon content but no relation was found between thickness and Nafion loading. Also, the performance was found to decrease as catalyst layer thickness increased.

Characteristics of the catalyst layer including porosity, area specific resistance, and active catalyst area were found to be either unaffected by the catalyst layer composition or insignificant factors in determining performance for the range of compositions considered here.

5.2 Future Research Recommendation.

This research has identified a range of carbon loading and Nafion percentages

for future research related to the optimization of fuel cell catalyst layers. By continuing to investigate construction methods of the catalyst layer, MEAs can be made to perform better at lower cost. The decal painting and hot-pressing method used to construct the catalyst layers can be improved further. For example, when the decals are made, the release of too much Teflon spray causes very poor performance. The Teflon left on the MEA surface blocks the diffusion of hydrogen and air through the catalyst layers. Teflon of 0.6 mg was enough to separate the MEA and decal and did not affect the overall performance. Another recommendation is to check the Nafion content in the solution. The manufacturer makes large amounts of solution and sells the solution in small bottles. The solution can be made more concentrated than specified by vaporization of the solvent.

Results from this research suggest that for the range of compositions considered here, the most important consideration seems to be the quality of the ionic pathways to the reaction sites. This was demonstrated by the significance of the Nafion film thickness and the effect of Nafion on the Tafel slope. Other approaches such as control of the microstructure may allow improvement of ionic pathways and yield reduced Nafion or better performance. The relative insensitivity of performance to active surface area within this research range suggests that the catalyst surface area could be decreased, thus leading to lower platinum cost without a major effect on performance.

One suggestion of manufacturing process is that a dry spraying method could be more easily and more accurately to construct the catalyst layer for a large production.

Manufactures could use a large Kapton film for a transporting decal and use a dry spraying method to apply the catalyst layer, and cut into a desired area for a single cell. The Kapton film is more hydrophilic than Teflon so that no releasing spry which could cause blacking the reactant goes through catalyst layer was needed. Also dry spraying method do not requires any liquid so that no baking time for vaporize liquid. These methods lead to reduce construction time and also reduce cost of manufacturing.

The performance of the best catalyst layers in this work is comparable to or better than results for other catalyst layers reported in the open literature. However, the results are still considerably less than the DOE targets for economical performance indicating that there is much work yet to be done.

References

[1] Srinivasan, S., Ticianelli, E.A., Derouin, C.R., and Redondo, A., 1988, "Advances in solid polymer electrolyte fuel cell technology with low platinum loading electrodes", Journal of Power Sources, **22**, pp. 359-375

[2-1] Paganin, V.A., Ticianelli, E.A., and Gonzalez, E.R., 1996, "Development and electrochemical studies of gas diffusion electrodes for polymer electrolyte fuel cells", Journal of Applied Electrochemistry, **26**, pp. 297-304.

[2] Wilson, M.S. and Gottesfeld, S., 1992, "Thin-film catalyst layers for polymer electrolyte fuel cell electrodes", Journal of Applied Electrochemistry, **22**, pp. 1-7.

[4] Ticianelli, E.A., Derouin, C.R., Redondo, A., and Srinivasan, S., 1988, "Methods to Advance Technology of Proton Exchange Membrane Fuel Cells", Journal of the Electrochemical Society, **135(9),** pp. 2209-2214.

[5] Watanabe, M., Igarashi, H., and Yosioka, K., 1995, "An Experimental Prediction of the Preparation Condition of Nafion-Coated Catalyst Layers for PEFCs", Electrochimica Acta, **40(3)**, pp. 329-334.

[6] Schulze, M., Schneider, A., and Gulzow, A., 2004, "Alteration of the distribution of the platinum catalyst in membrane-electrode assemblies during PEFC operation", Journal of Power Sources, **127**, pp. 213-221.

[7] Gasteiger, H.A., Panels, J.E., and Yan, S.G., 2004, "Dependence of PEM fuel cell performance on catalyst loading", Journal of Power Sources, **127**, pp. 162-171.

[8] Bender, G., Zawodzinski, Thomas A., and Saab, Andrew P., 2003, "Fabrication of high precision PEFC membrane electrode assemblies", Journal of Power Sources, **124**, pp. 114-117.

[9] Xie, J., Garzon, F., Zawodzinski, T., and Smith, W., 2004, "Ionomer Segregation in Composite MEAs and Its Effect on Polymer Electrolyte Fuel Cell Performance", Journal of the Electrochemical Society, **151,** pp. A1084-A1093

[10] Poltarzewski, Z., Staiti, P., Alderucci, V., Wieczorek, W., and Giordano, N., 1992, "Nafion Distribution in Gas Diffusion Electrodes for Solid-Polymer-Electrolyte-Fuel-Cell Applications", Journal of the Electrochemical Society, **139(2)**, pp. 761-765.

[11] Srinivasan, S., 1989, "Fuel Cells for Extraterrestrial and Terrestrial applications", Journal of the electrochemical society, **136**, pp. 41C-48C.

[12] Mehta, V., and Cooper, J., 2003, "Review and analysis of PEM fuel cell design and manufacturing", Journal of Power Sources, **114**, pp. 32-53.

[13] O'Hayre, R., Lee, S., Cha, S., Prinz, F., 2002, "A sharp peak in the performance of sputtered platinum fuel cells at ultra-low platinum loading", Journal of Power Sources, **109**, pp. 483-493.

[14] Eriksson, L., Johansson, E., Kettaneh-Wold, N., Wikstrom, C., and Wold, S., 1999, *Design of Experiments,* Umetrics, New Jersey, pp. 165-189.

[15] Wilson, M.S. and Gottesfeld, S., 1992, "High Performance Catalyzed Membranes of Ultra-low Pt Loadings for Polymer Electrolyte Fuel Cells", Journal of the Electrochemical Society, **139(2)**, pp. L28-L30.

[16] Passalacqua, E., Lufrano, F., Squadrito, G., Patti, A., and Giorgi, L., 2001, "Nafion content in the catalyst layer of polymer electrolyte fuel cells: effects on structure and performance", Electrochimica Acta, **46**, pp. 799-805.

[17] Antolini, E., Giorgi, L., Pozio, A., and Passalacqua, E., 1999, "Influence of Nafion loading in the catalyst layer of gas-diffusion electrodes for PEFC", Journal of Power Sources, **77**, pp. 136-142.

[18] Springer, T., Zawodzinski, T., and Gottesfeld, S., 1991, "Polymer Electrolyte Fuel Cell Model", Journal of the Electrochemical Society, **138(8)**, pp. 2234-2342.

[19] Litster, S., and McLean, G., 2004, "PEM fuel cell electrodes", Journal of Power Sources, **130**, pp. 61-76.

[20] O'Hayre, R., Cha, S., Colella, W., and Prinz, F., 2006, *Fuel Cell Fundamentals,*

Wiley, New York, pp. 201-232.

[21] Uchida, M., Aoyama, Y., Eda, N., and Ohta, A., 1995, "Investigation of the Microstructure in the Catalyst Layer and Effects of Both Perfluorosulfonate Ionomer and PTFE-Loaded Carbon on the Catalyst Layer of Polymer Electrolyte Fuel Cells", Journal of the Electrochemical Society, **142(12)**, pp. 4143-4149.

[22] Chun, Y., Kim, C., Peck, D., and Shin, D., 1998, "Performance of a Polymer Electrolyte Membrane Fuel Cell with Thin Film Catalyst Electrodes", Journal of Power Sources, **71**, pp. 174-178.

[23] Henderson, K., 2005, "Evaluation of the Effect of Microporous Sublayer Design and Fabrication on Performance and Adhesion in PEM Fuel Cell Assemblies", (Master thesis, Virginia Polytechnic Institute and State University, 2005).

[24] Sole, J., 2006, "Investigation of Novel Gas Diffusion Media for Application in PEM Fuel Cell Ribbon Assemblies", (Master thesis, Virginia Polytechnic Institute and State University, 2006).

[25] Russell, J., 2003, "Investigation of the Effect of Catalyst Layer Composition on the Performance of PEM Fuel Cells", (Master thesis, Virginia Polytechnic Institute and State University, 2003).

[26] S. Kocha, in *Handbook of Fuel Cells-Fundamentals, Technology and Applications*, W. Veilstich, A. Lamm, and H. Gasteiger, Editors, Vol. 3, p. 538, Wiley, Weinhem (2003).

[27] Larminie, J. and Dicks, A., 2003, *Fuel Cell Systems Explained,* Wiley, New York, pp. 94-100.

Appendix A: Performance data

A.1 MEA 1 data

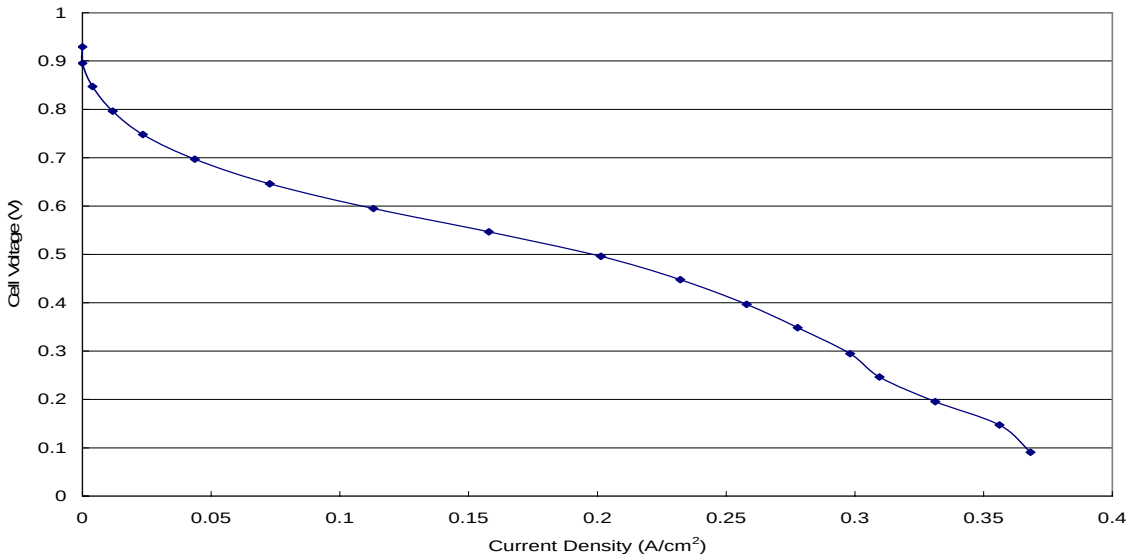

Figure A.1.1. Polarization curves for MEA 1.

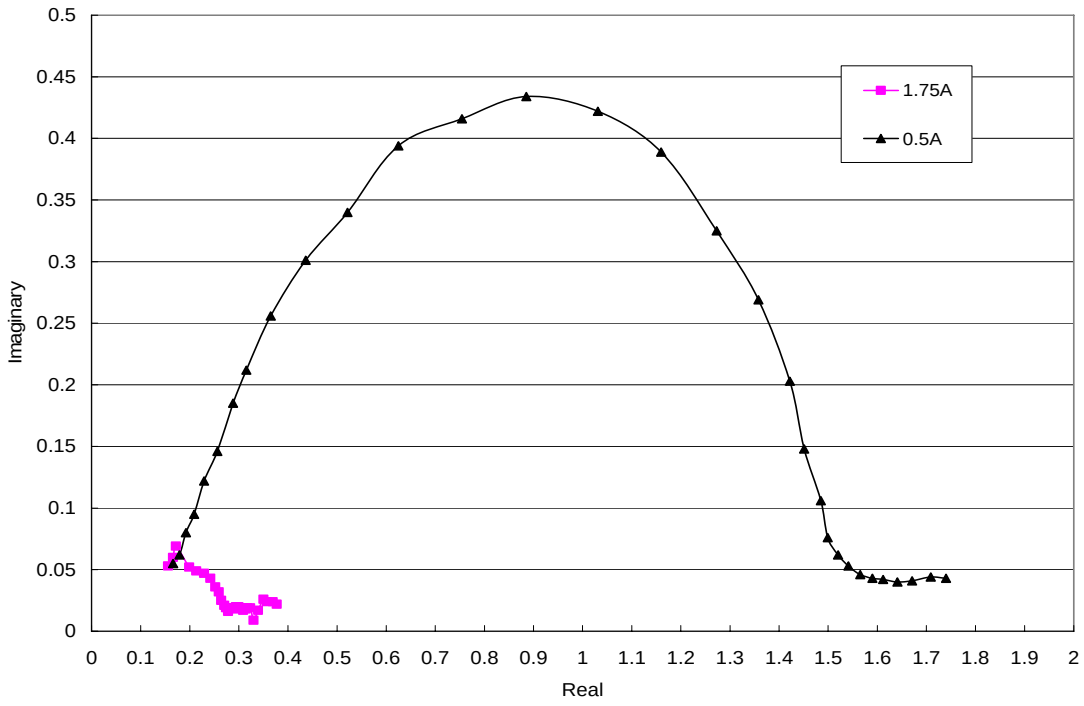

Figure A.1.2. Electrochemical impedance spectroscopy for MEA 1.

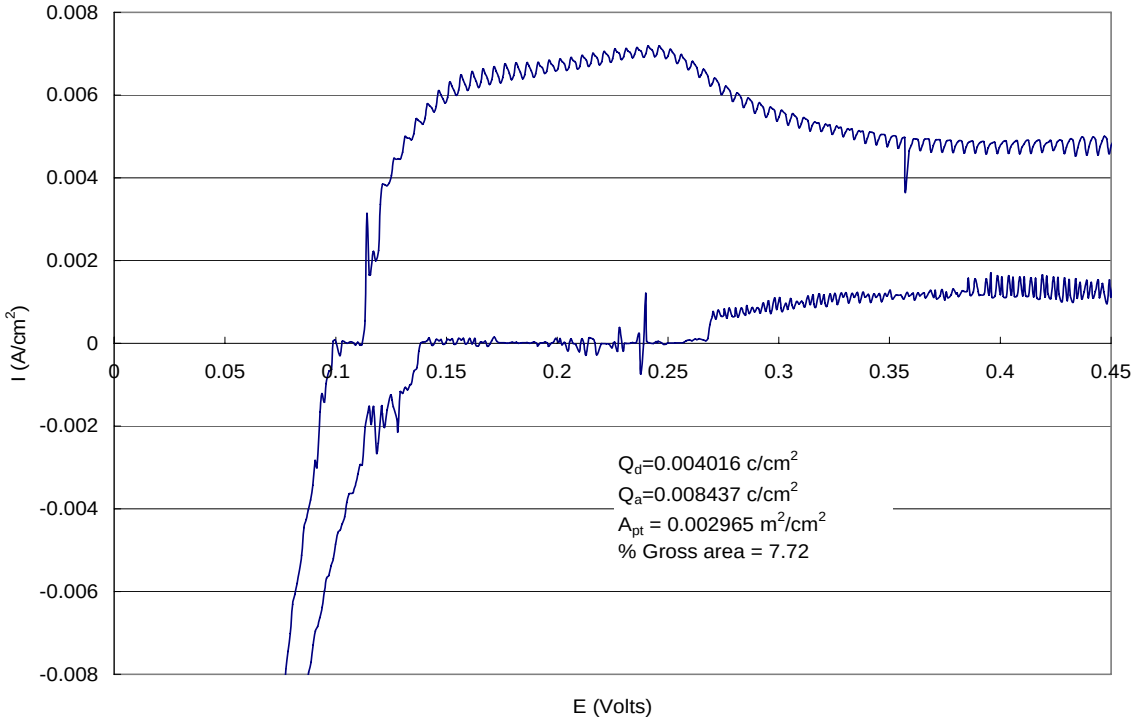

Figure A.1.3. Cyclic voltammetry for MEA 1.

A.2 MEA 2 data

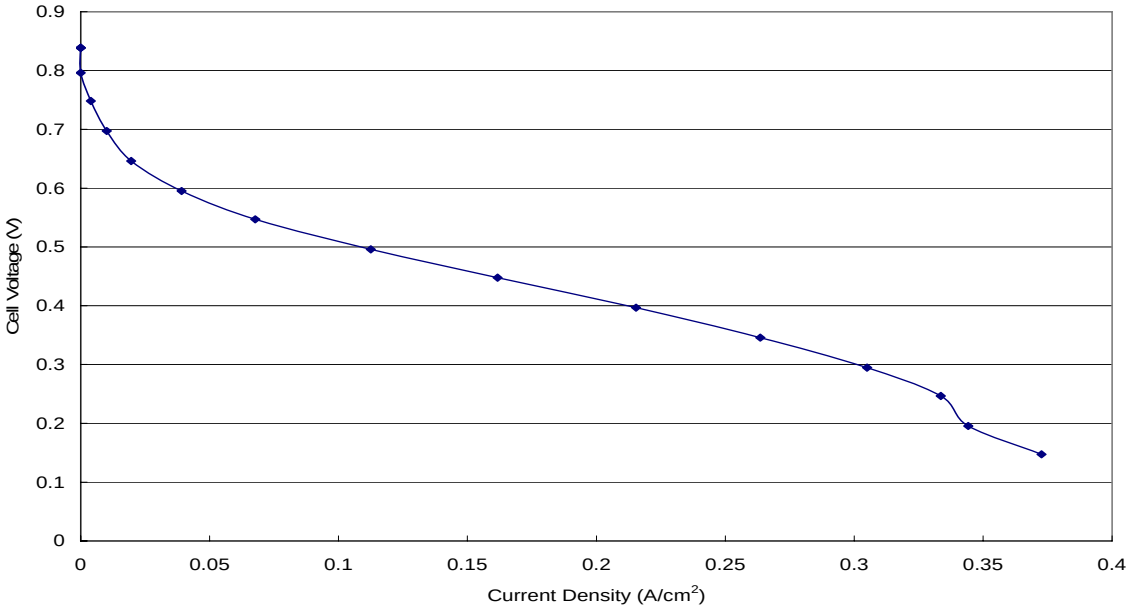

Figure A.2.1. Polarization curves for MEA 2.

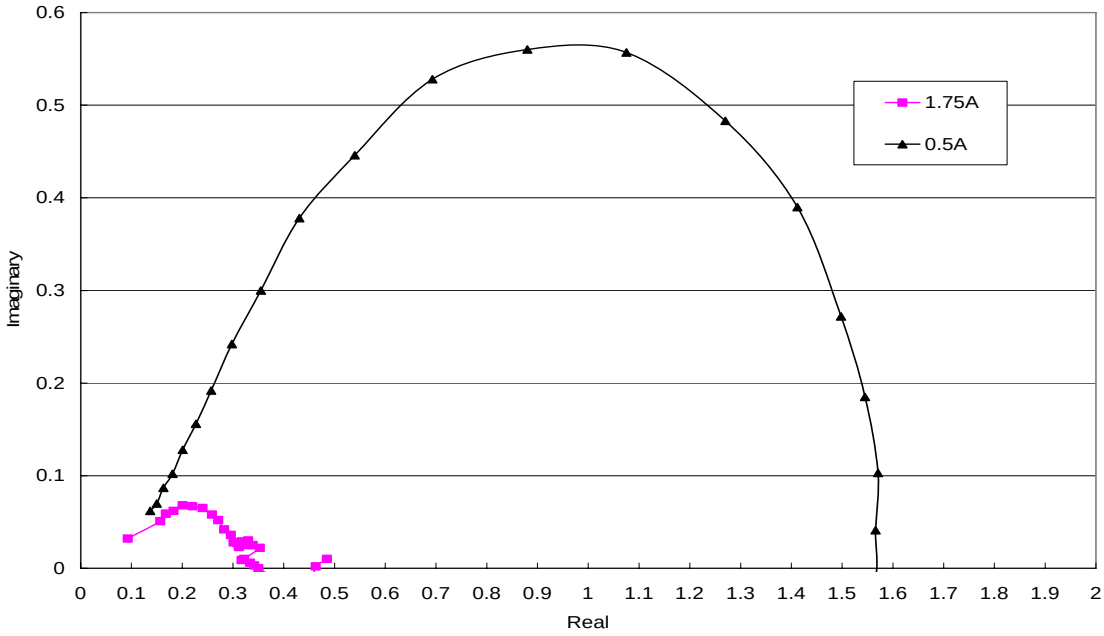

Figure A.2.2. Electrochemical impedance spectroscopy for MEA 2.

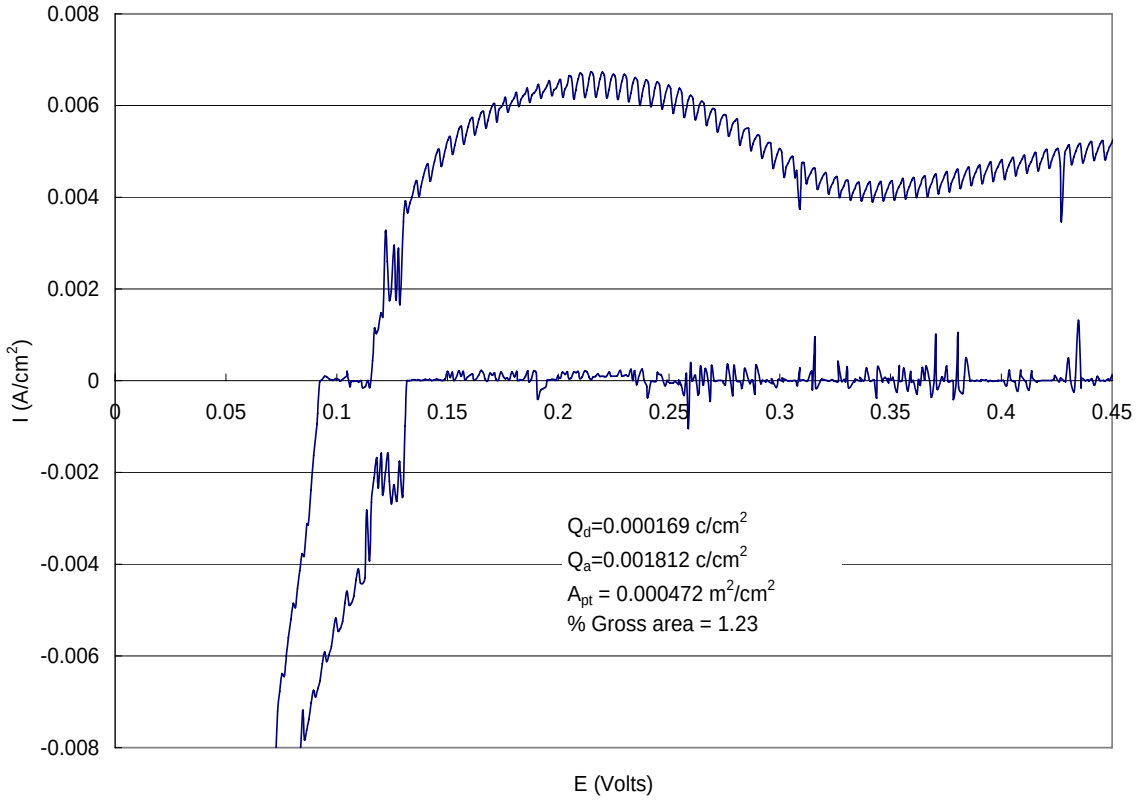

Figure A.2.3. Cyclic voltammetry for MEA 2.

A.3 MEA 3 data

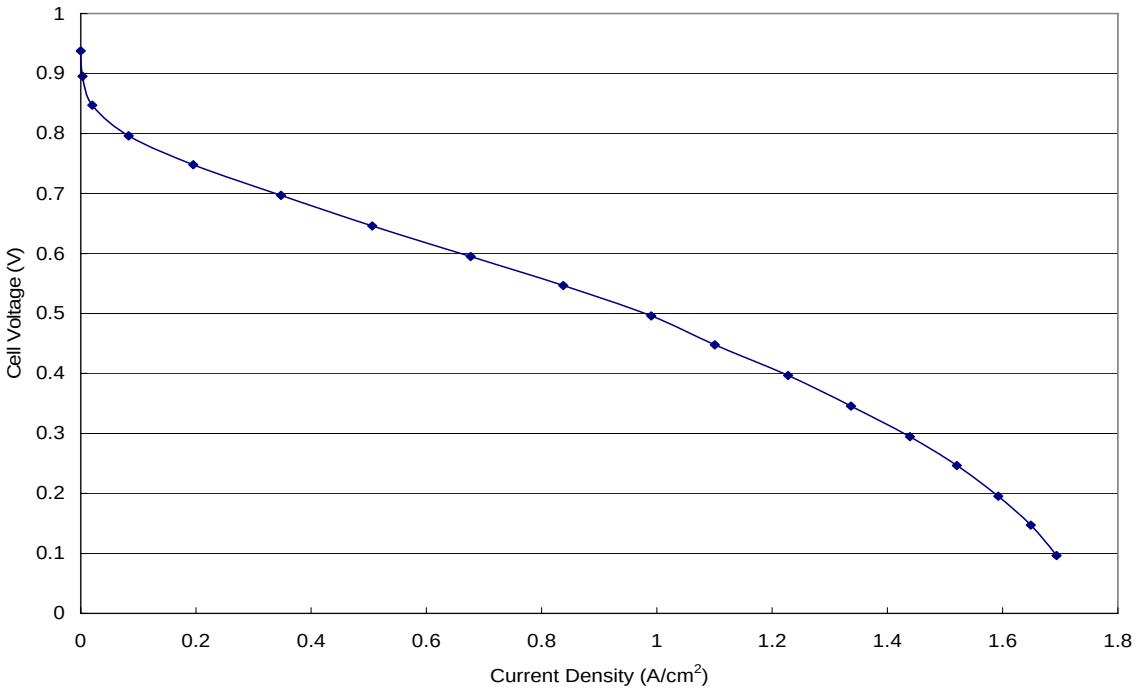

Figure A.3.1. Polarization curves for MEA 3.

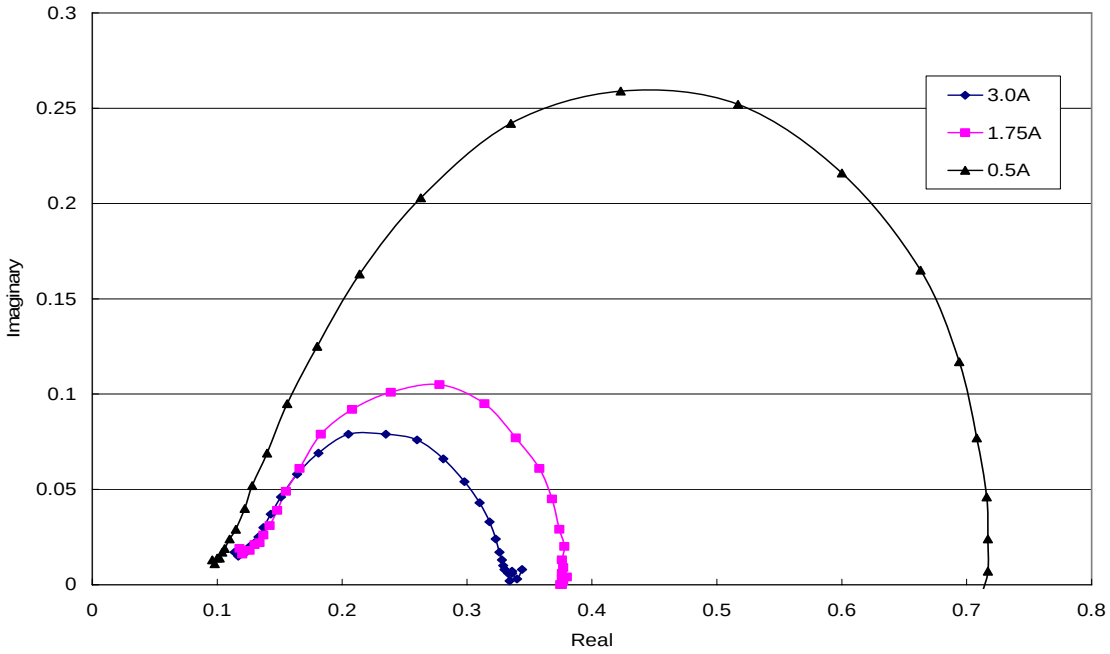

Figure A.3.2. Electrochemical impedance spectroscopy for MEA 3.

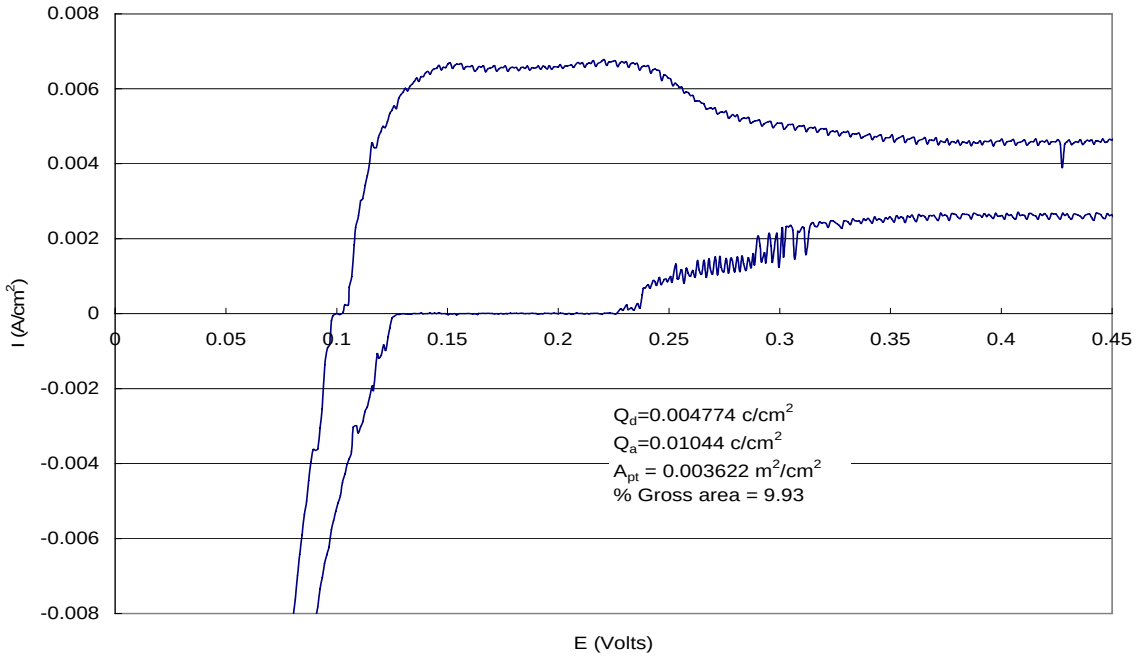

Figure A.3.3. Cyclic voltammetry for MEA 3.

A.4 MEA 4 data

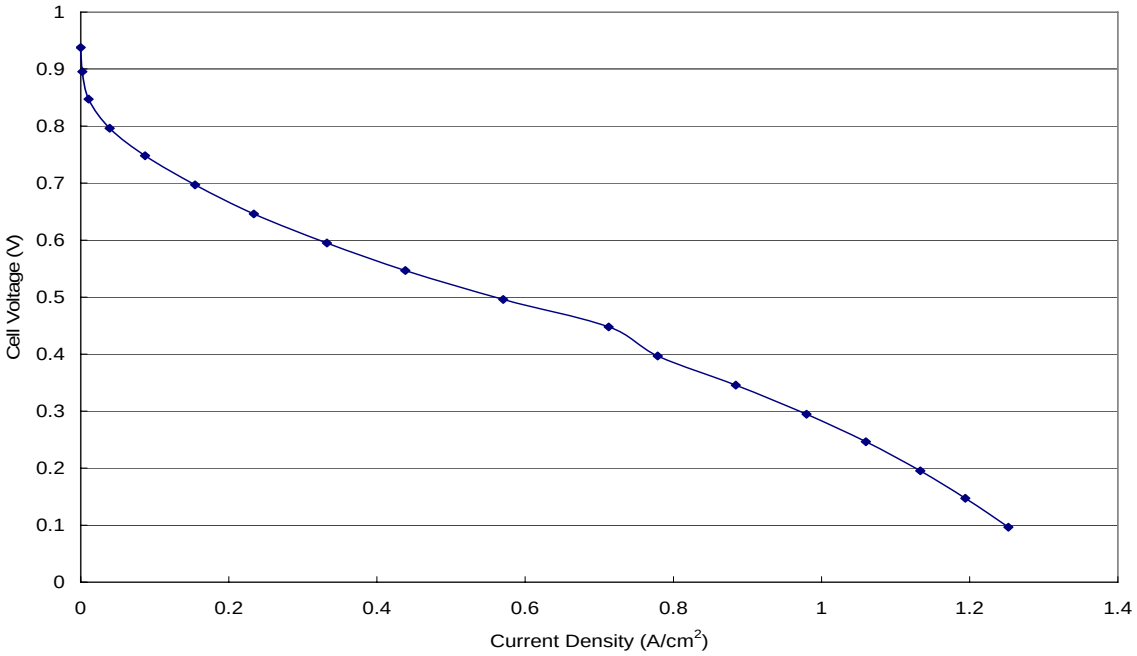

Figure A.4.1. Polarization curves for MEA 4.

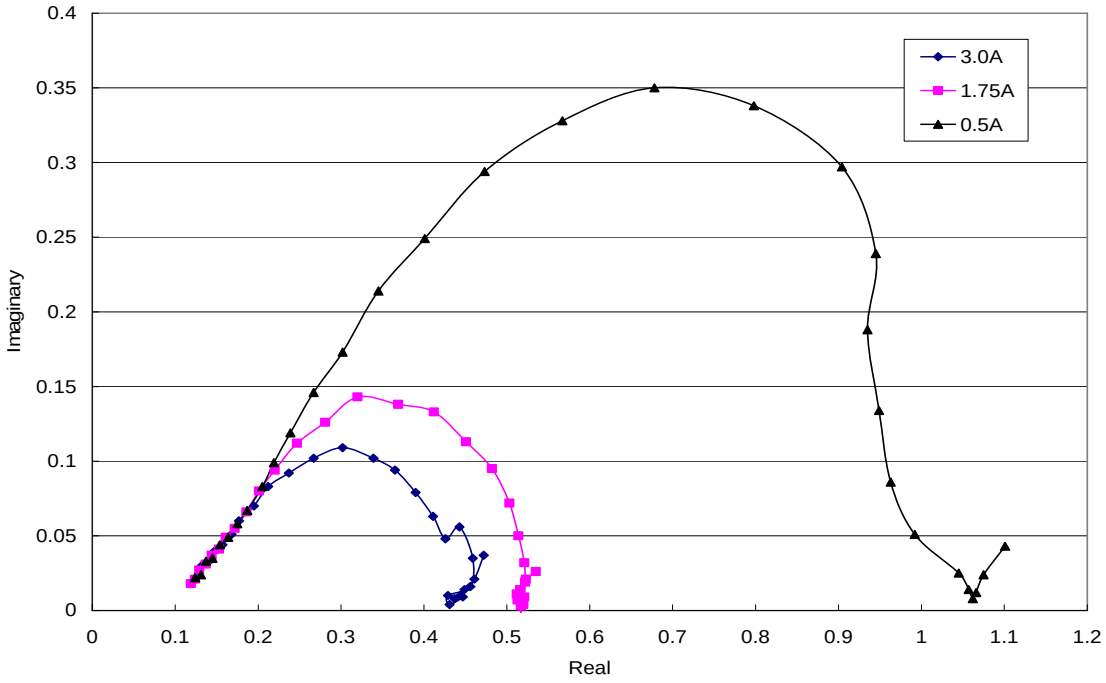

Figure A.4.2. Electrochemical impedance spectroscopy for MEA 4.

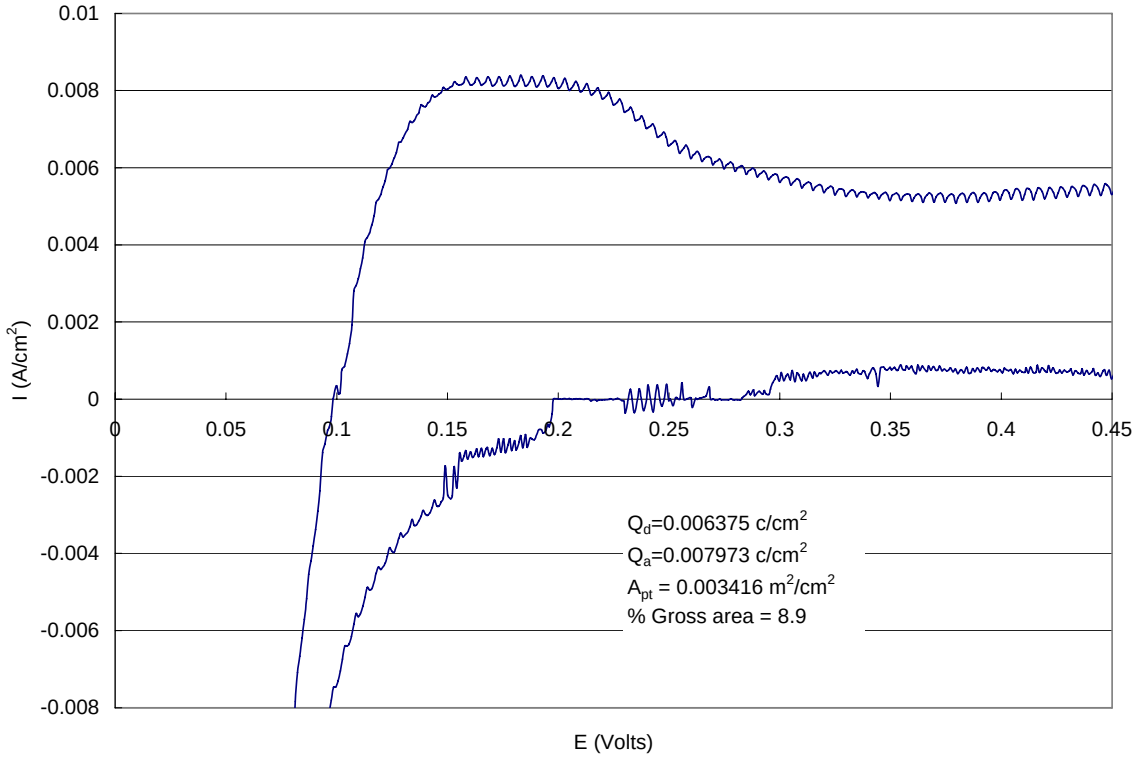

Figure A.4.3. Cyclic voltammetry for MEA 4.

A.5 MEA 5 data

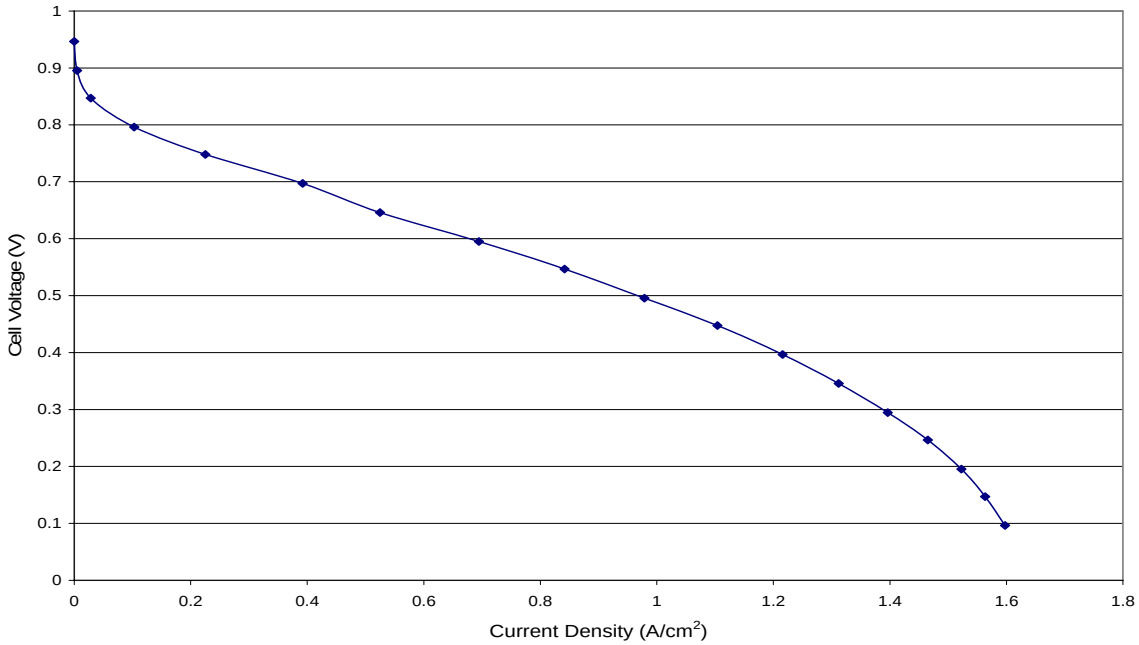

Figure A.5.1. Polarization curves for MEA 5.

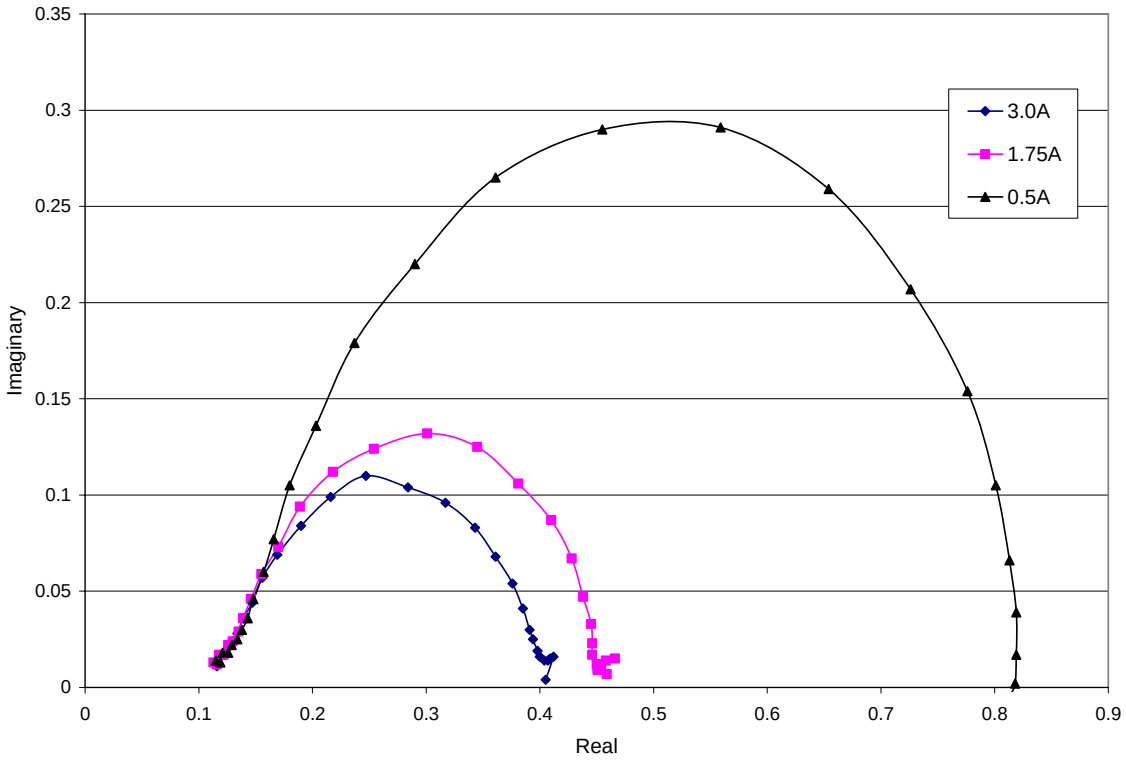

Figure A.5.2. Electrochemical impedance spectroscopy for MEA 5.

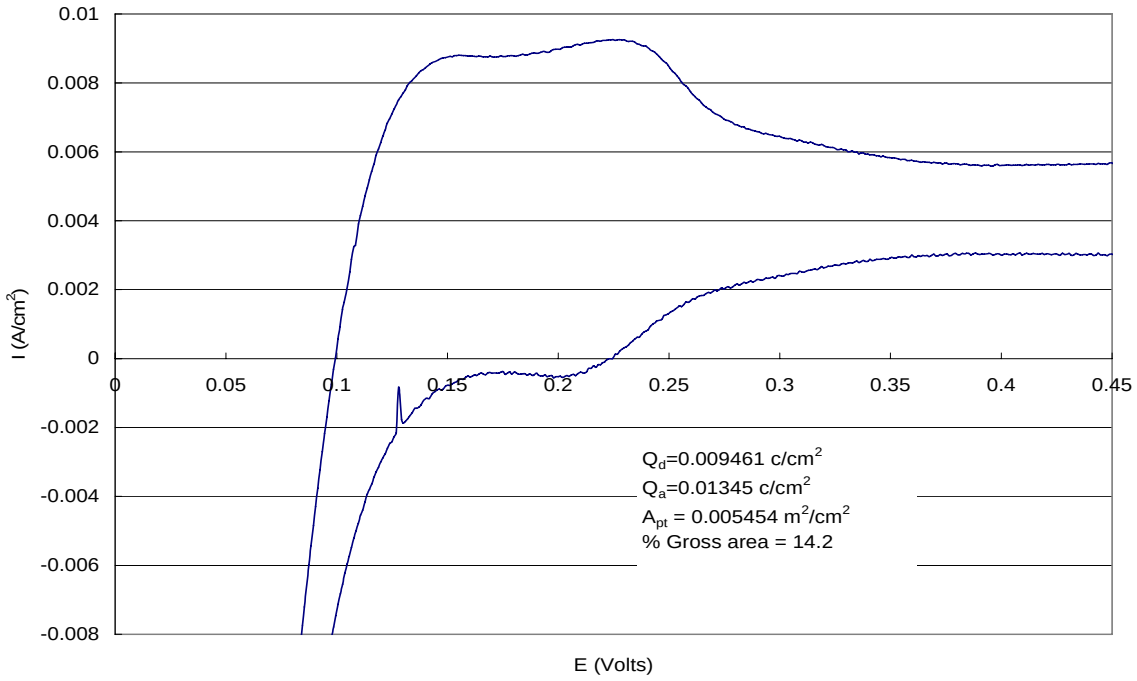

Figure A.5.3. Cyclic voltammetry for MEA 5.

A.6 MEA 6 data

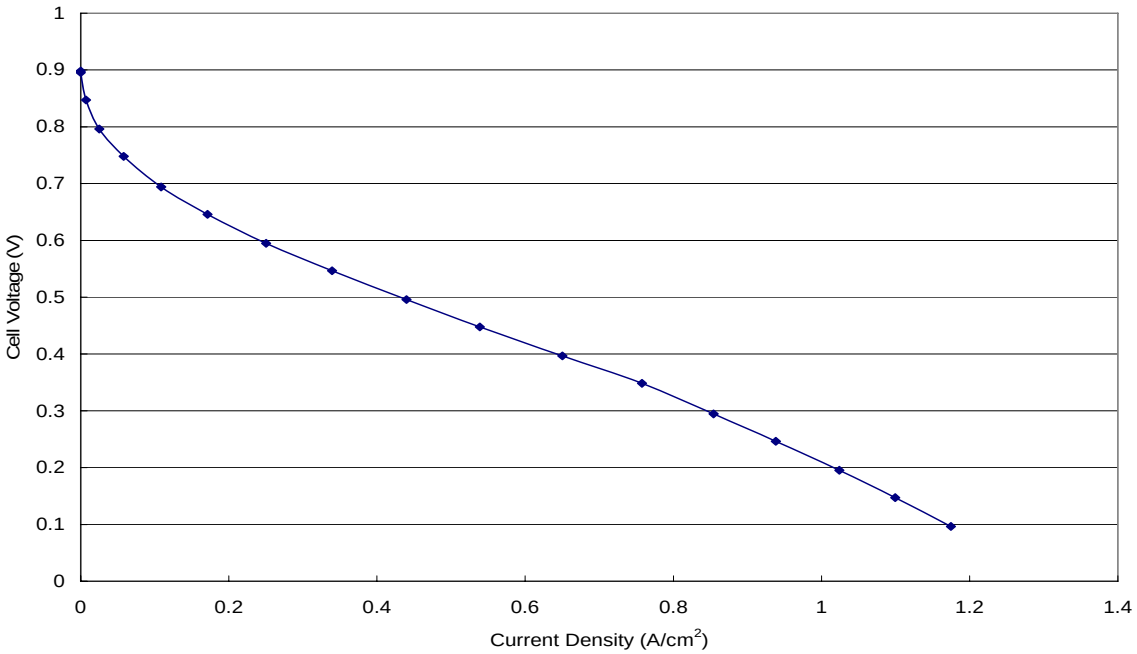

Figure A.6.1. Polarization curves for MEA 6.

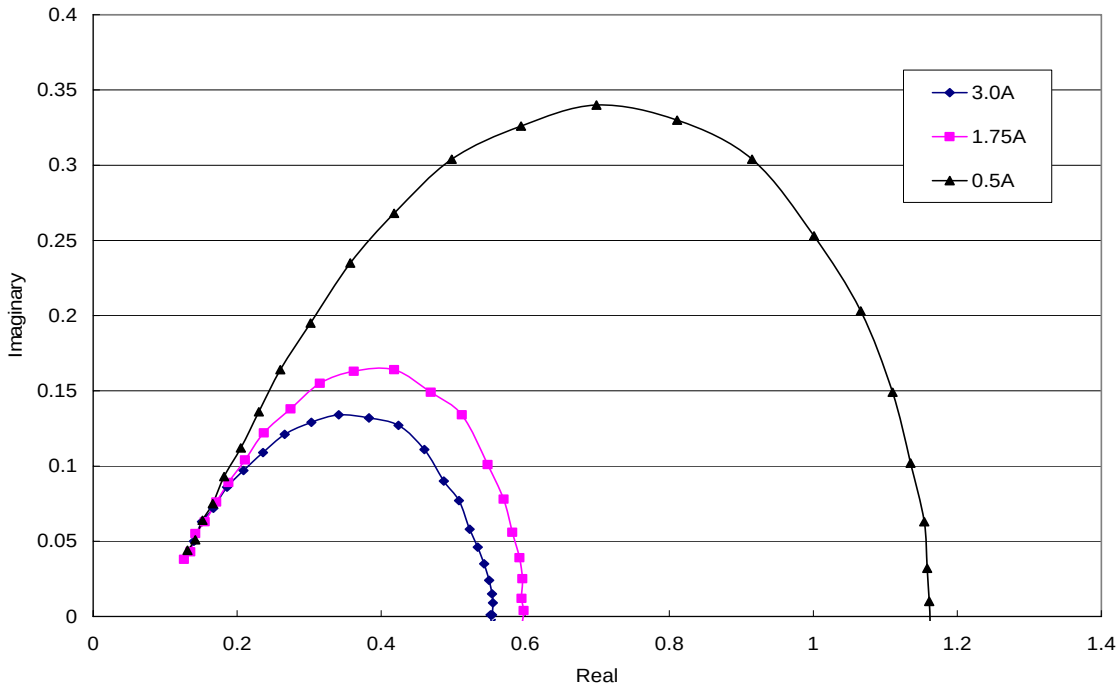

Figure A.6.2. Electrochemical impedance spectroscopy for MEA 6.

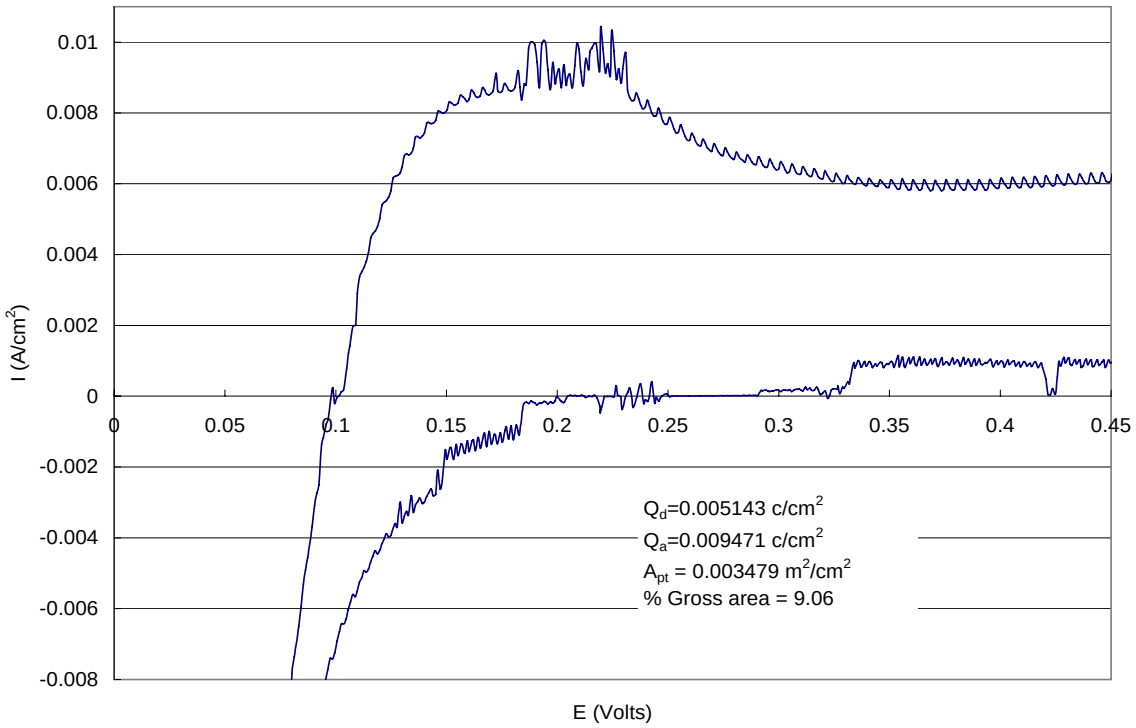

Figure A.6.3. Cyclic voltammetry for MEA 6.

A.7 MEA 7 data

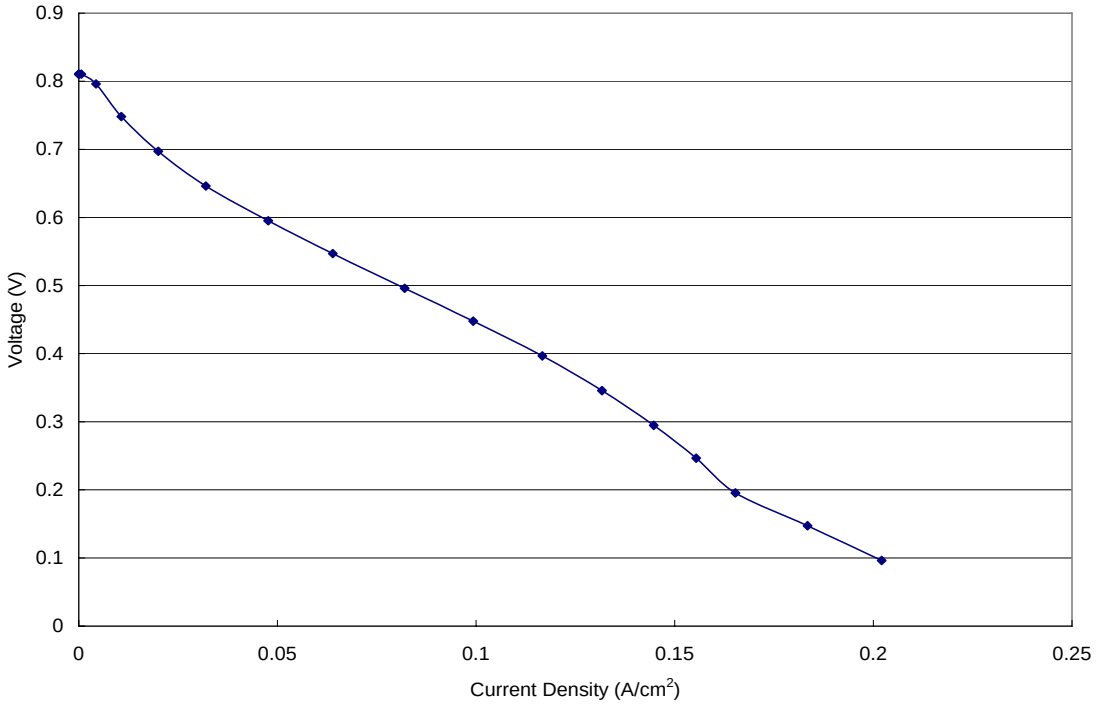

Figure A.7.1. Polarization curves for MEA 7.

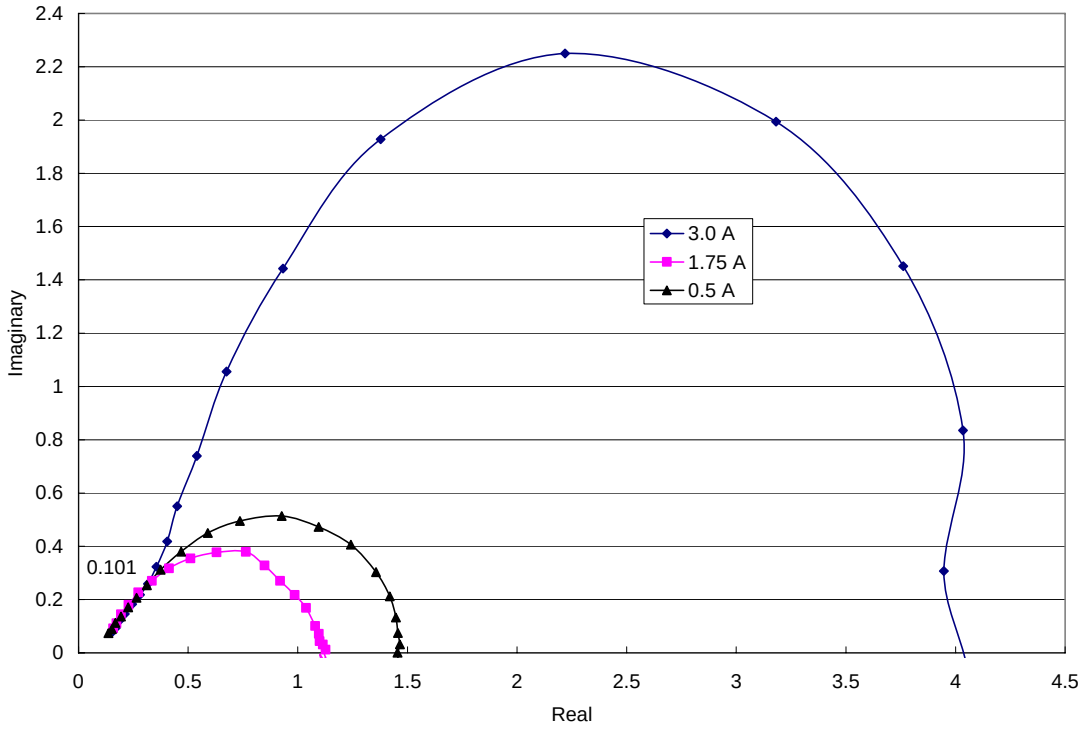

Figure A.7.2. Electrochemical impedance spectroscopy for MEA 7.

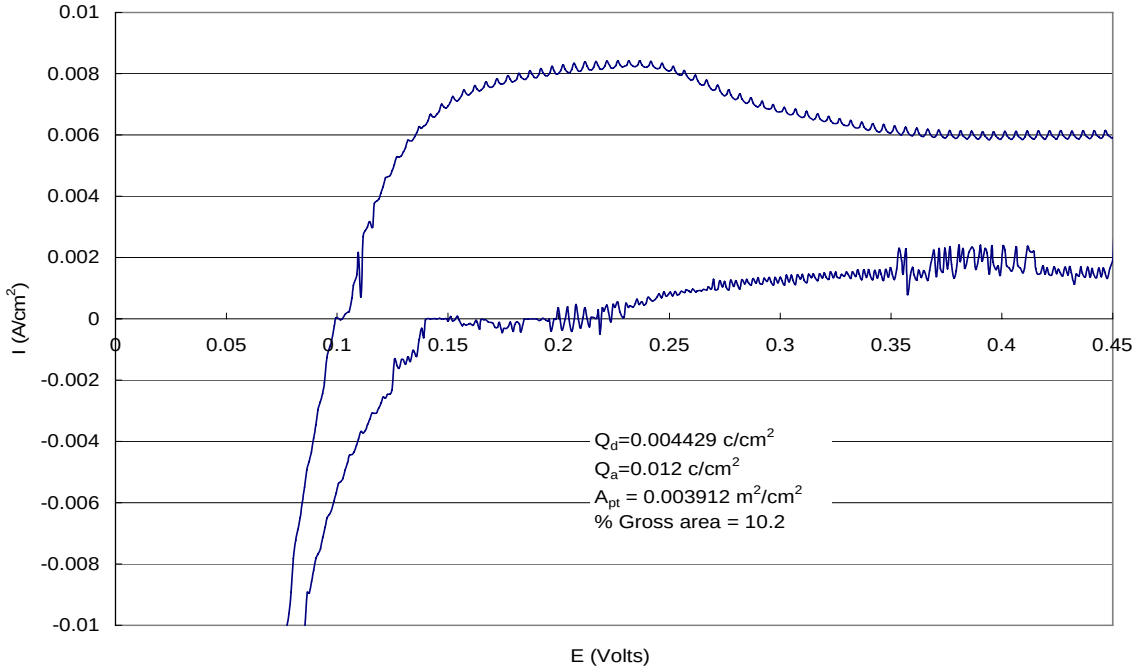

Figure A.7.3. Cyclic voltammetry for MEA 7.

A.8 MEA 8 data

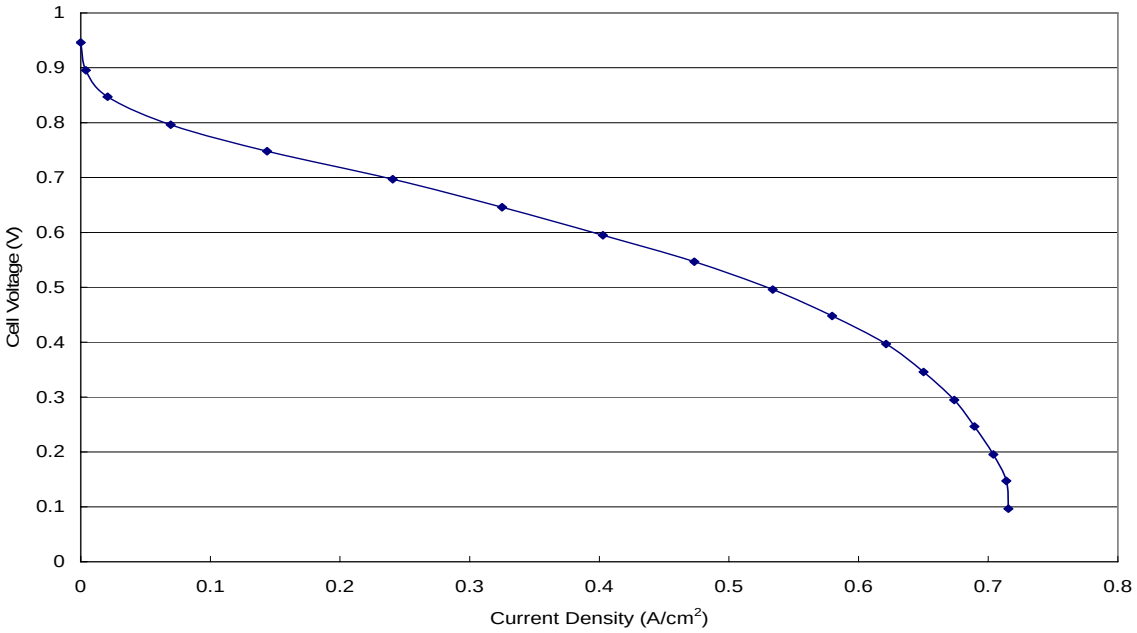

Figure A.8.1. Polarization curves for MEA 8.

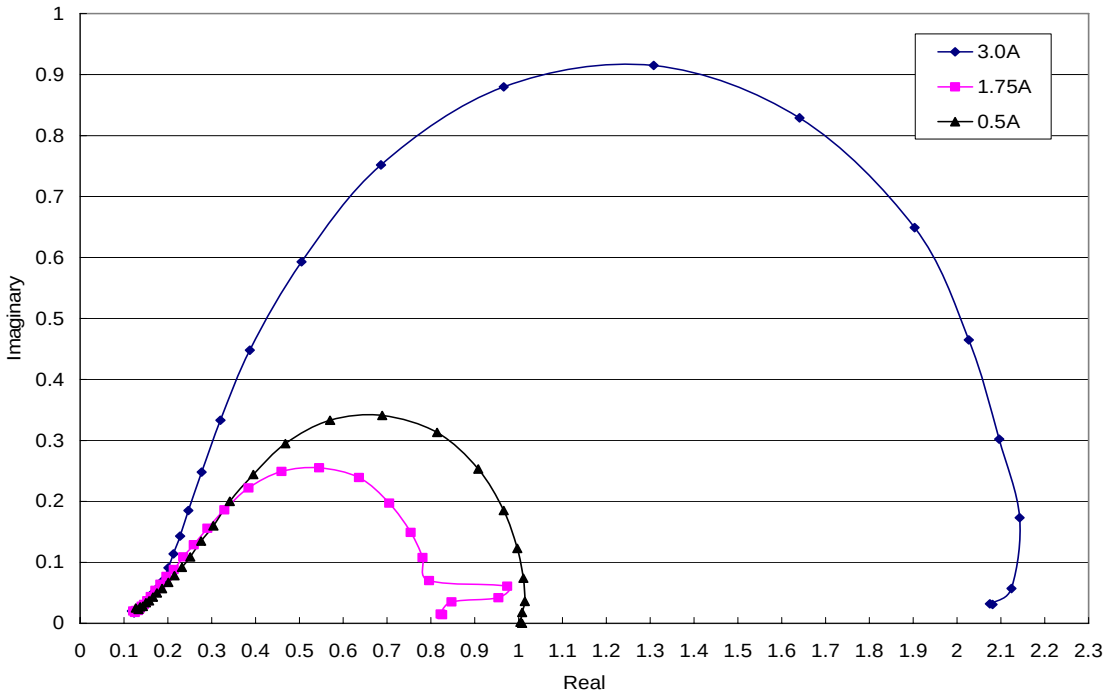

Figure A.8.2. Electrochemical impedance spectroscopy for MEA 8.

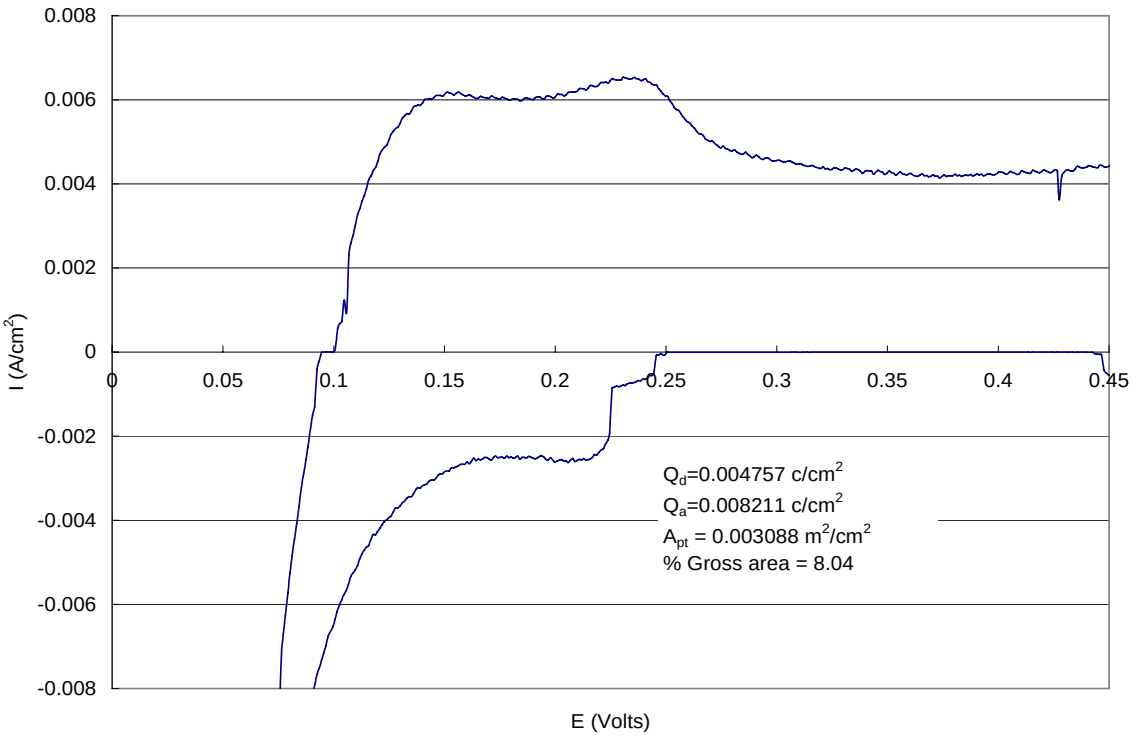

Figure A.8.3. Cyclic voltammetry for MEA 8.

A.9-1 MEA 9-1 data

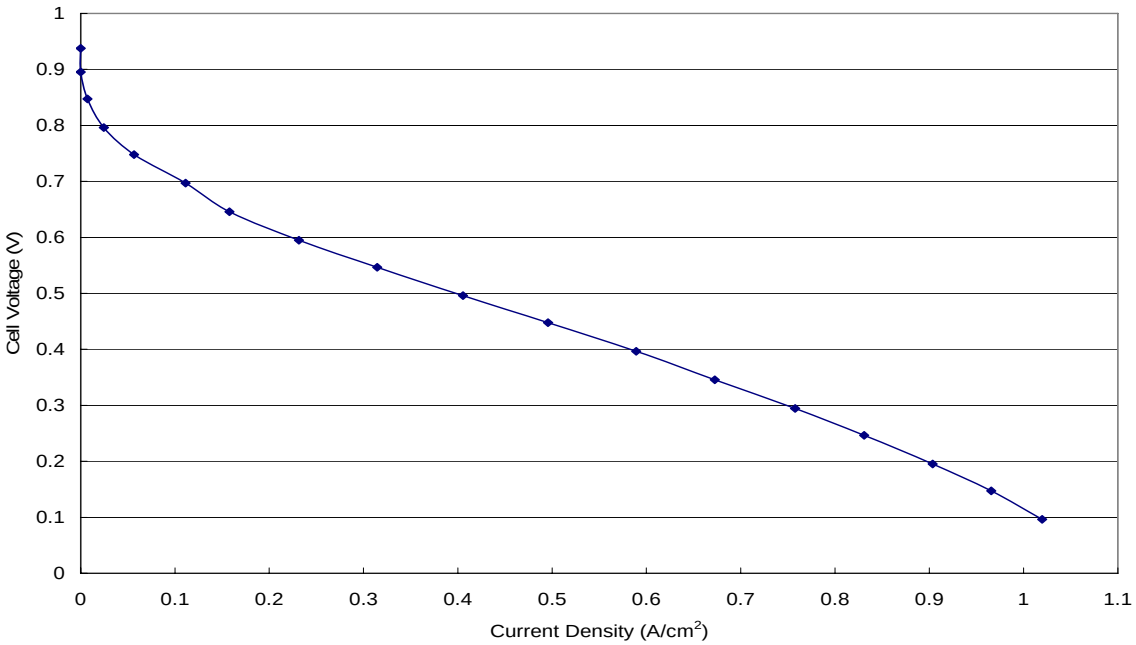

Figure A.9-1.1. Polarization curves for MEA 9-1.

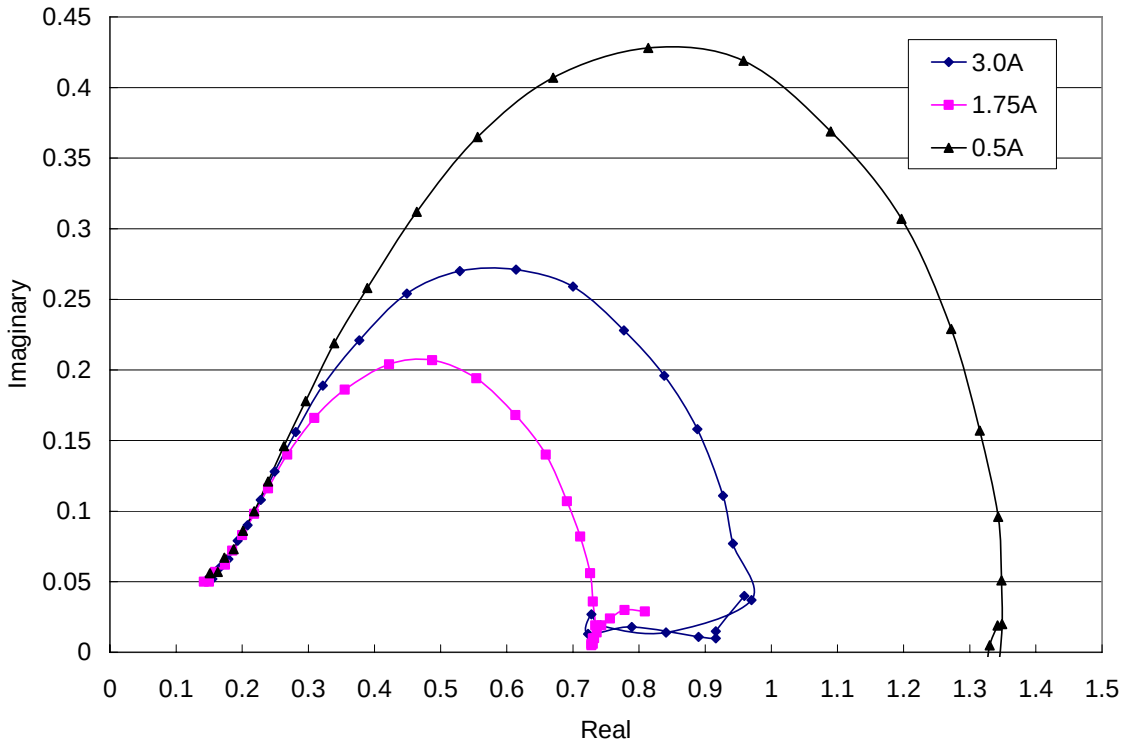

Figure A.9-1.2. Electrochemical impedance spectroscopy for MEA 9-1.

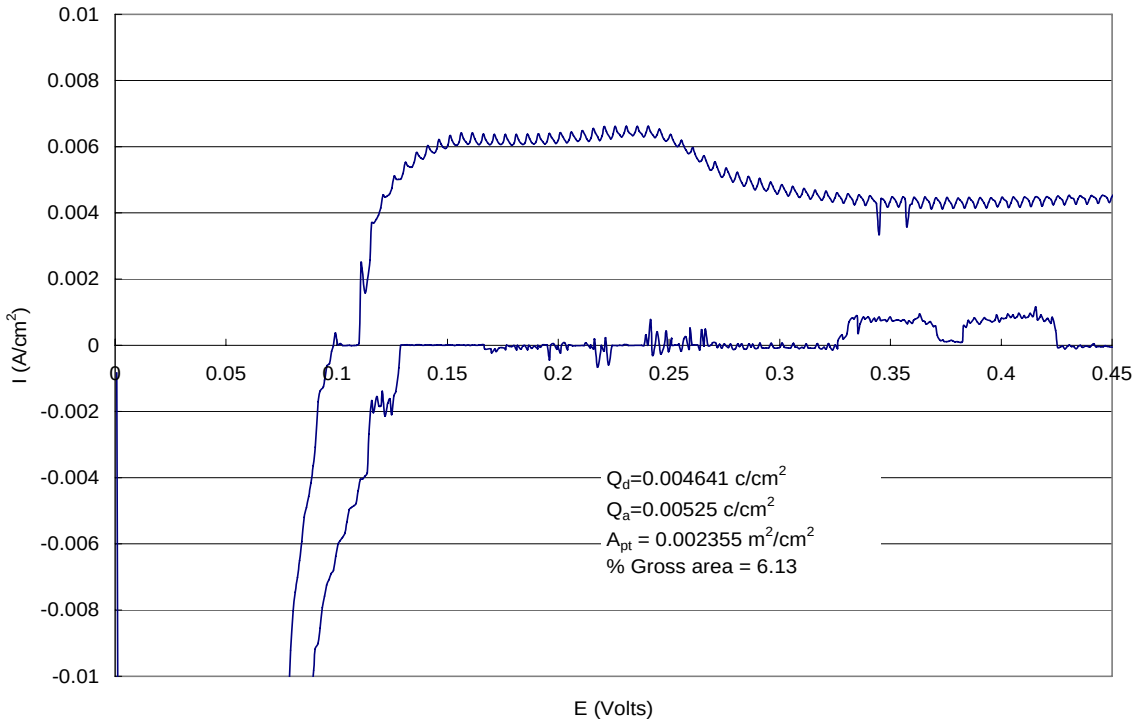

Figure A.9-1.3. Cyclic voltammetry for MEA 9-1.

A.9-2 MEA 9-2 data

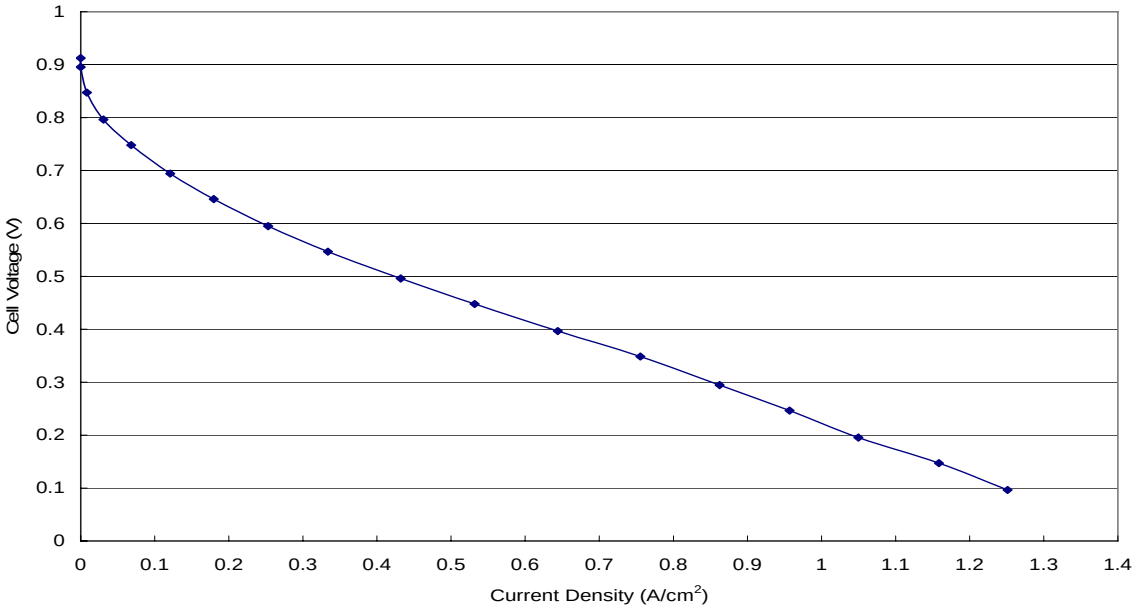

Figure A.9-2.1. Polarization curves for MEA 9-2.

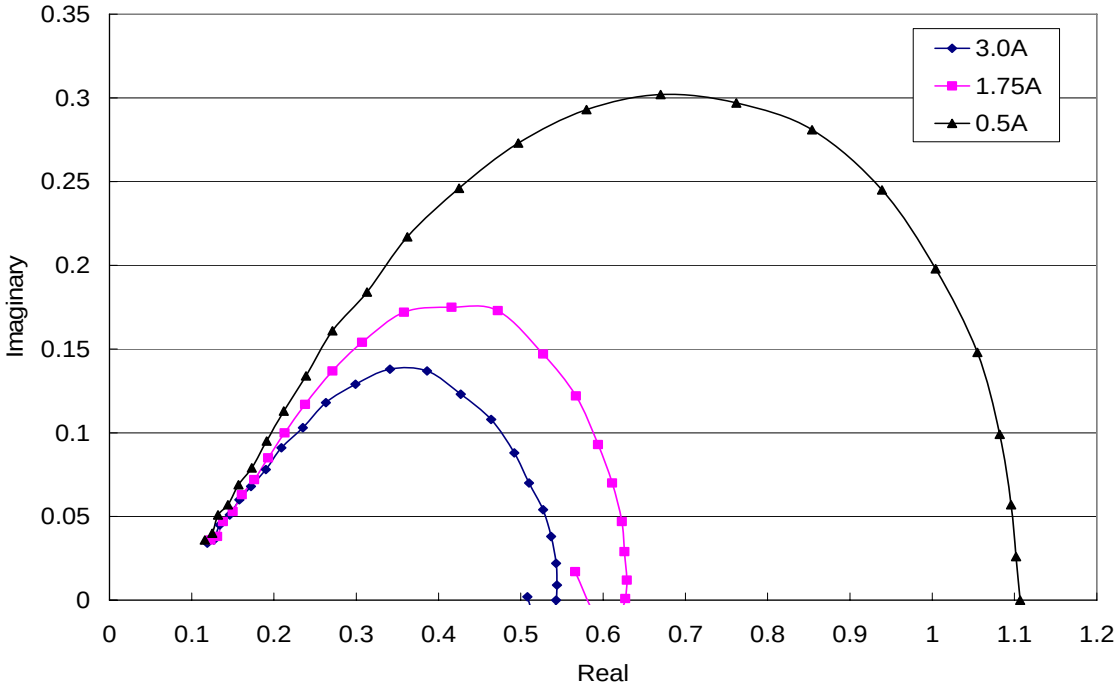

Figure A.9-2.2. Electrochemical impedance spectroscopy for MEA 9-2.

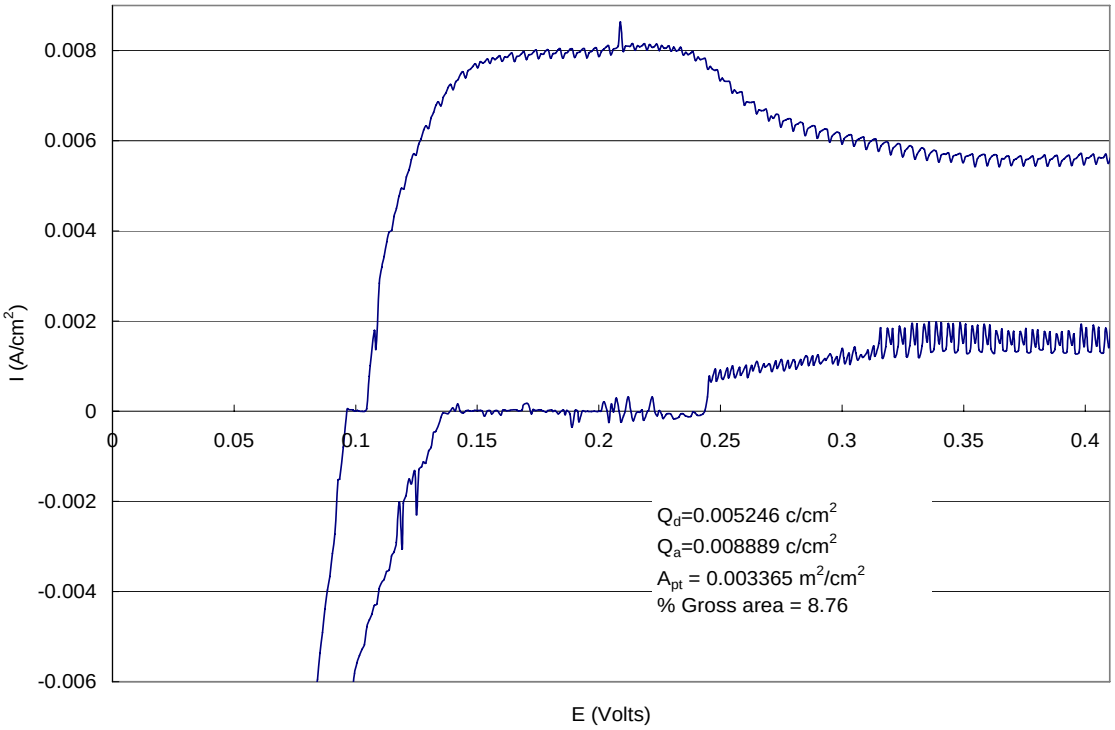

Figure A.9-2.3. Cyclic voltammetry for MEA 9-2.

A.9-3 MEA 9-3 data

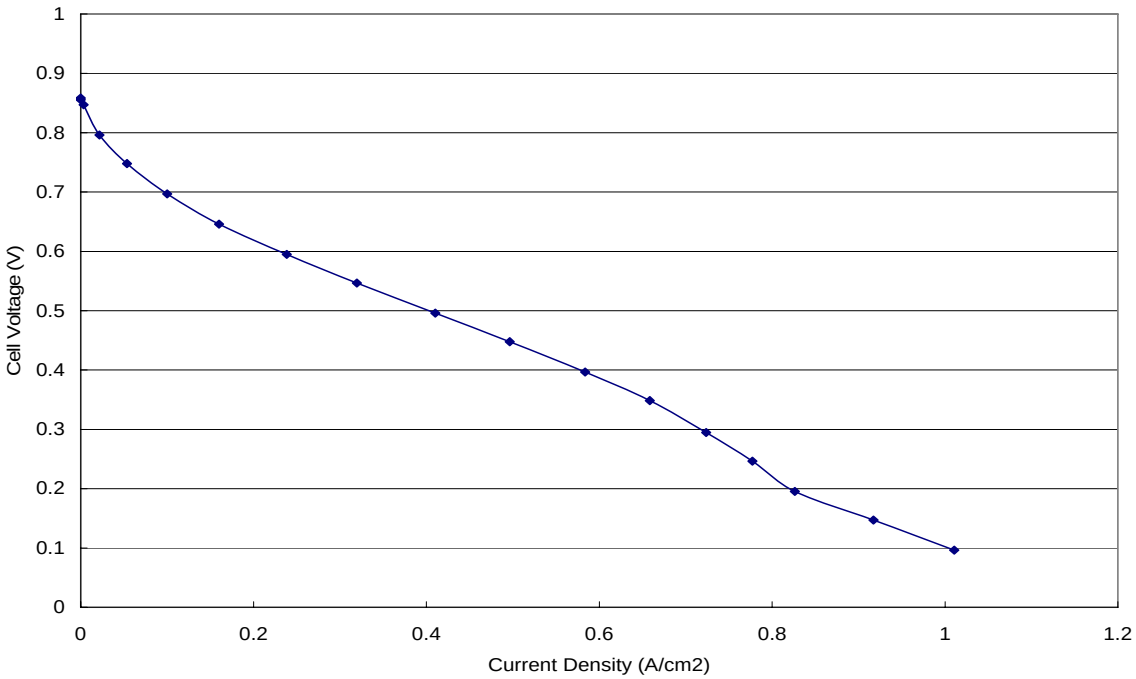

Figure A.9-3.1. Polarization curves for MEA 9-3.

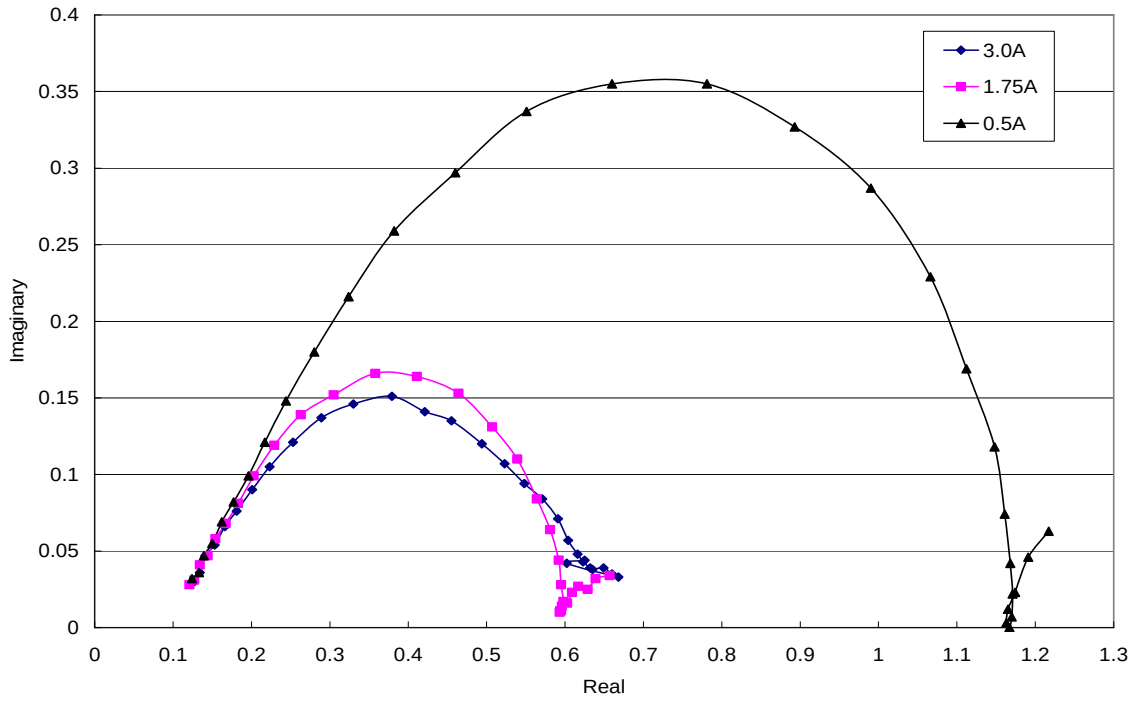

Figure A.9-3.2. Electrochemical impedance spectroscopy for MEA 9-3.

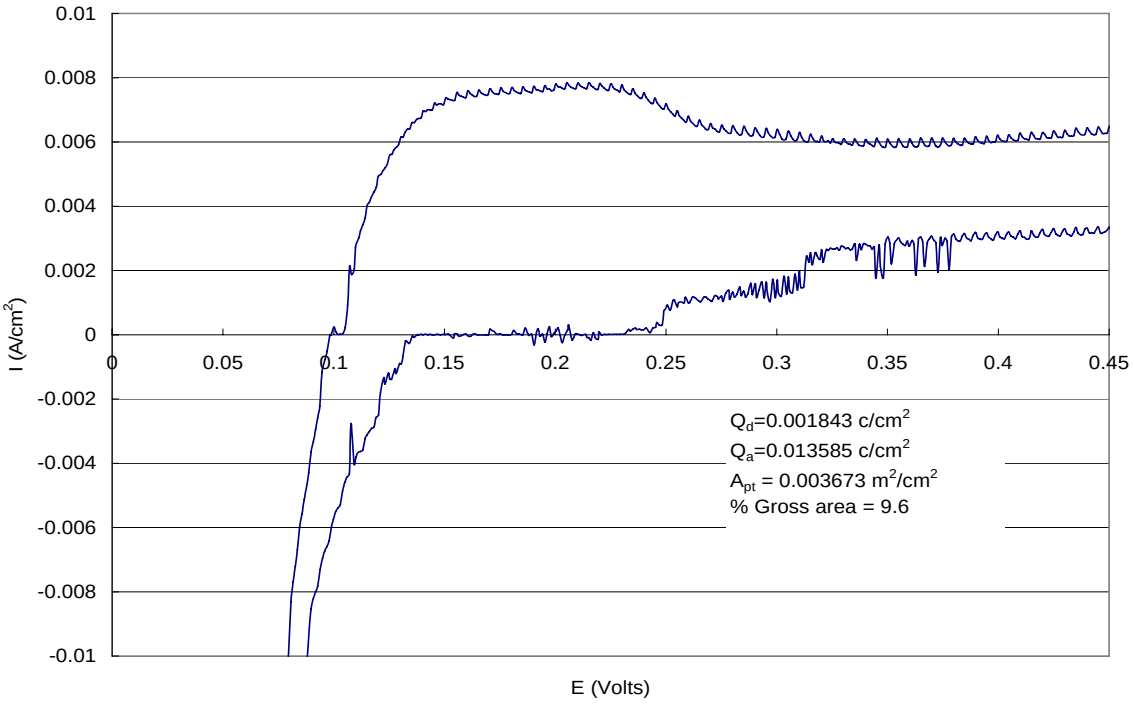

Figure A.9-3.3. Cyclic voltammetry for MEA 9-3.

Appendix B: SEM Pictures of Catalyst Layer Samples

B.1 SEM Images of MEA 1

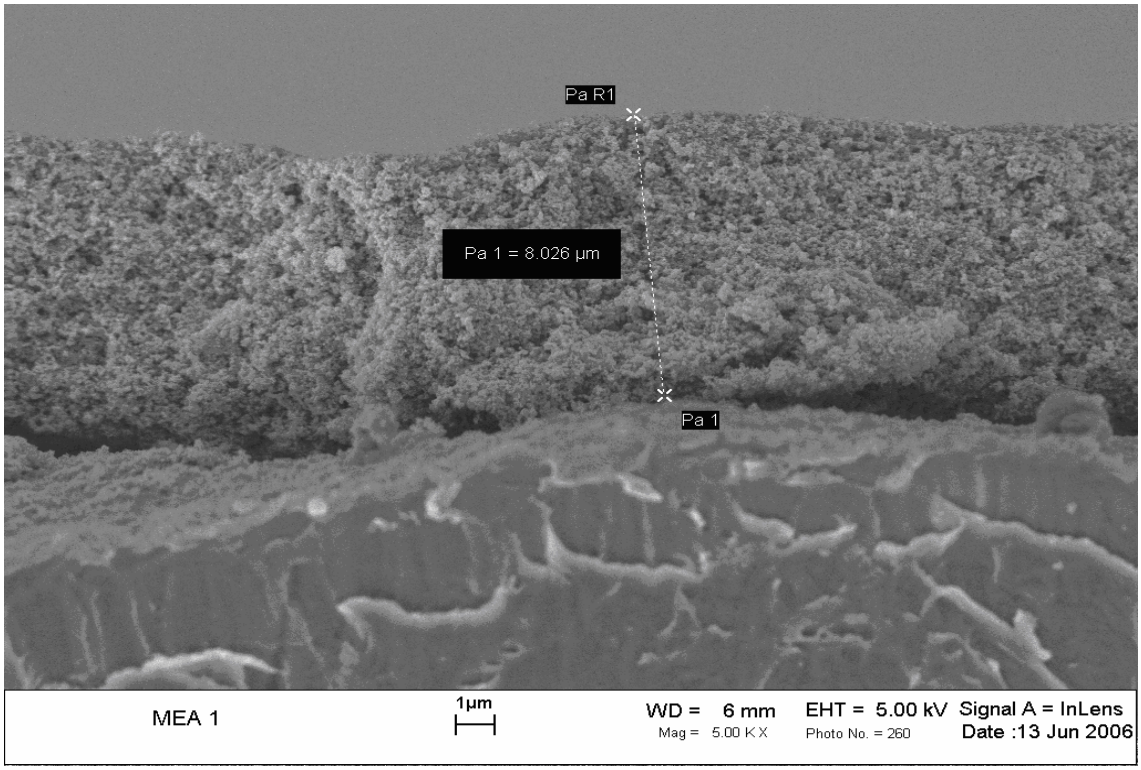

Figure B.1.1 MEA 1 at 5,000x magnification.

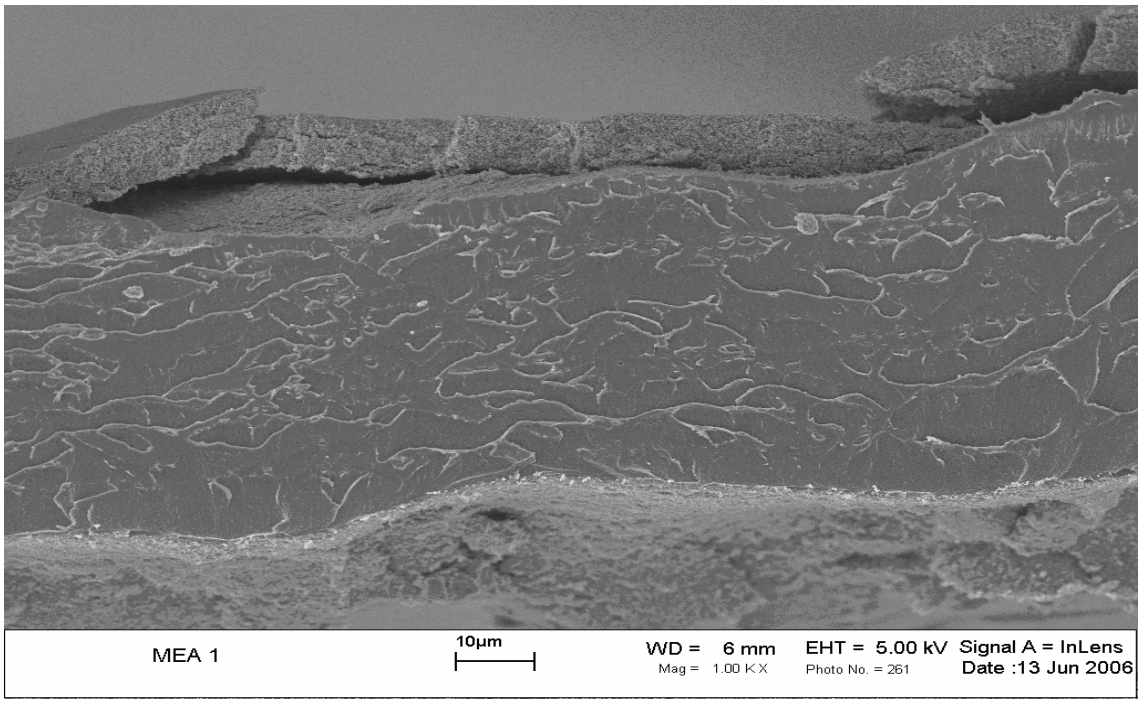

Figure B.1.2 MEA 1 at 1,000x magnification.

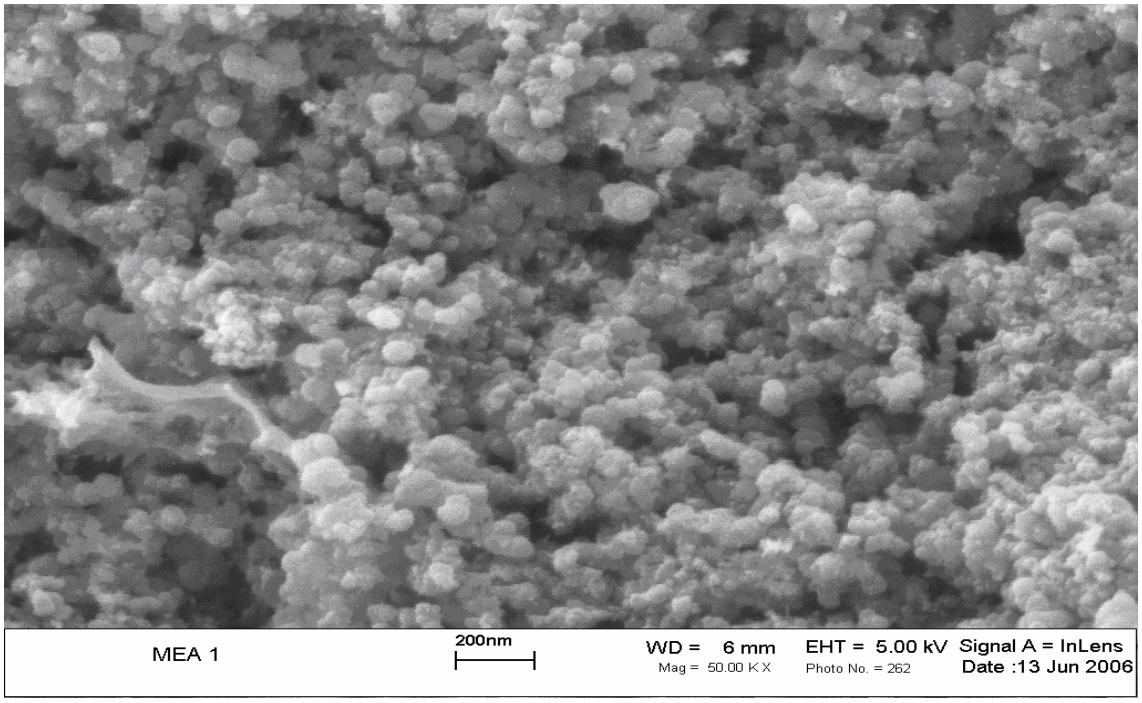

Figure B.1.3 MEA 1 at 100,000x magnification.

B.2 SEM Images of MEA 2

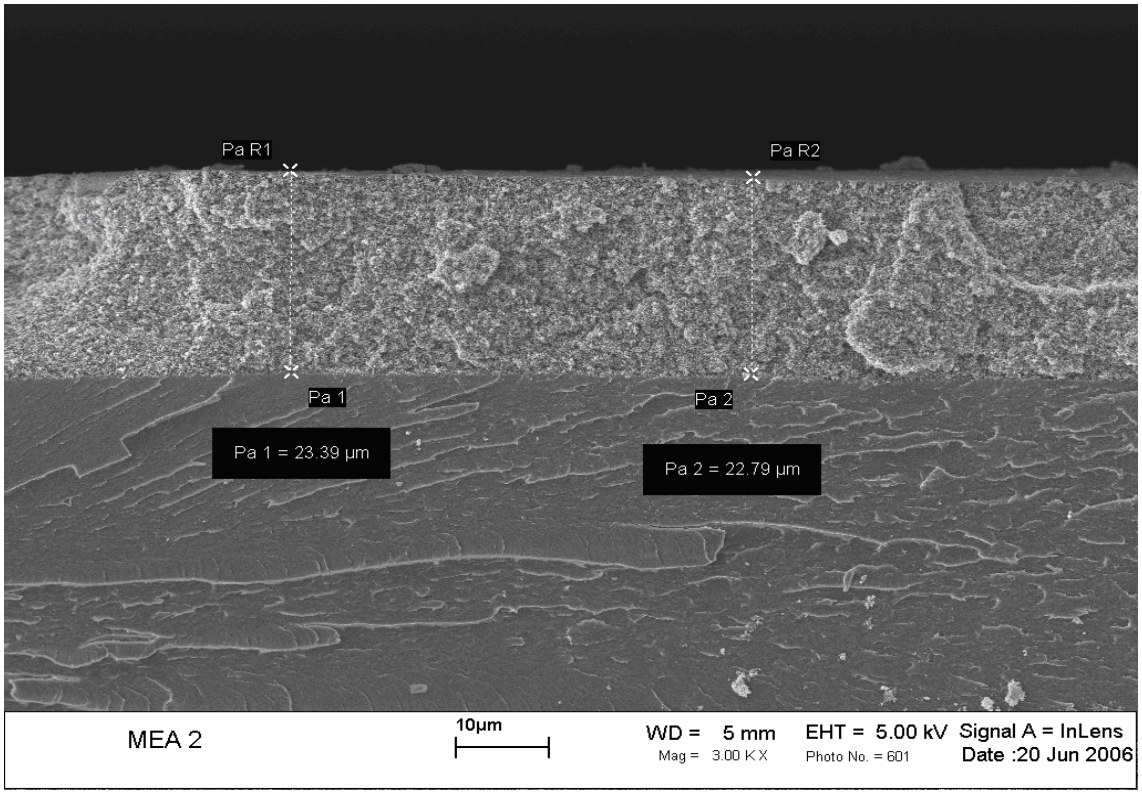

Figure B.2.1 MEA 2 at 3,000x magnification.

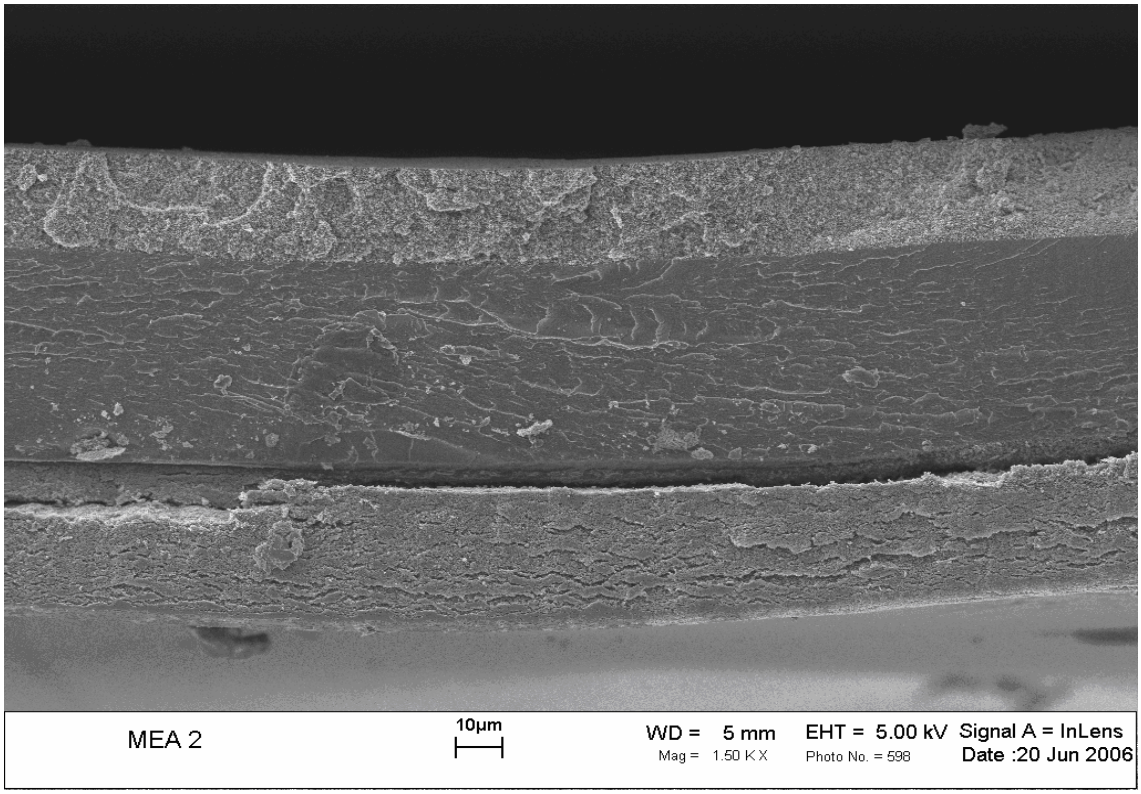

Figure B.2.2 MEA 2 at 1,500x magnification.

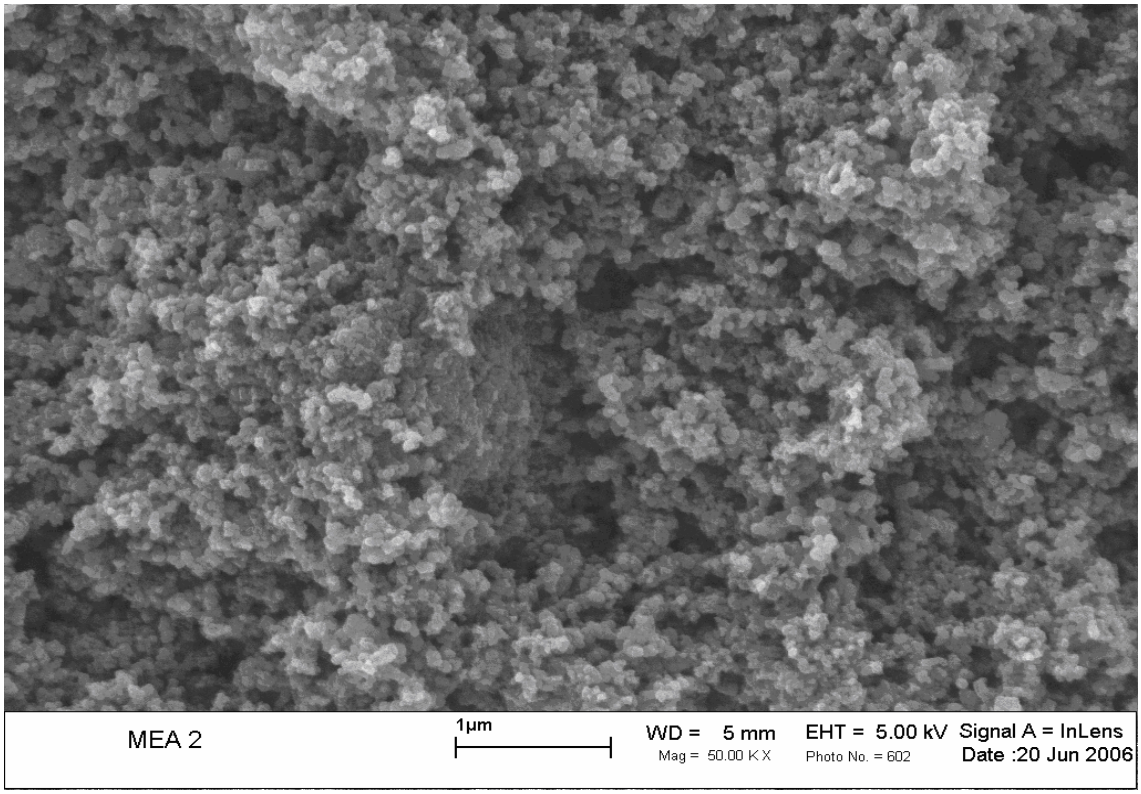

Figure B.2.3 MEA 2 at 50,000x magnification

B.3 SEM Images of MEA 3

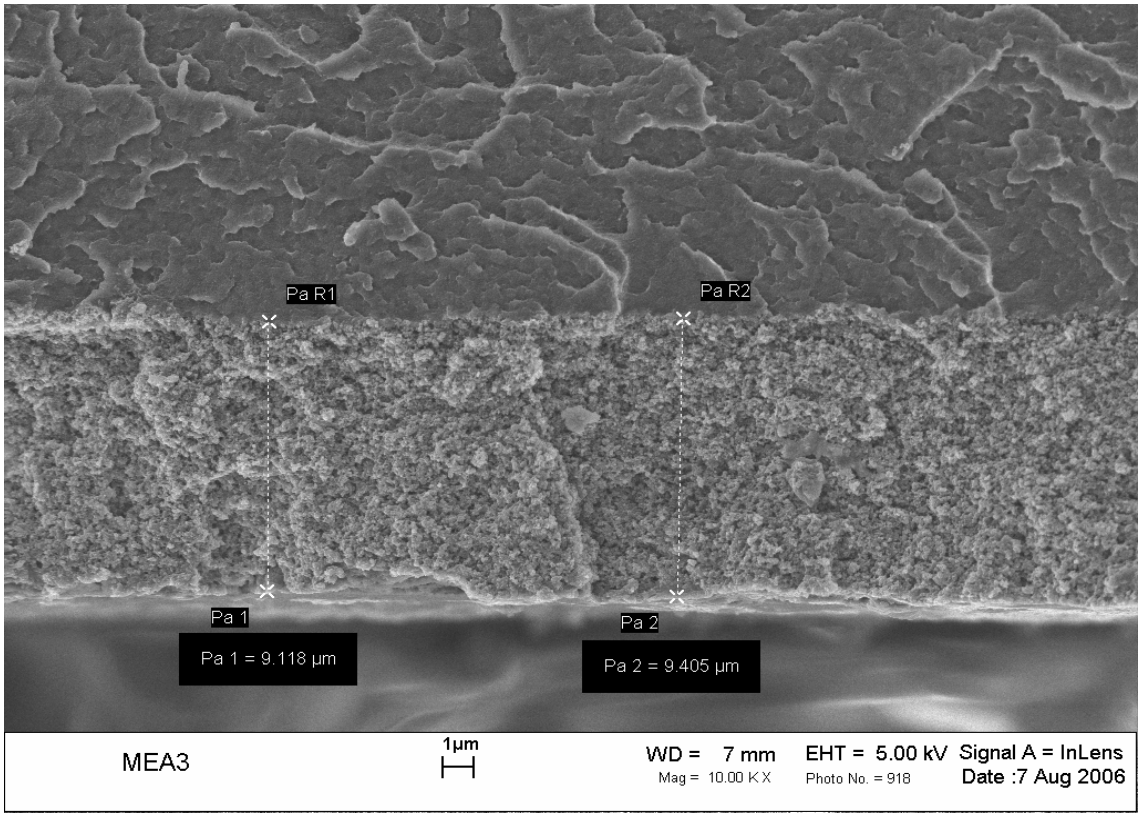

Figure B.3.1 MEA 3 at 10,000x magnification.

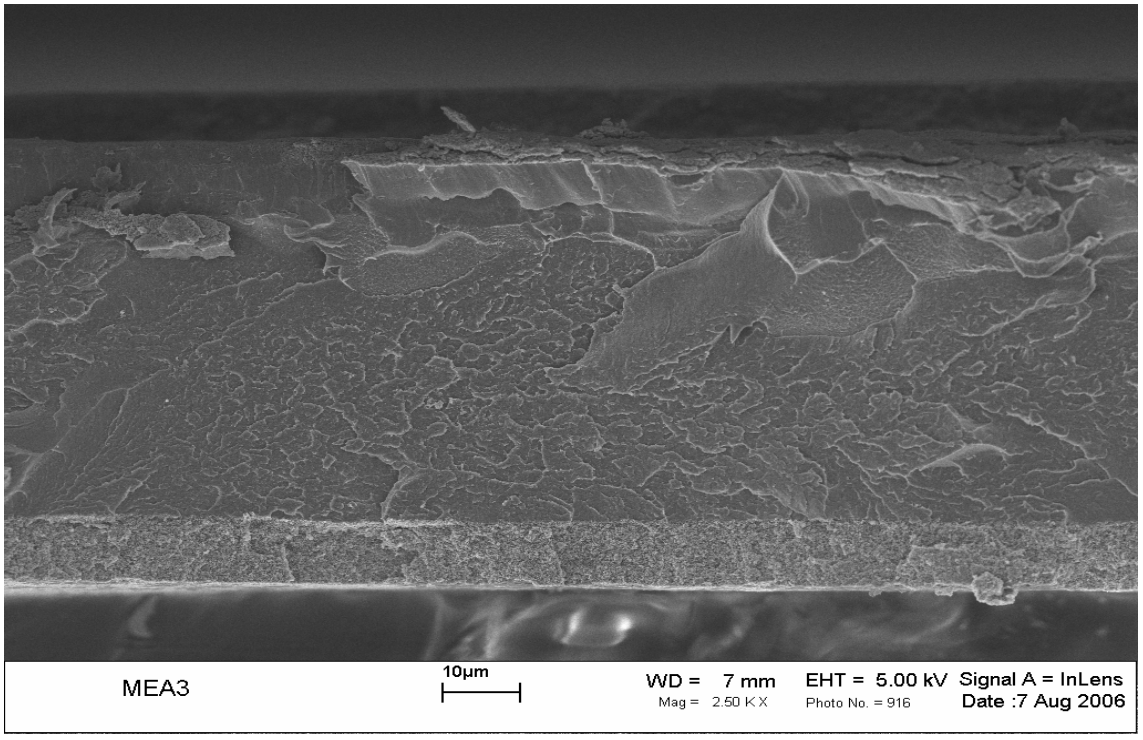

Figure B.3.2 MEA 3 at 3,000x magnification.

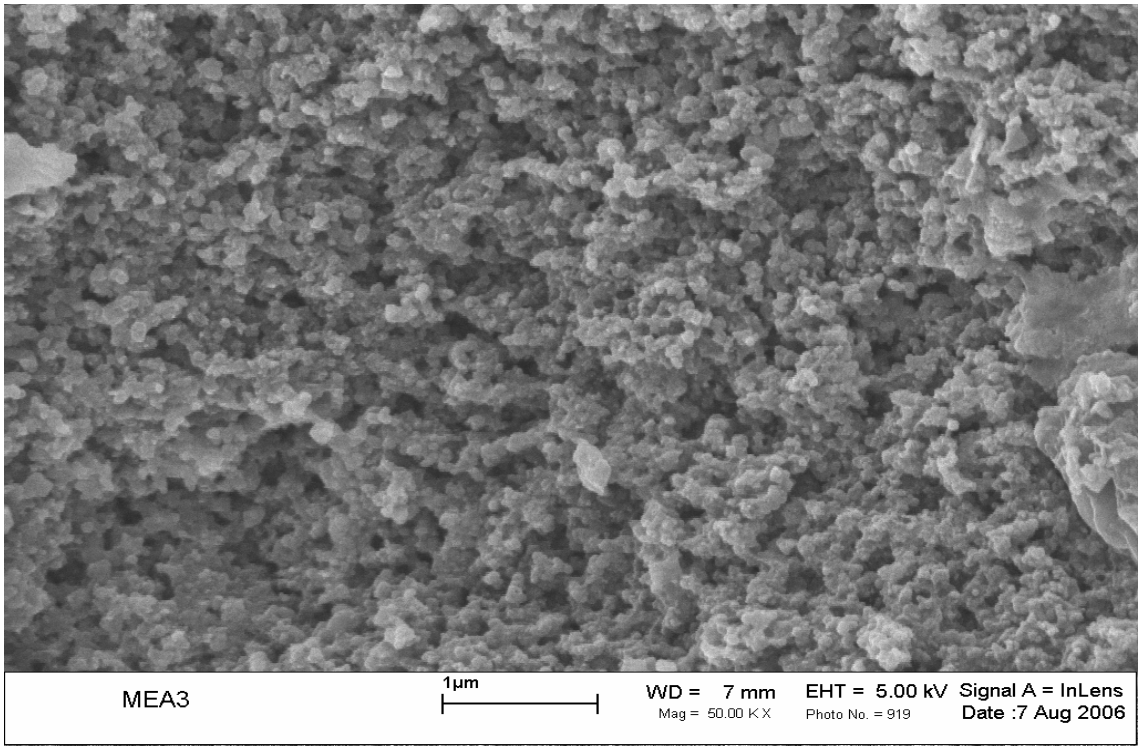

Figure B.3.3 MEA 3 at 50,000x magnification.

B.4 SEM Images of MEA 4

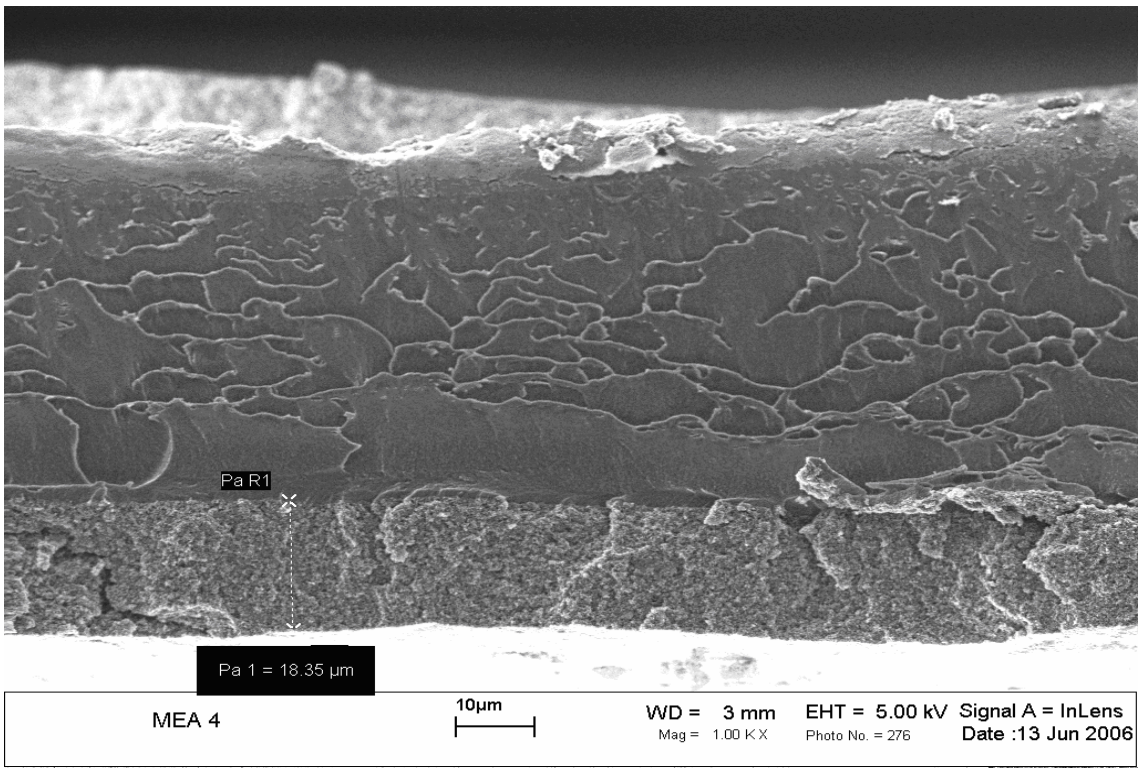

Figure B.4.1 MEA 4 at 1000x magnification.

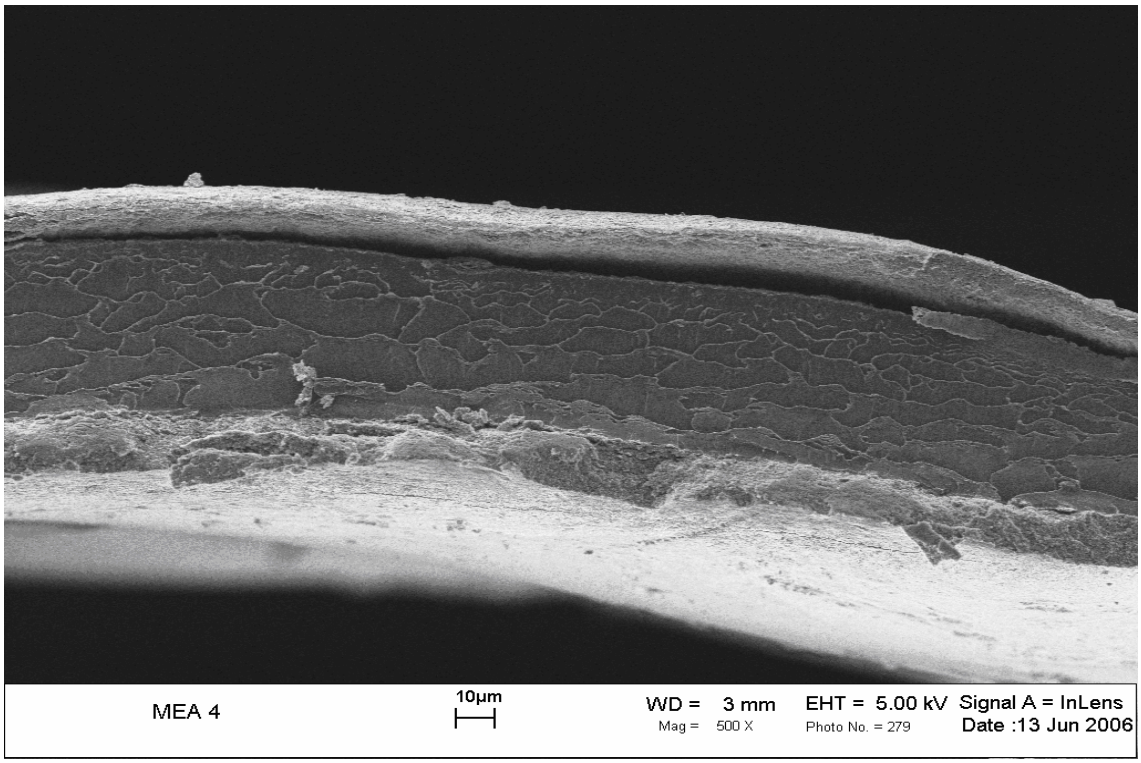

Figure B.4.2 MEA 4 at 500x magnification.

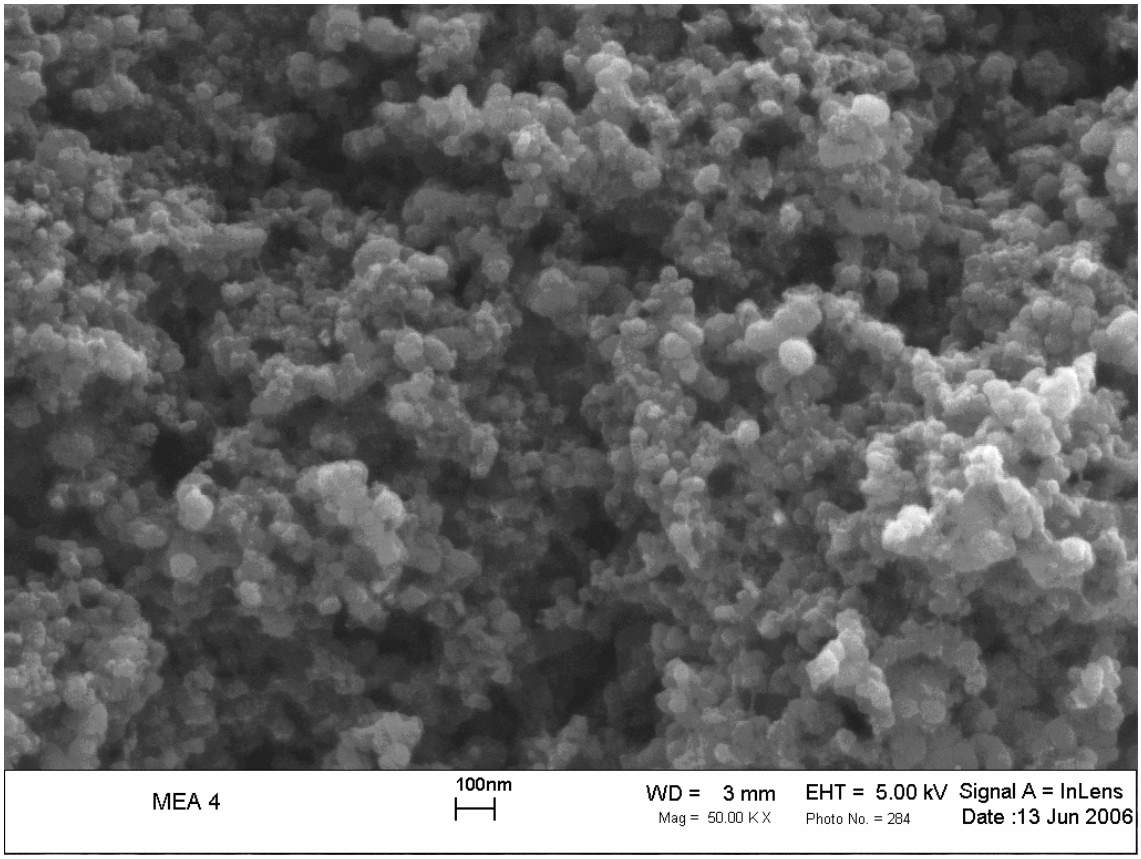

Figure B.4.3 MEA 4 at 50,000x magnification.

B.5 SEM Images of MEA 5

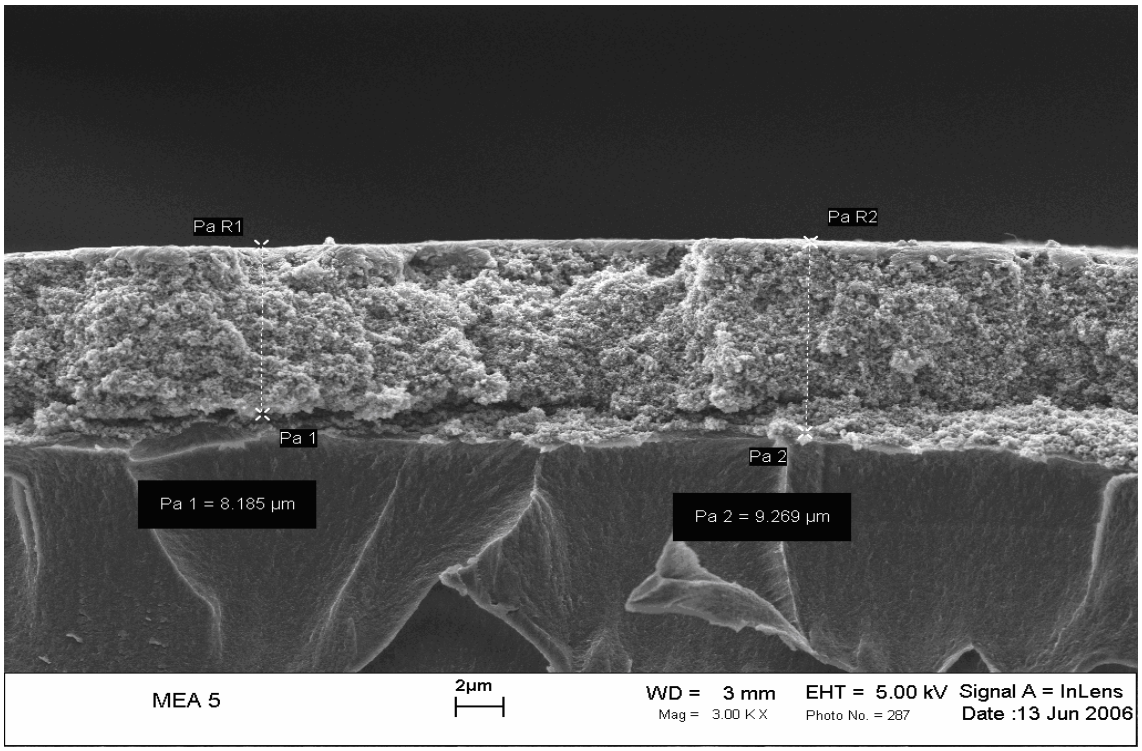

Figure B.5.1 MEA 5 at 3000x magnification.

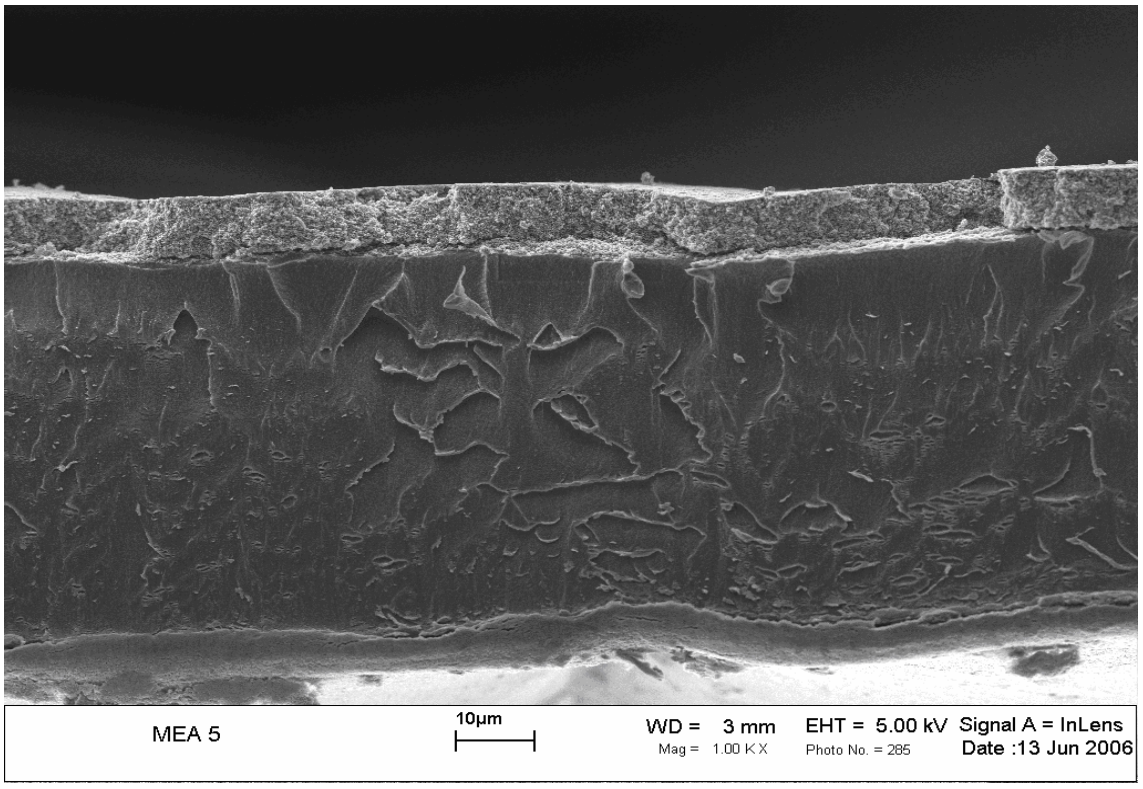

Figure B.5.2 MEA 5 at 1000x magnification.

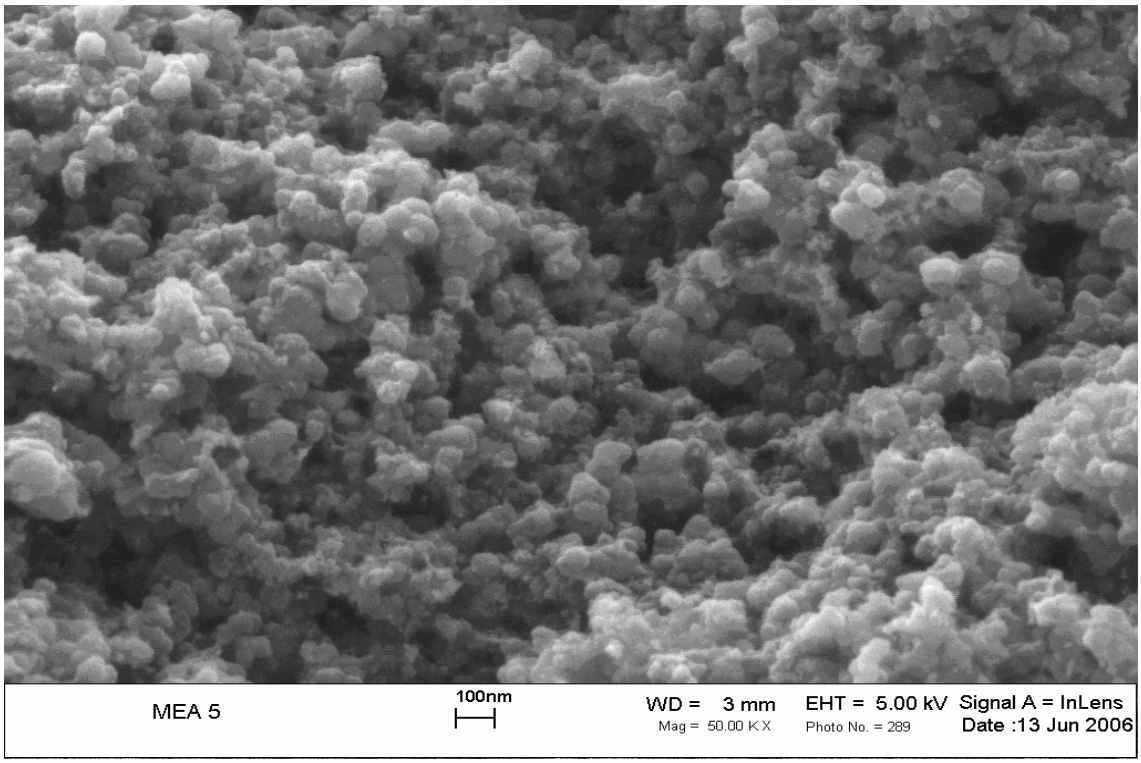

Figure B.5.3 MEA 5 at 50,000x magnification.

B.6 SEM Images of MEA 6

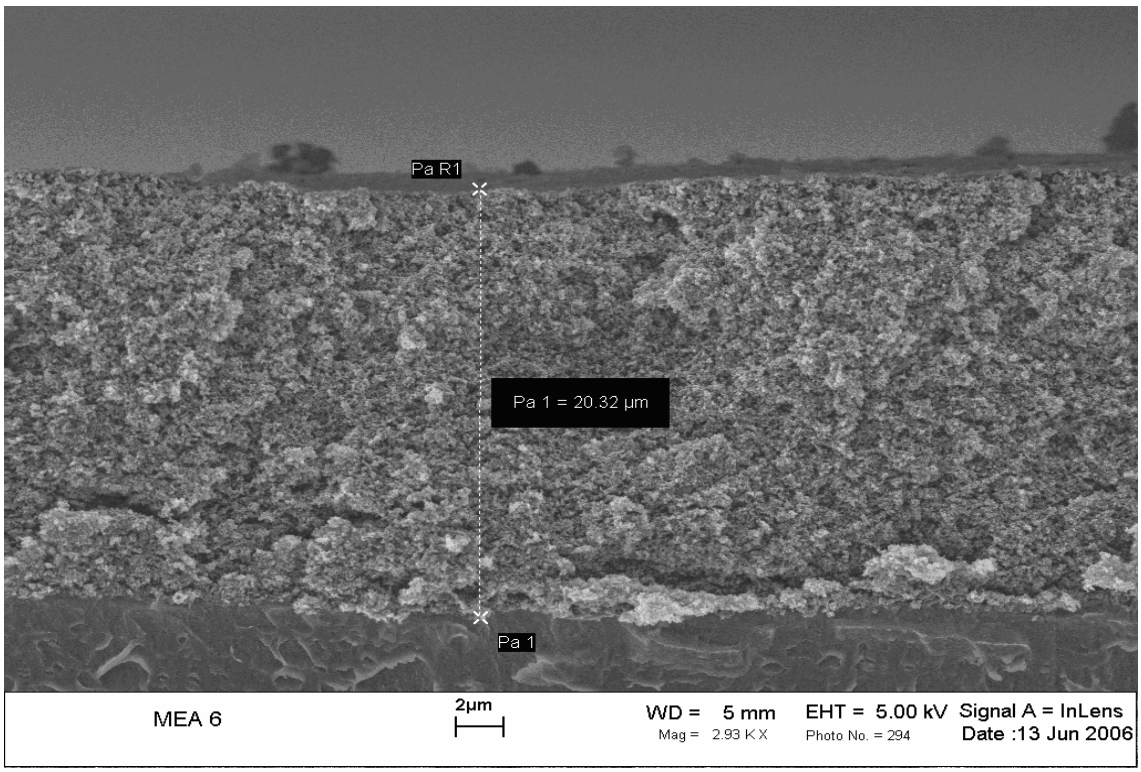

Figure B.6.1 MEA 6 at 3000x magnification.

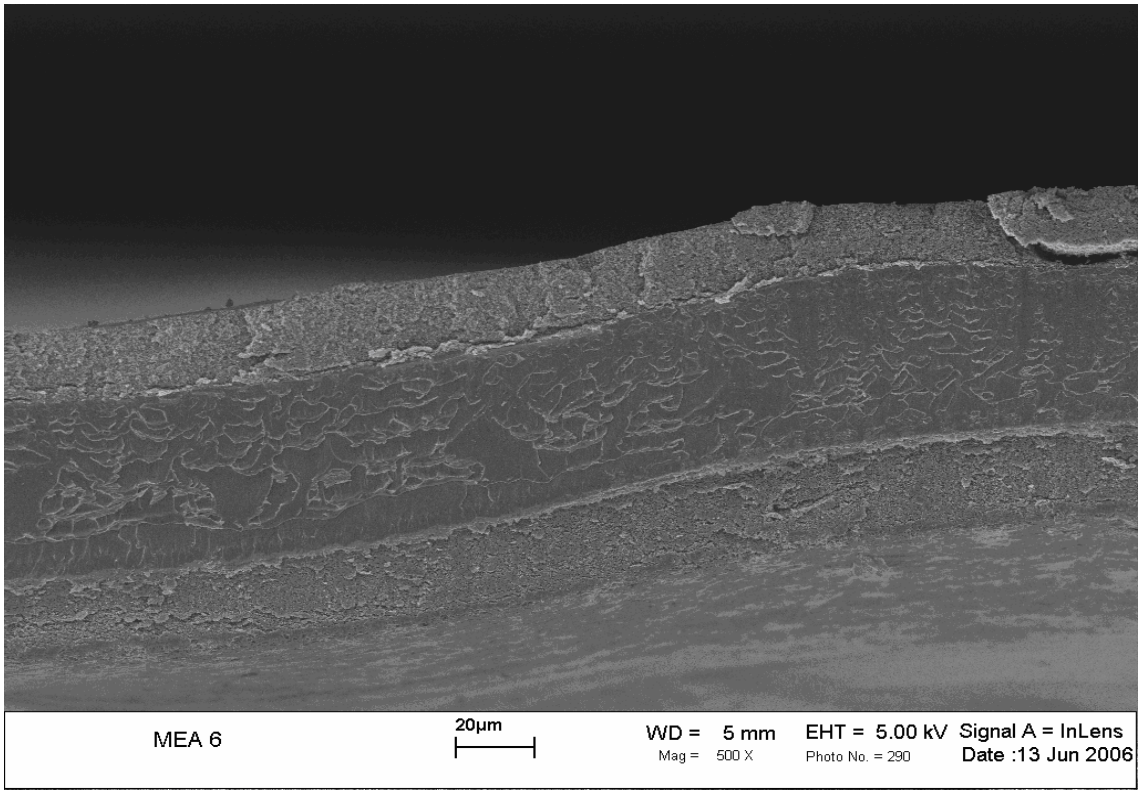

Figure B.6.2 MEA 6 at 500x magnification.

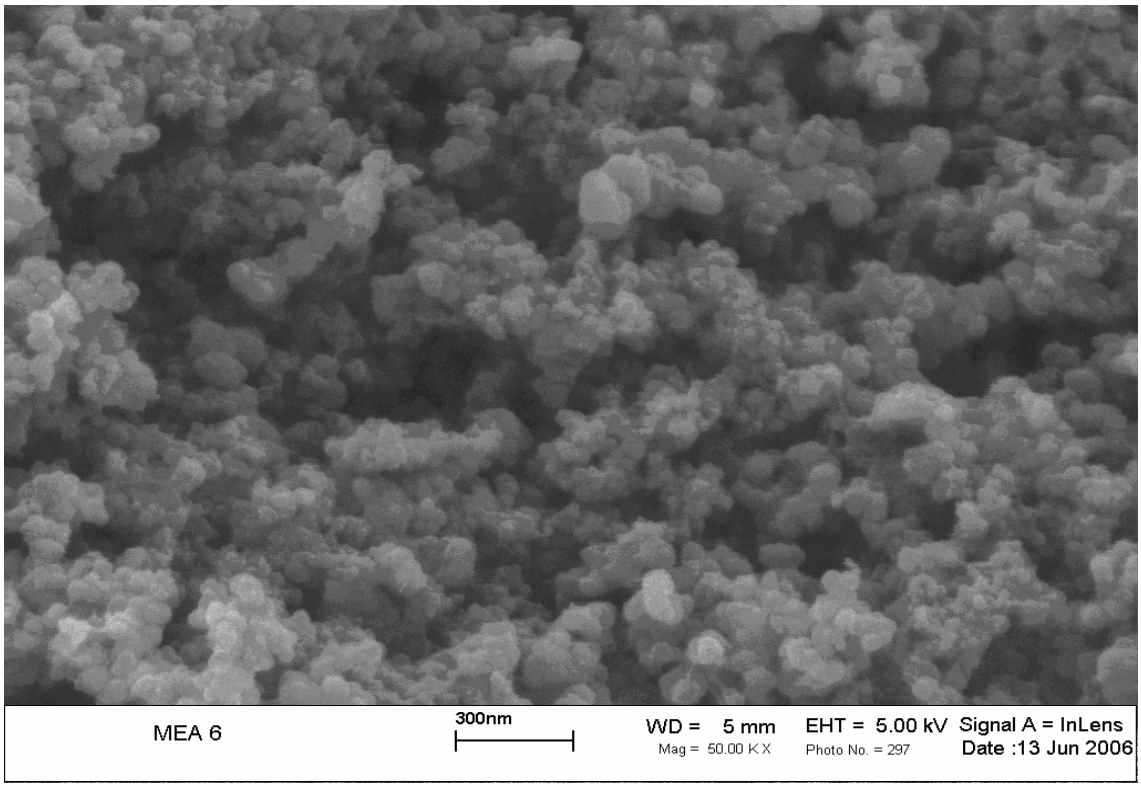

Figure B.6.3 MEA 6 at 50,000x magnification.

B.7 SEM Images of MEA 7

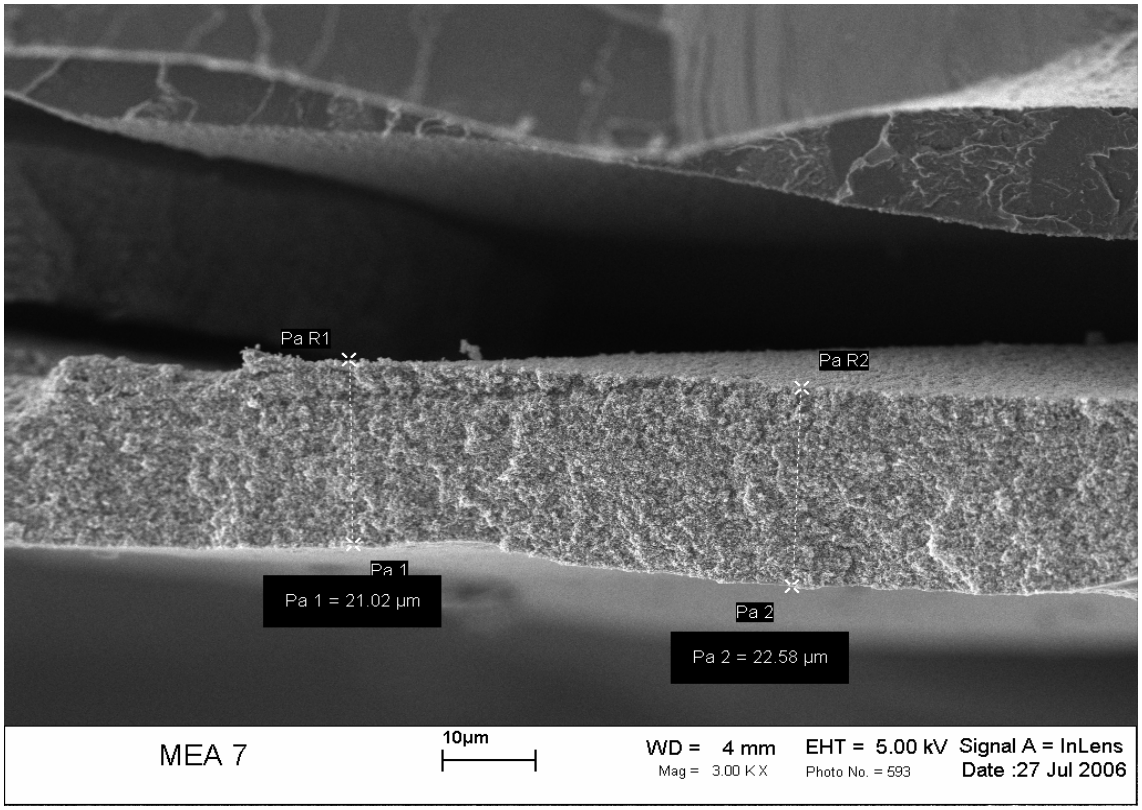

Figure B.7.1 MEA 7 at 1000x magnification.

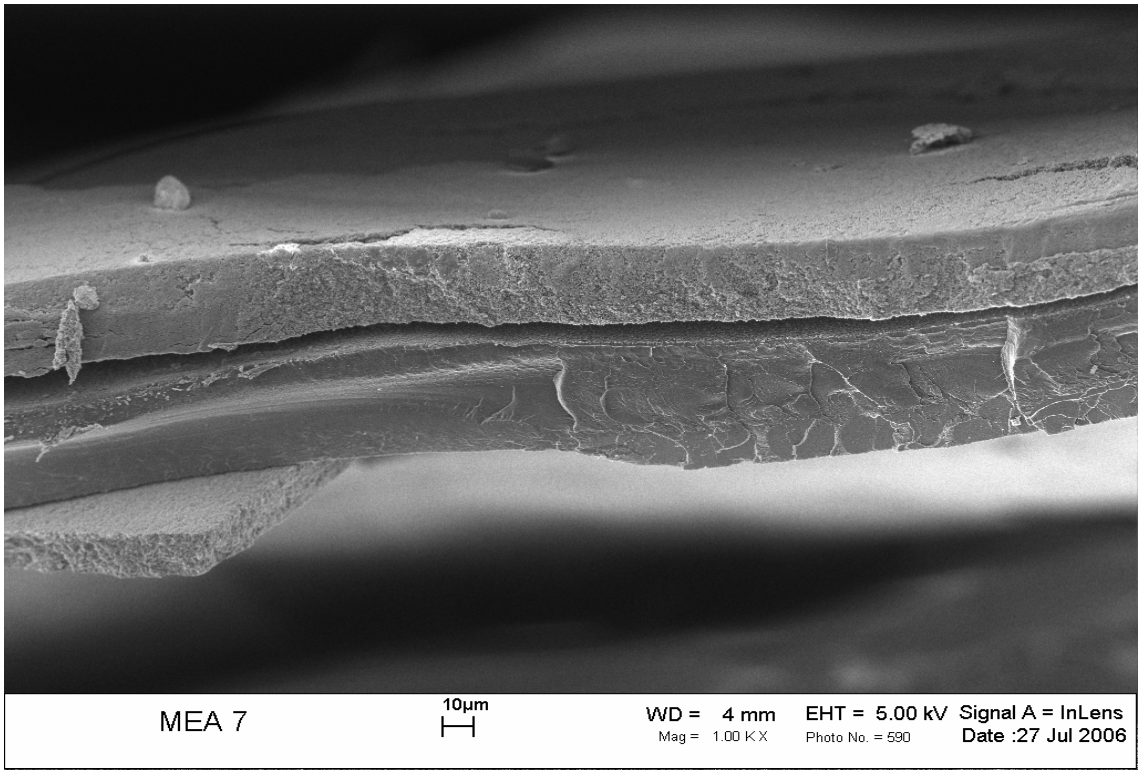

Figure B.7.2 MEA 7 at 1,000x magnification.

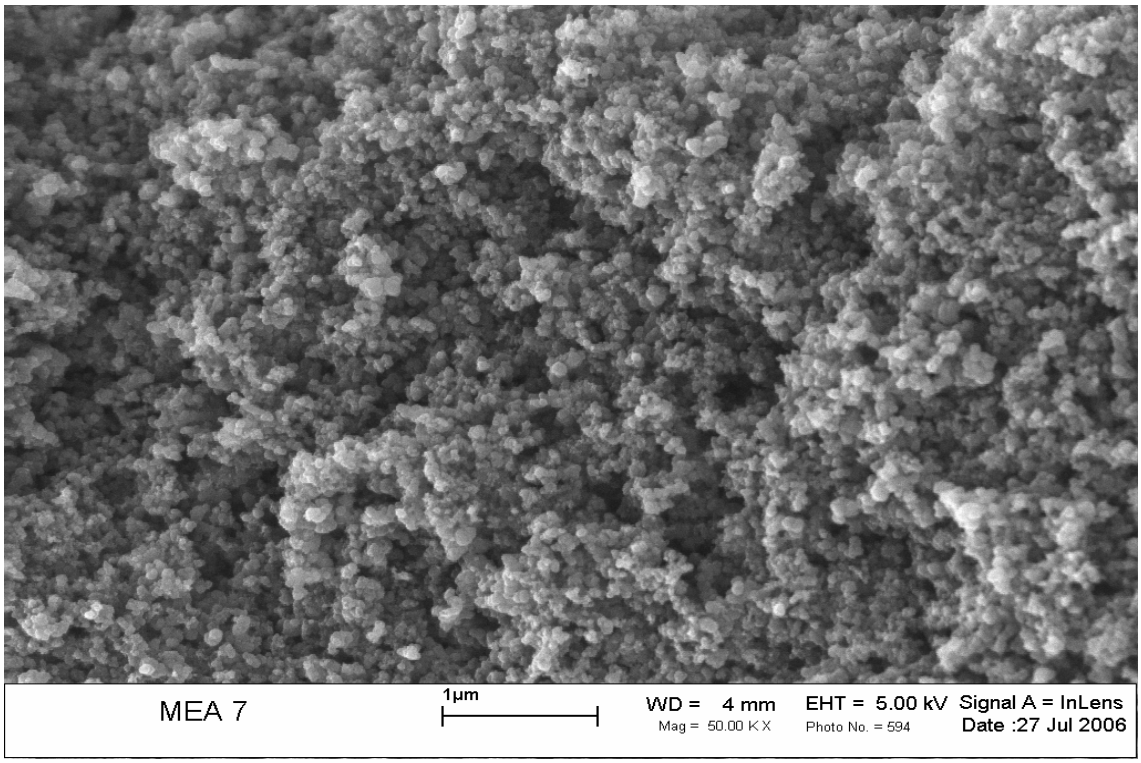

Figure B.7.3 MEA 7 at 50,000x magnification.

B.8 SEM Images of MEA 8

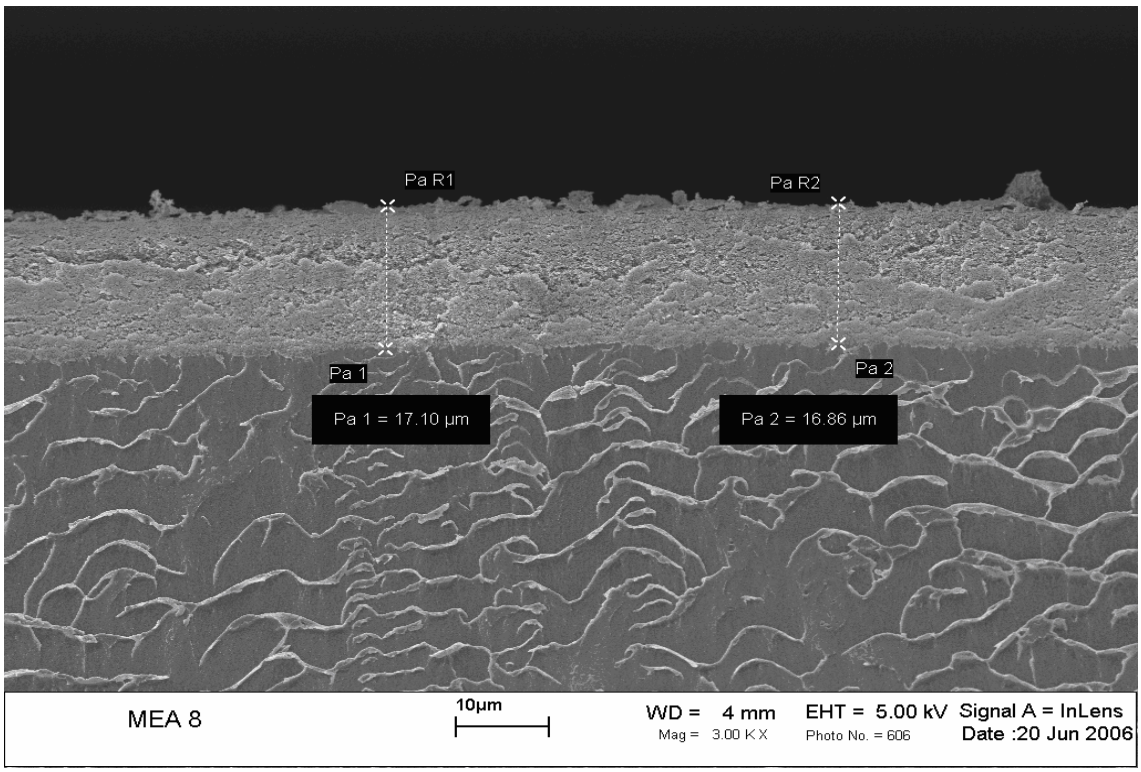

Figure B.8.1 MEA 8 at 3,000x magnification.

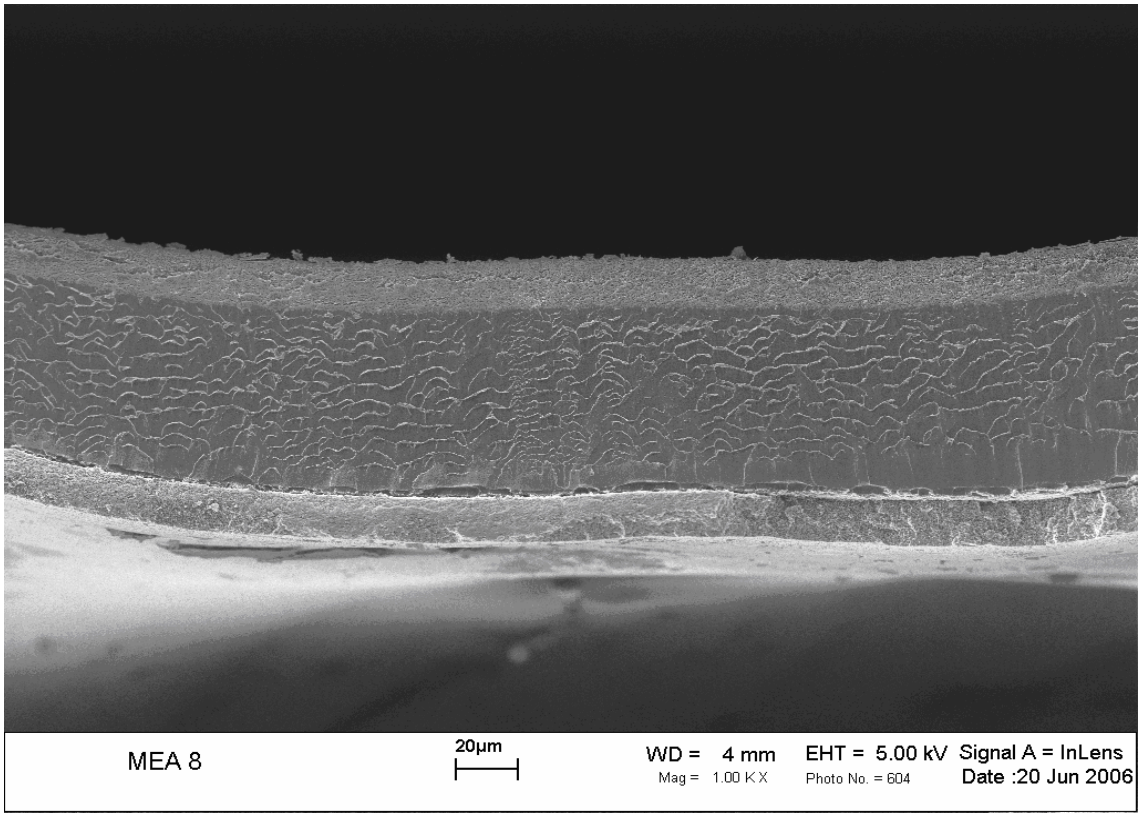

Figure B.8.2 MEA 8 at 1,000x magnification.

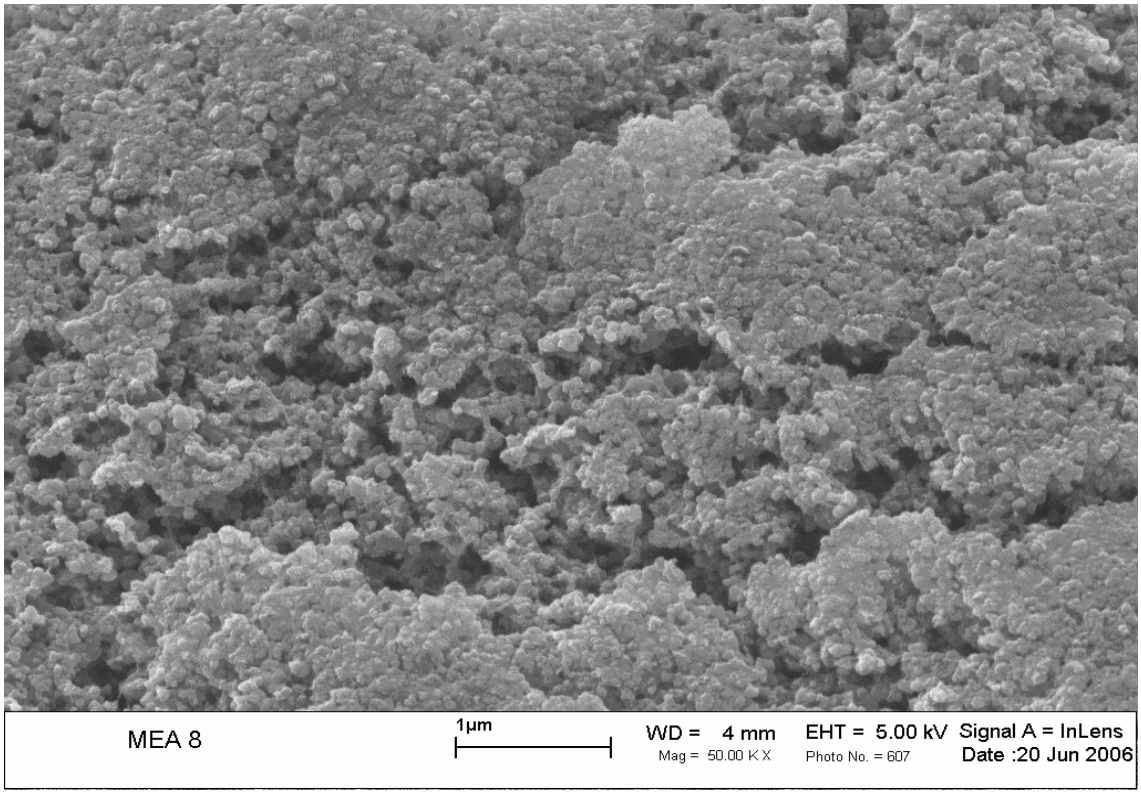

Figure B.8.3 MEA 8 at 50,000x magnification.

B.9-1 SEM Images of MEA 9-1

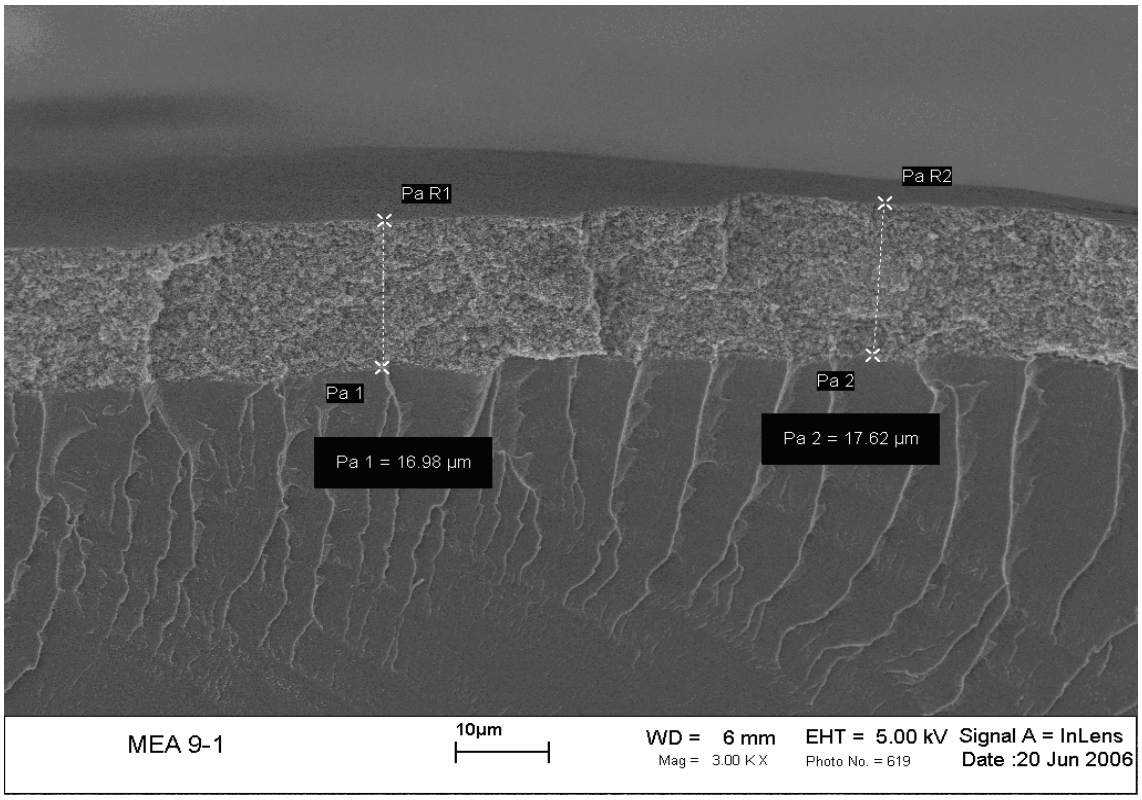

Figure B.9-1.1 MEA 9-1 at 3,000x magnification.

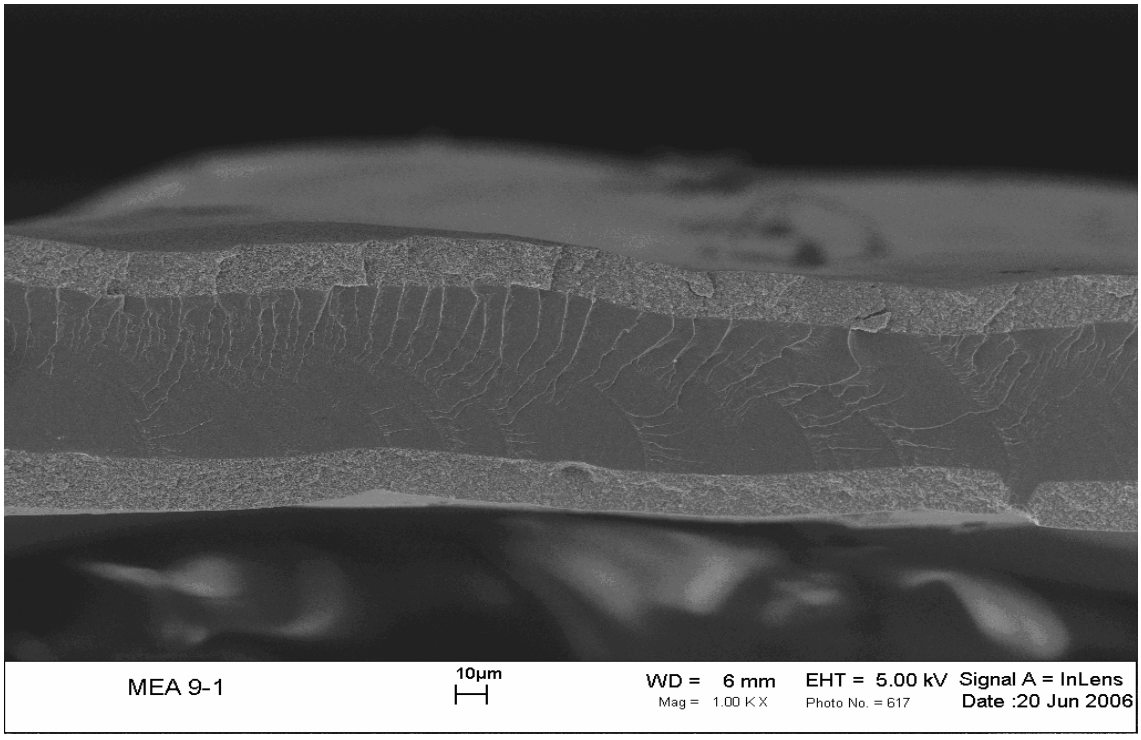

Figure B.9-1.2 MEA 9-1 at 1,000x magnification.

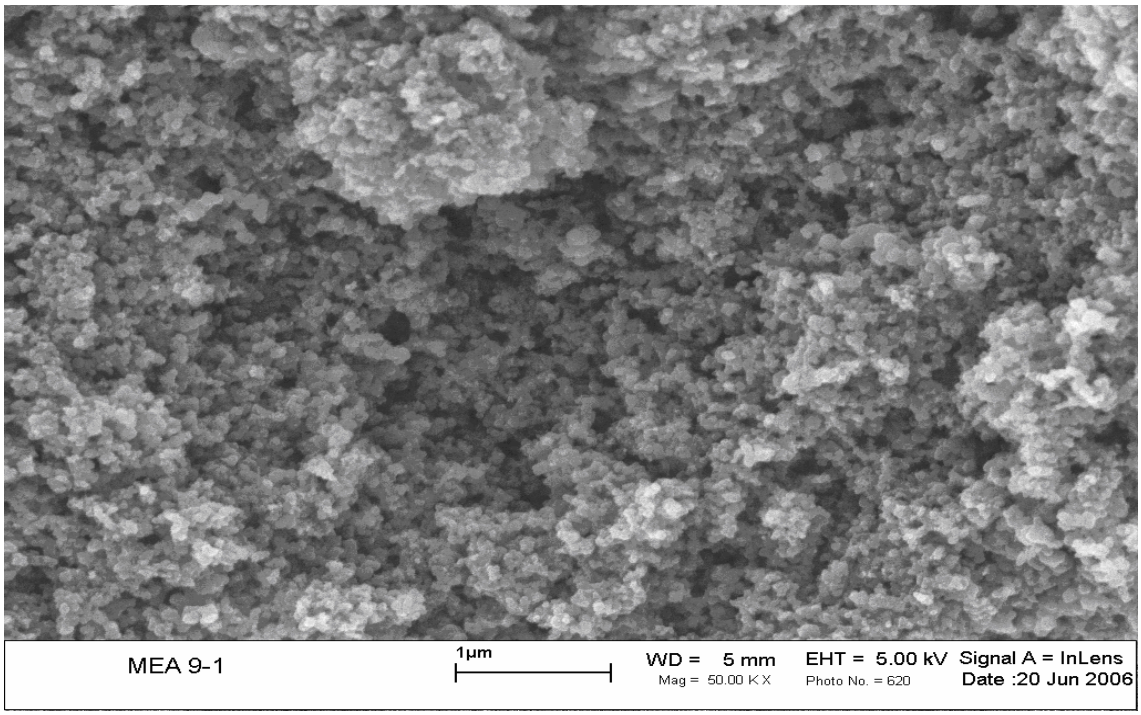

Figure B.9-1.3 MEA 9-1 at 50,000x magnification.

B.9-2 SEM Images of MEA 9-2

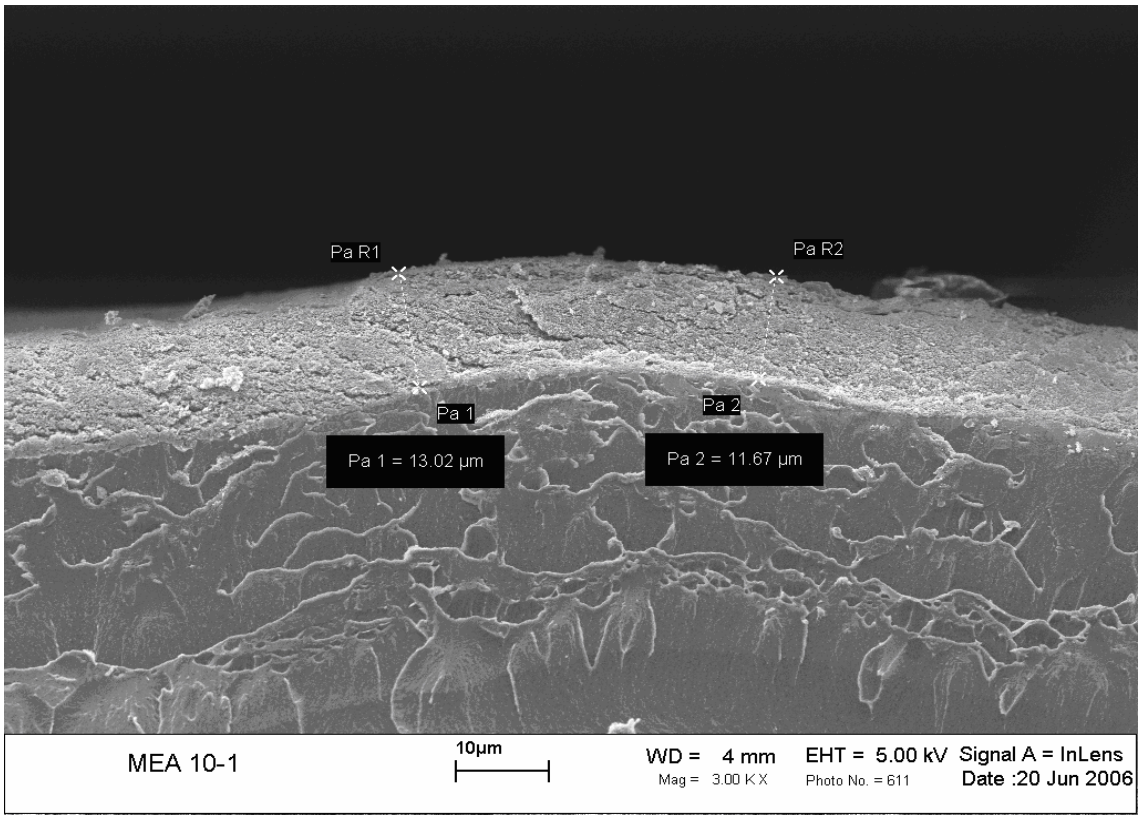

Figure B.9-2.1 MEA 9-2 at 3,000x magnification.

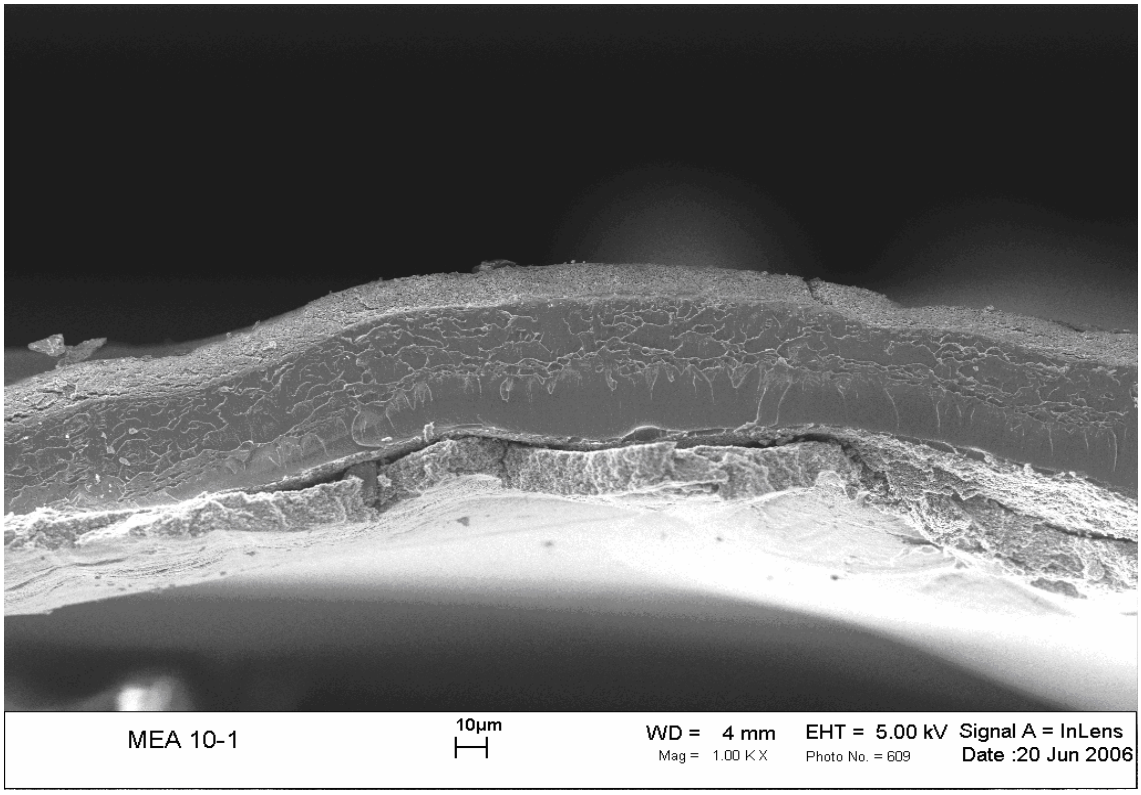

Figure B.9-2.2 MEA 9-2 at 1,000x magnification.

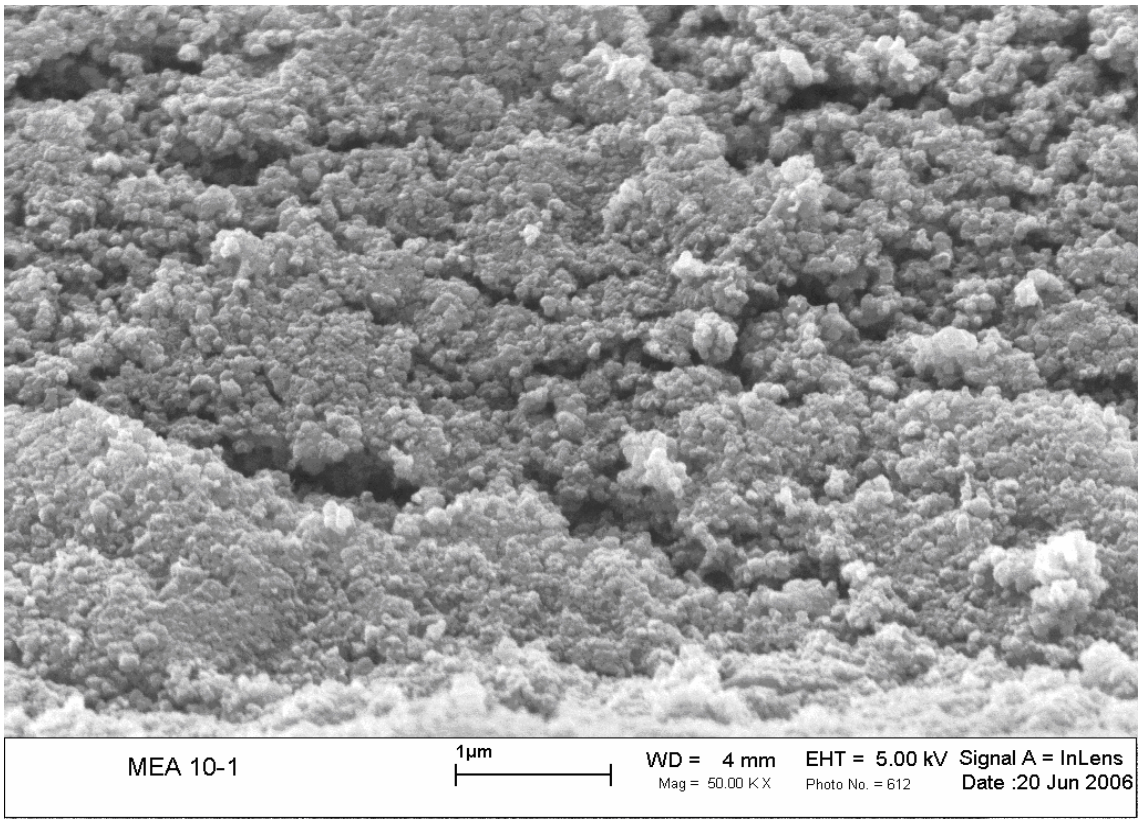

Figure B.9-2.3 MEA 9-2 at 50,000x magnification.

B.9-3 SEM Images of MEA 9-3

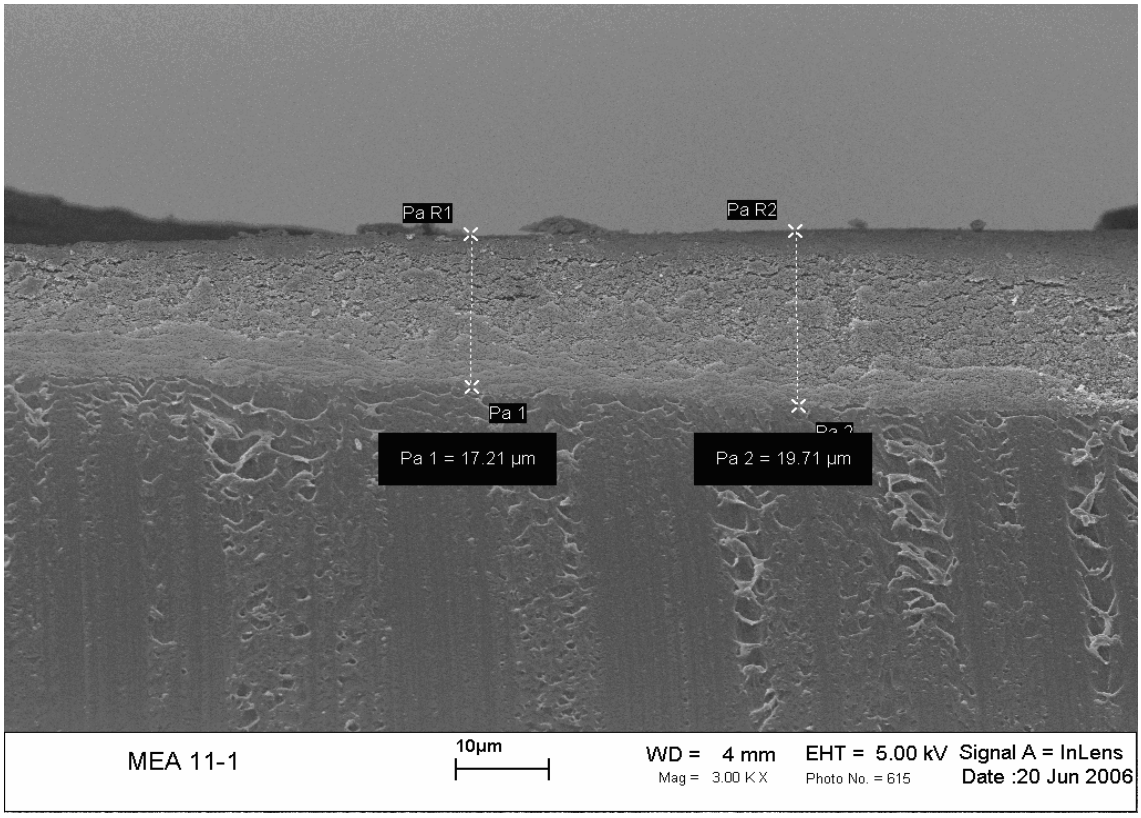

Figure B.9-3.1 MEA 9-3 at 3,000x magnification.

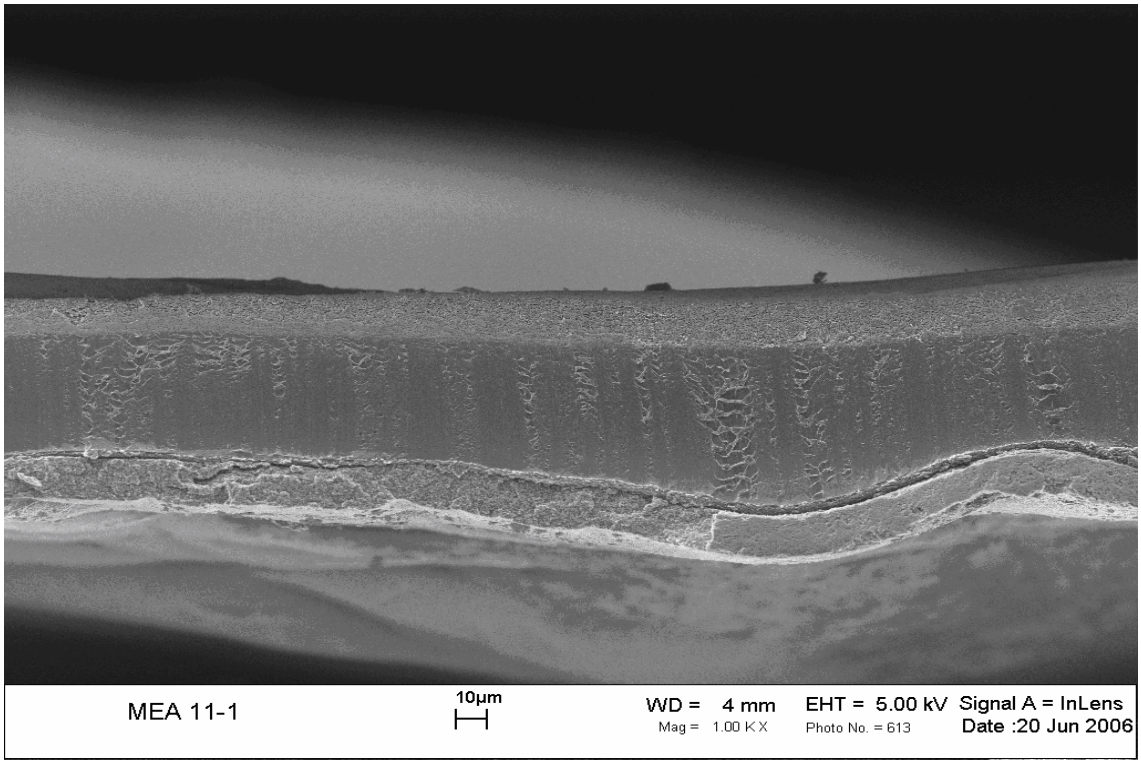

Figure B.9-3.2 MEA 9-3 at 1,000x magnification.

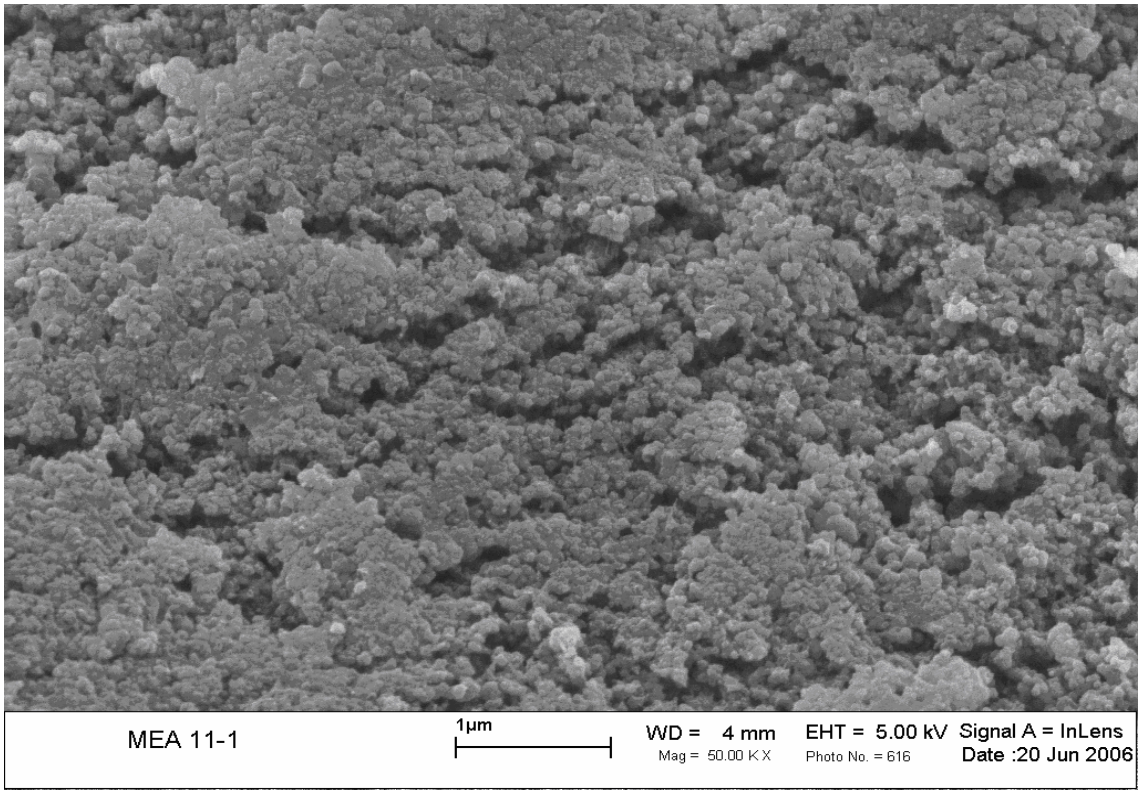

Figure B.9-3.3 MEA 9-3 at 50,000x magnification.

Vitae

EDUCATION

Master of Science, Mechanical Engineering, expected July 2006
Virginia Polytechnic Institute and State University (Virginia Tech), Blacksburg, VA
Thesis: *Experimental Investigation of the Effect of Composition on the Performance and Characteristics of PEM Fuel Cell Catalyst Layer*s
Advisor: Dr. Michael W. Ellis
Bachelor of Science, Mechanical Engineering, received May 2002
Milwaukee School of Engineering, Milwaukee, WI.

ACHIEVEMENTS

Scholarship in senior year for academic achievement.
Dean's list since Fall 2000.
Graduated With Honors.
Successfully completed the Fundamentals of Engineering Examination.

SENIOR PROJECT

SAE Aero Design Project: Designing and building composite for wings and fuselage.

EXPERIENCE

Kangnam District Office Seoul, Korea,
Government Service for 2 years
Accomplishments:

- Worked in Recycle Department
- Worked in a team environment making responsible decisions

HONORS & ORGANIZATIONS

Director of Public Relations Division in Korean Student Association At Western Illinois University for 2 years.